Exciton harvesting and multiplication in near-infrared organic light-emitting diodes

永田, 亮

出版情報：九州大学, 2020, 博士（工学）, 課程博士
バージョン：
権利関係：

2020
Doctor thesis

Exciton harvesting and multiplication in near-infrared organic light-emitting diodes

Ryo Nagata

Department of Chemistry and Biochemistry
Graduate School of Engineering
Kyushu University

Contents

Chapter 4. Development of highly efficient NIR-TADF molecule

Chapter 5. Summary and future perspective

Chapter 1

Introduction

1.1. Background and motivation

1.1.1. Near-infrared application

Near-infrared (NIR) wavelength region (700 ~ 2000 nm) has many advantages such as high transmissivity and non-invasiveness for organisms, suppressed light scattering in air, and low optical loss in silicon-based optical fibers. This has led to the development of inorganic light-emitting diodes (LEDs), inorganic laser diodes (LDs), and inorganic photodetectors (PDs), as well as to the development of new applications such as bio-optical sensing and imaging, optical distance measurement (*e.g.*, LiDAR), and optical communications. In particular, the development of NIR applications in the medical field has been remarkable recently. In fact, pulseplethysmography (PPG) [1] and blood oxygen saturation measurement (pulse oximetry) [2], which use NIR probe light, have become indispensable medical technologies for health care management and diagnosis. Moreover, NIR light is used not only for bio-sensing but also for bio-therapy (*e.g.*, photoimmunotherapy [3] and photothermal therapy [4]). Besides, NIR-LDs and NIR-LEDs are frequently used in security authentication such as iris, fingerprint, vein, and face recognition. Therefore, the development of an efficient NIR light source with additional value such as non-toxicity and flexibility will further expand the potential application and accelerate the commercial exploitation of NIR light source technology.

1.1.2 Organic light-emitting diodes

One promising candidate that potentially accelerate the development of NIR technology is organic LEDs (OLEDs) [5], which utilize both unique features of organic semiconducting materials, *i.e.*, luminescent and semiconducting properties. In fact, OLEDs have been attracting significant attention in recent years due to their excellent features as a light source such as ultra-flexibility, light-weight, the possibility of a low-cost fabricating process and the high uniformity of electroluminescence (EL). Therefore, OLEDs are expected to be complementarily used for various applications that are difficult with inorganic LEDs. In fact, OLEDs have been commercialized as a

display for large area TVs and smartphones, and its industrial market continues to expand year by year.

Figure 1-1 shows the schematic illustration of a conventional OLED structure consisted of several organic semiconductor layers with a total thickness of about 100 nm, including hole transporting layer (HTL), emitting layer (EML) and electron transporting layer (ETL), a transparent anode such as indium-tin-oxide (ITO), and a reflective cathode with a low work function and high reflectivity at visible wavelength such as aluminum (Al). When applied external electrical field to the OLEDs, at first, holes are injected from the anode to the highest occupied molecular orbital (HOMO) of the hole transporting material, while electrons are injected from the cathode to the lowest unoccupied molecular orbital (LUMO) of the electron transporting materials simultaneously. As a result, radical cations and radical anions are formed in the hole and electron transporting layers, respectively. The injected charges (holes and electrons) are then transported along with the applied electric field and recombine on an emitter molecule, resulting in a high energy hole-electron pair called “exciton”. The excitons can release the excited state energy as EL when the exciton backs to its’ ground state (S_0). OLEDs, therefore, are self-emitting devices, and the radiative molecules themselves determine their EL spectra. Thus, it is possible to develop OLEDs that display EL in not only visible wavelength regions but also in the UV and NIR wavelength regions by designing and utilizing appropriate molecules. In particular, OLEDs that emit efficient NIR-EL has been expected to open up new possibilities for not only display applications but also sensing light sources.

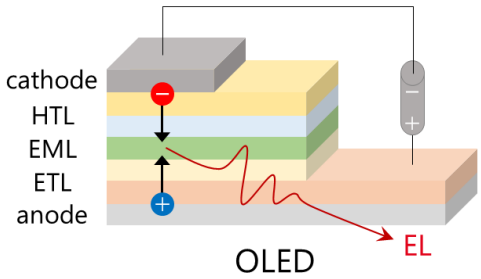

Fig. 1-1. Typical device structure of reported OLEDs

1.1.3. Exciton production efficiency

To improve the overall EL efficiency of OLEDs, significant efforts have been made from various perspectives such as material design and device architecture. Here, the overall external EL quantum

efficiency (η_{EQE}) of OLEDs is expressed as a product of four factors: (1) charge balance of injected holes and electrons (γ), (2) PL quantum yield of the emitter (φ_{PL}), (3) radiative exciton production efficiency (η_γ), and (4) light outcoupling efficiency (η_{out}), as shown in **Eq. 1-1**.

$$\eta_{EQE} = \gamma \times \eta_\gamma \times \varphi_{PL} \times \eta_{out} \qquad \text{(Eq. 1-1)}$$

From the perspective of material design, a great number of researchers have been working especially for achieving the ideal η_γ in OLEDs, where the lowest excited spin-singlet state (S_1) and the lowest excited spin-triplet state (T_1) are directly generated at a ratio of 1:3 based on the spin statistic rule [6]. Therefore, when using a fluorescent material as the emitter in OLEDs, only a spin-allowed fluorescent transition from S_1 to S_0 can be harvested as EL. Therefore, the theoretical maximum of radiative exciton production efficiency (η_γ) is limited to only 25% [5]. Thus, the material that possesses triplet harvesting ability is essential for achieving ideal η_γ in OLEDs, though a phosphorescent transition from pure T_1 to S_0 is essentially spin-forbidden.

For some organic materials, however, an efficient intersystem crossing (ISC) from S_1 to T_1 [7] and successive intense room-temperature phosphorescence, *i.e.*, the radiative transition from T_1 to S_0 [8], has been experimentally observed. Based on perturbation theory, it can be understood that the wavefunction for the triplet of the materials is not a purely zero-order wavefunction but instead a mixture of the singlet nature by perturbation such as spin-orbit coupling (SOC). In other words, the spin-state of organic molecules that we observe and think of as a triplet (or singlet) excited state is slightly mixed with the information of the singlet (or triplet) states. Here, up to the first-order perturbation for the sake of simplicity, the wavefunction of real triplet state ($\psi_T{}'$) is expressed as the linear combination of the wavefunction of pure singlet (ψ_S) and pure triplet (ψ_T) states, as shown in **Eq. 1-2**.

$$\psi_T' = \psi_T + \lambda\psi_S \qquad \text{(Eq. 1-2)}$$

where the first-order mixing coefficient (λ) is expressed as **Eq. 1-3**.

$$\lambda \approx \frac{H_{SOC}}{\Delta E_{ST}} \qquad \text{(Eq. 1-3)}$$

Here, ΔE_{ST} is the energy splitting between the excited singlet and triplet states, and H_{SOC} is the spin-orbit coupling (SOC) element value, which consists of spin-orbit coupling constant (ξ_{SOC}), spin (S) and orbital (L) angular momentum of electron, as described in **Eq. 1-4**.

$$H_{SOC} = \xi_{SOC} \; S \cdot L \qquad \text{(Eq. 1-4)}$$

Based on **Eq. 1-4**, the reported large ISC rate constant (k_{ISC}) of ~10^{11} s^{-1} in the purely organic compound, benzophenone [9], is explained by El-Sayed rule [9]. In benzophenone, ISC from $^1(n,\pi^*)$ to $^3(\pi,\pi^*)$ involves the electron transition on the oxygen atom, which induces the magnetic momentum of L (μ_L). Here, the generated μ_L can interact with the magnetic momentum of S (μ_S) originating from the spin-flip, leading to a large H_{SOC} value for the efficient ISC.

According to **Eq. 1-4**, the utilization of heavy atoms effectively achieves strong singlet-triplet spin-mixing and eventual room temperature phosphorescence, since ξ_{SOC} is proportional to the fourth power of the nuclear charge (Z). In fact, the phosphorescence rate constant (k_{phos}) of 2-bromonaphthalene is more than two orders of magnitude larger than that of unsubstituted naphthalene [8]. Using this strategy, various efficient room-temperature-phosphorescent (RTP) materials have been intensely developed in the research of OLEDs using heavy atoms such as iridium (Ir, Z = 77) [10,11] and platinum (Pt, Z = 78) [12,13] (**Figure 1-3**). In RTP materials, the spin selection rule in the ISC process between S_1 and T_n states and the phosphorescent process between T_1 and S_0 are relaxed, leading to ultimately high $\varphi_{PL(phos)}$ of ~100% [14]. Indeed, high η_{EQE} reaching the theoretical upper limit has been already achieved in phosphorescent OLEDs as early as the 2000s [10,11]. However, as efficient RTP materials generally contain expensive, rare, and toxic metals, it is desirable to develop purely organic alternatives with no environmental or bio-toxicity.

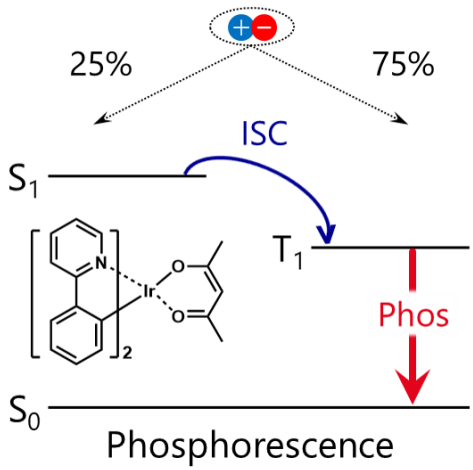

Fig. 1-3. Emission mechanism of room temperature phosphorescence

Based on **Eq. 1-3**, another possible approach for enhanced singlet-triplet spin-mixing is the reduction of ΔE_{ST}. Here, ΔE_{ST} is expressed as the exchange integral between wavefunction of the highest occupied molecular orbital (ψ_{HOMO}) and the lowest unoccupied molecular orbital (ψ_{LUMO}), as shown in **Eq. 1-5**.

$$\Delta E_{ST} = 2 \iint \psi_{HOMO}(1)\psi_{LUMO}(2)\frac{1}{r_{12}}\psi_{HOMO}(2)\psi_{LUMO}(1)d\tau_1\tau_2 \quad \text{(Eq. 1-5)}$$

where r_{12} is the distance between the electrons 1 and 2, indicating that the spatial separation between HOMO and LUMO is required for small ΔE_{ST}. If a strong mixing of S_1 and T_n states can be achieved by lowering the ΔE_{ST}, both forward ISC and reverse ISC (RISC) become spin-allowed transitions. In such a case, triplet excitons are harvested as delayed fluorescence from S_1 during ISC/RISC cycles because the phosphorescence channel is still shut-off, which are called thermally activated delayed fluorescence (TADF) (**Figure 1-4**). TADF behaviors have first found in Eosin Y [15] (therefore, also called E-type delayed fluorescence), and the current big wave for TADF interest was prompted by its exploitation for improving η_γ in OLEDs [16,17,18]. TADF materials have been rapidly developed because they show significant triplet harvesting ability without using rare, noble, and toxic metals.

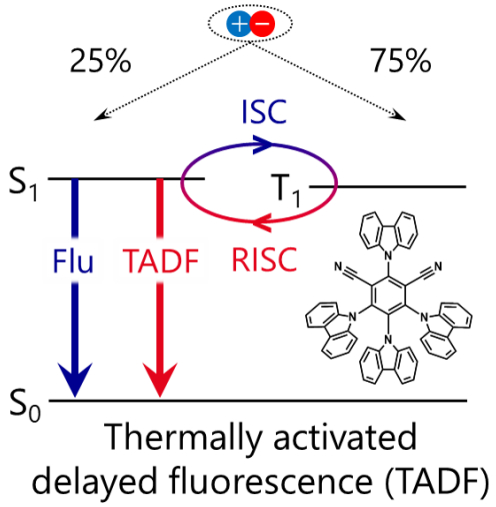

Fig. 1-4. Emission mechanism of TADF

In general, the design of TADF materials involves introducing structural twisting between the electron-donating (D) and electron-accepting (A) moieties to obtain the effective spatial separation between the HOMO and LUMO to reduce the ΔE_{ST}, resulting in efficient RISC [17]. Based on this molecular design concept, a lot of D-A type TADF materials exhibiting an intramolecular charge-transfer (CT) transition have been developed using a wide variety of π-conjugated aromatics [18,19,20,21,22], and recent design strategy of TADF materials has been further expanded into n-π^* type [23], excited-state intramolecular proton transfer (ESIPT) type [24], multi-resonance type

[25,26]. As a result, high η_{EQE} reaching the theoretical upper limit has been already achieved in TADF-OLEDs in blue to the deep-red region [18-22,25,26].

1.1.3 Current status and challenges in NIR-OLEDs

As well as visible OLEDs, recent NIR-OLEDs have made great progress in terms of η_{EQE}. **Figure 1-5** and **Table 1-1** show η_{EQE} against peak EL wavelength of representative NIR-OLEDs and the chemical structures of NIR fluorescent, phosphorescent, and TADF materials reported so far [27,28]. Here in NIR-OLEDs, the development of Pt-complexes has been remarkable, and in fact, significantly high η_{EQE} of 24% (EL peak at 740 nm) and 3.8% (EL peak at 900 nm) have already been achieved in Pt-complex based phosphorescent OLEDs [29,30].

However, η_{EQE} of rare-metal-free NIR-TADF-OLEDs has been behind from that of NIR-phoshorecent-OLEDs, though various D-A type structures employing pyrazinophenanthrene [31], pyrazinoacenaphthene [32], quinoxaline [33], benzothiadiazole [34], and boron-curcuminoid [35] are developed for achieving TADF property. Moreover, the reverse intersystem crossing rate constant (k_{RISC}) values of the reported NIR-TADF materials are still on the order of ~10^4 s^{-1} [32], leading to the significant η_{EQE} roll-off in high current operation, which is caused by the accumulation of triplet excitons [36,37,38,39]. In addition, although the operational device stability is strongly required for practical use, only a handful of reports have mentioned the operational device stability of NIR-TADF-OLEDs [40]. Here, the triplet management is also essential for improved device stability, since device degradation can be induced by bond dissociation from higher lying triplet excited states [41]. Thus, it is highly desirable to develop highly efficient NIR-TADF materials with large k_{RISC} for achieving η_γ of ~100% even at high current region with high operational durability. Besides, if narrow band-gap fluorescent materials are used as terminal emitters, *i.e.*, TADF-assisted fluorescence (TAF) system [42], an increase of driving voltage and the deteriorated charge balance induced by charge trapping on narrow-gap emitting molecules are serious problem. Therefore, it is also desirable to explore the possibility of TADF materials not only as the triplet sensitizer but also as a bipolar host.

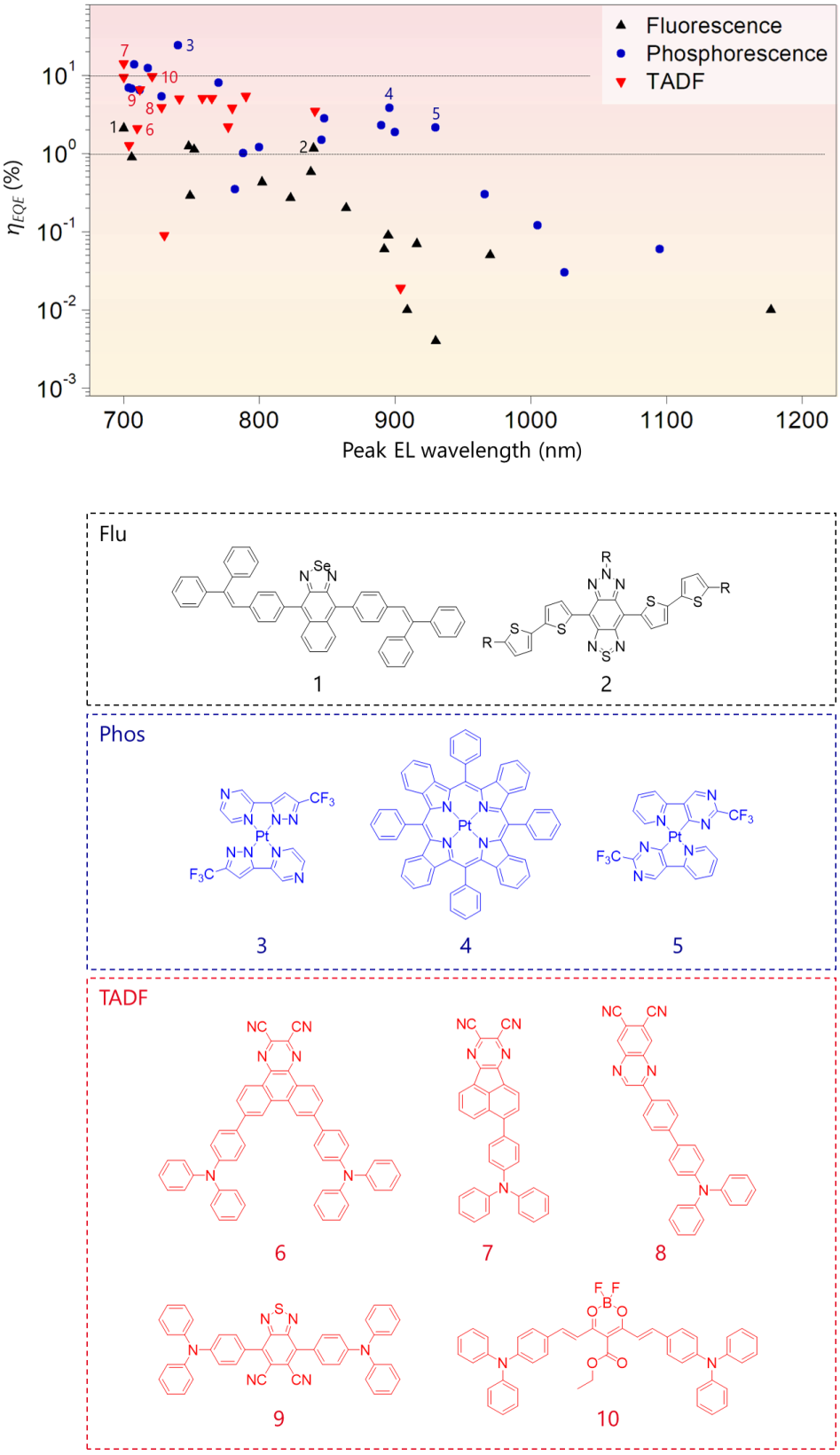

Fig. 1-5. Summary of External EL quantum efficiency against EL peak wavelength for reported NIR-OLEDs with the chemical structures of representative NIR emitters. The numbers beside the plots correspond to the numbers below the compounds [27,28].

Table 1-1. EL properties of state-of-the-art NIR-OLEDs

OLED type	Compound name	EL peak [nm]	η_{EQE_max} [%]
Fluorescence	NSeD	700	2.1
	TQ	748	1.2
		752	1.1
		823	0.3
	BTT*	840	1.2
	DCPA	838	0.6
		916	0.1
Phosphorescence	Ir(DBPz)	708	13.7
		728	5.4
		788	1.0
	$Pt(fprpz)_2$	740	24
	Pt(tptnp)	896	3.8
	$Pt(2\text{-pyridylpyrimidine})_2$	890	2.3
		900	1.9
		930	2.1
TADF	TPA-DCPP	710	2.1
	TPACNBz	712	6.6
	YD24	721	9.7
	TPA-QCN	700	9.4
		728	3.9
	POZ-DBPHZ	741	5
	TPAAP	700	14.1
		765	5.1
	APDC-DTPA	777	2.2
	CAT1	904	0.019
	TPAAZ	1010	0.003

Here, in addition to the TADF materials, the development of novel exciton-sensitizing materials is even more preferable for achieving η_γ of more than 100% to realize high power NIR light source. One path to breaking the η_γ limit is a singlet fission process [43], in which two triplet excitons are created from one singlet exciton as described in **Figure 1-6**. Since the triplet pair (TT) intermediating a singlet fission process has entire singlet nature, singlet fission is a spin-allowed process. In fact, recent studies have reported that the rate constant of a singlet fission process can reach ~10^{13} s^{-1} [44].

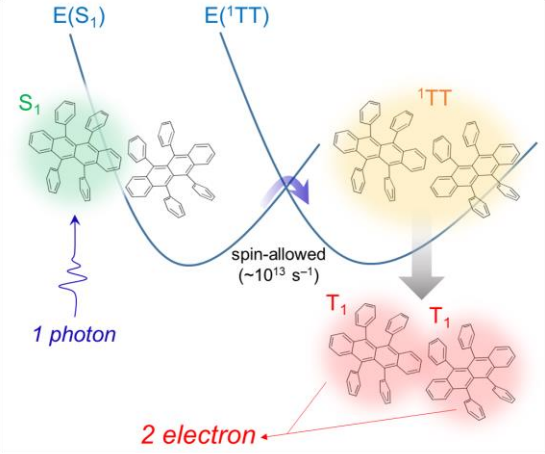

Fig. 1-6. Singlet fission process

In order to promote an efficient singlet fission process, the relative configuration of the energy levels: $S_1 > 2T_1$ or $S_1 = 2T_1$ must be satisfied. Since the singlet fission process is based on the intermolecular interaction between two neighboring molecules, the strength of the electronic interaction between the neighboring molecules is essentially an important factor. Due to the importance of energetic configuration and intermolecular distance, most of the previous reports are related to materials that can form crystalline morphologies, such as polyacene derivatives [45], oligophenylene derivatives [46], and carotenoid derivatives [47]. Recently, there have also been some reports on molecules that exhibit an intramolecular singlet fission process, which is promising for overcoming the limitations of intermolecular interactions [48].

Research on the fundamental physics of a singlet fission process started with the photophysical study of an anthracene single crystal in 1965 [49]. In 1968, the singlet fission process was proposed as the main origin for the low φ_{PL} in tetracene single crystals [45], which was justified by the analysis using a magnetic field in 1969 [50,51]. Later, in the 1980s, this research area came back into the spotlight with the observation of a singlet fission process in carotenoid derivatives [47] and conjugated polymers [52]. After the proposal by Nozik *et al.* in 2006 [53], the device applications of a singlet fission process have been intensively studied in the field of organic photovoltaics (OPVs), since singlet fission intrinsically has the potential for breaking the Shockley-Queisser limit [54]. In fact, in 2013, Baldo *et al.* reported the realization of an external quantum efficiency of over 100% in OPVs by utilizing a singlet fission process [55]. The sensitization by a singlet fission process is also beneficial for luminescence, and indeed there are some reports in which NIR photoluminescence originating from nanocrystals were obtained by energy transfer of triplet excitons generated by a

singlet fission process [56,57]. To date, however, there has been no research on OLEDs utilizing a singlet fission process.

Note that φ_{PL} of emitting materials is another serious problem especially in the NIR region. The φ_{PL} is defined as "the number of emitted photons per the number of absorbed photons", and φ_{PL} of almost 100% can be easily achieved in many fluorescent emitters in the visible region with a radiative rate constant of about 10^8-10^9 s^{-1} with a negligible ISC process [58]. In the NIR region, however, a dramatic decrease in φ_{PL} is generally observed, and this can be explained by the energy gap law [59-62], which indicates that the energy gap between the ground and excited states (ΔE) decreases in the NIR luminescence process, causing an exponential increase in the non-radiative decay rate constant (k_{nr}) due to a large overlap in the wave functions of the two states (**Figure 1-7**).

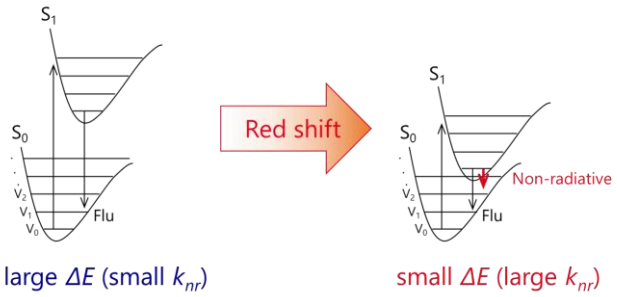

Fig. 1-7. Schematic of the energy gap law

Since k_{nr} also strongly depends on the reorganization energy of the promoting vibrational modes (λ_M) (**Figure 1-8**) [62], the decrease of λ_M is essentially required for achieving high φ_{PL}. In fact, a recent study on NIR phosphorescent materials has experimentally revealed the relationship between λ_M and φ_{PL}, *i.e.*, large λ_M, was found in the materials with low φ_{PL} [63]. Thus, it is desirable to explore rigid molecular skeletons with a sterically hindered substituent.

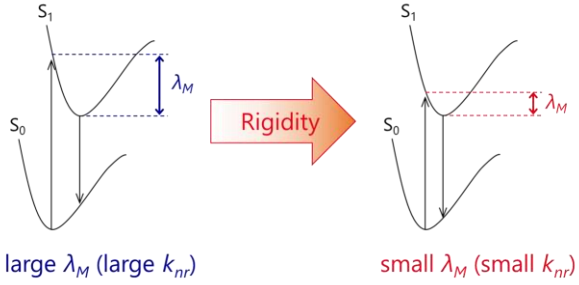

Fig. 1-8. Schematic of reorganization energy in the energy gap law

Further, in the deactivation processes of NIR molecules, the energy of the excited states can be also dissipated to the surrounding organic matrix as thermal energy, because the excited states located in the low energy region resonates with the vibrational overtones of the C-H stretching and O-H stretching vibrations specific to organic molecules. Therefore, to suppress such vibrational

deactivation processes, reducing the vibrational mode energy by halogen substitution such as fluorination is also effective [64].

1.2 Purposes and outline

The purpose of this thesis is the improvement of the overall η_{EQE} of NIR-OLEDs and the establishment of comprehensive material and device design rules for efficient NIR-OLEDs. This thesis is organized as follows.

In **Chapter 2**, I investigated the utilization of triplet harvesting processes, *i.e.*, TADF processes for the enhancement of η_γ in NIR-OLEDs. Using the TADF materials which emit in the visible region, as an energy donor to NIR-dyes, I demonstrated the NIR emission originated via the RISC process in the TADF host matrix and the successive FRET from TADF to NIR dyes. In the OLED characterization, η_{EQE} of the TADF host-based NIR-OLEDs is about 6 times higher than that of the conventional fluorescent host-based NIR-OLEDs due to the harvesting of electrically generated triplet excitons through an efficient RISC process on the TADF host. Further, I experimentally demonstrated that the TADF materials consisting of the electron-donating and electron-accepting moieties intrinsically have a high hole and electron mobility and are useful as a bipolar host material.

In **Chapter 3**, I focused on the singlet fission process as the exciton multiplication process, and utilized the triplet exciton generated by the singlet fission process for NIR luminescence. From the magnetic field dependence of the visible and NIR luminescence intensities, I found that it is possible to realize η_γ above the theoretical upper limit of 100% by exploiting of a singlet fission process in NIR-OLEDs.

In **Chapter 4**, I developed a novel NIR-TADF molecule with a rigid electron-accepting unit to achieve high φ_{PL} at 700~1000 nm, useful for biological sensing and imaging applications. The newly developed NIR-TADF molecule showed an emission peak at 729 nm in a 10wt%-doped film and its φ_{PL} exceeded 40%. The NIR-TADF molecule also functioned as an efficient energy donor for the NIR fluorescent molecule emitting around 900 nm. The NIR-OLEDs using the co-deposited film as an

emitting layer showed the η_{EQE} values of 13.4% with EL peak at 734 nm and 1.1% with EL peak at 901 nm, which are the highest η_{EQE} reported for NIR-TADF-OLEDs in each wavelength. Furthermore, by integrating the developed NIR-OLEDs with a conventional organic photodiode (OPD), I realized "all-organic" PPG sensing both in the 700 nm and 900 nm region.

In **Chapter 5**, the conclusions of this work and the future perspectives for highly efficient NIR-OLEDs are described.

References

1. A. V. J. Challoner, C. A. Ramsay, A photoelectric plethysmograph for the measurement of cutaneous blood flow. *Phys. Med. Biol.* **19**, 317 (1974)
2. T. Aoyagi, Pulse oximetry: its invention, theory, and future. *J. Anesth.* **17**, 259 (2003)
3. M. Mitsunaga, M. Ogawa, N. Kosaka, L. T. Rosenblum, P. L. Choyke, H. Kobayashi, Cancer cell-selective in vivo near infrared photoimmunotherapy targeting specific membrane molecules. *Nat. Med.* **17**, 1685 (2011)
4. A. B. Akimov, V. E. Seregin, K. V. Rusanov, E. G. Tyurina, T. A. Glushko, V. P. Nevzorov, O. F. Nevsorova, E. V. Akimova, Nd:YAG interstitial laser thermotherapy in the treatment of breast cancer. *Lasers Surg. Med.* **22**, 257 (1998)
5. C. W. Tang, S. A. VanSlyke, Organic electroluminescent diodes. *Appl. Phys. Lett.* **51**, 913 (1987)
6. M. A. Baldo, D. F. O'Brien, M. E. Thompson, S. R. Forrest, Excitonic singlet-triplet ratio in a semiconducting organic thin film. *Phys. Rev. B* **60**, 14422 (1999)
7. R. W. Anderson Jr., R. M. Hochstrasser, H. Lutz, G. W. Scott, Direct measurements of energy transfer between triplet states of molecules in liquids using picosecond pulses. *J. Chem. Phys.* **61**, 2500 (1974)
8. N. J. Turro, G. J. Kavarnos, T. Cole Jr., P. Scribe, J. C. Dalton, Molecular photochemistry. XXXIX. External heavy-atom-induced spin-obital coupling. Spectroscopic study of naphthonorbornanes. *J. Am. Chem. Soc.* **93**, 1032 (1971)
9. M. A. El-Sayed, The Radiationless Processes Involving Change of Multiplicity in the Diazenes. *J. Chem. Phys.* **36**, 573 (1962)

10. M. A. Baldo, S. Lamansky, P. E. Burrows, M. E. Thompson, S. R. Forrest, Very high-efficiency green organic light-emitting devices based on electrophosphorescence. *Appl. Phys. Lett.* **75**, 4 (1999)

11. C. Adachi, M. A. Baldo, M. E. Thompson, S. R. Forrest, Nearly 100% internal phosphorescence efficiency in an organic light-emitting device. *J. Appl. Phys.* **90**, 5048 (2001)

12. M. A. Baldo, D. F. O'Brien, Y. You, A. Shoustikov, S. Sibley, M. E. Thompson, S. R. Forrest, Highly efficient phosphorescent emission from organic electroluminescent devices. *Nature* **395**, 151 (1998)

13. C. Borek, K. Hanson, P. I. Djurovich, M. E. Thompson, K. Aznavour, R. Bau, Y. Sun, S. R. Forrest, J. Brooks, L. Michalski, J. Brown, Highly Efficient, Near-Infrared Electrophosphorescence from a Pt–Metalloporphyrin Complex. *Angew. Chem. Int. Ed.* **46**, 1109 (2007)

14. Y. Kawamura, K. Goushi, J. Brooks, J. J. Brown, H. Sasabe, C. Adachi, 100% phosphorescence quantum efficiency of Ir(III) complexes in organic semiconductor films. *Appl. Phys. Lett.* **86**, 0711044 (2005)

15. S. Boudin, Phosphorescence des solutions glycériques d'éosine influence des iodures. *J. Chim. Phys.* **27**, 285 (1930)

16. A. Endo, M. Ogasawara, A. Takahashi, D. Yokoyama, Y. Kato, C. Adachi, Thermally Activated Delayed Fluorescence from Sn^{4+}–Porphyrin Complexes and Their Application to Organic Light Emitting Diodes — A Novel Mechanism for Electroluminescence. *Adv. Mater.* **21**, 4802 (2009)

17. K. Goushi, K. Yoshida, K. Sato, C. Adachi, Organic light-emitting diodes employing efficient reverse intersystem crossing for triplet-to-singlet state conversion. *Nat. Photon.* **6**, 253 (2012)

18. H. Uoyama, K. Goushi, K. Shizu, H. Nomura, C. Adachi, Highly efficient organic light-emitting diodes from delayed fluorescence. *Nature* **492**, 234 (2012)

19. K. Sato, K. Shizu, K. Yoshimura, A. Kawada, H. Miyazaki, C. Adachi, Organic Luminescent Molecule with Energetically Equivalent Singlet and Triplet Excited States for Organic Light-Emitting Diodes. *Phys. Rev. Lett.* **110**, 247401 (2013)

20. S. Hirata, Y. Sakai, K. Masui, H. Tanaka, S. Y. Lee, H. Nomura, N. Nakamura, M. Yasumatsu, H. Nakanotani, Q. Zhang, K. Shizu, H. Miyazaki, C. Adachi, Highly efficient blue electroluminescence based on thermally activated delayed fluorescence. *Nat. Mater.* **14**, 330 (2015)

21. H. Kaji, H. Suzuki, T. Fukushima, K. Shizu, K. Suzuki, S. Kubo, T. Komino, H. Oiwa, F. Suzuki, A. Wakamiya, Y. Murata, C. Adachi, Purely organic electroluminescent material realizing 100% conversion from electricity to light. *Nat. Commun.* **6**, 8476 (2015)

22. T. Yang, B. Liang, Z. Cheng, C. Li, G. Lu, Y. Wang, Construction of Efficient Deep-Red/Near-Infrared Emitter Based on a Large π-Conjugated Acceptor and Delayed Fluorescence OLEDs with External Quantum Efficiency of over 20%. *J. Phys. Chem. C* **123**, 18585 (2019)

23. J. Li, Q. Zhang, H. Nomura, H. Miyazaki, C. Adachi, Thermally activated delayed fluorescence from $^{3}n\pi^{*}$ to $^{1}n\pi^{*}$ up-conversion and its application to organic light-emitting diodes. *Appl. Phys. Lett.* **105**, 013301 (2014)

24. M. Mamada, K. Inada, T. Komino, W. J. Potscavage Jr., H. Nakanotani, C. Adachi, Highly Efficient Thermally Activated Delayed Fluorescence from an Excited-State Intramolecular Proton Transfer System. *ACS Cent. Sci.* **3**, 769 (2017)

25. T. Hatakeyama, K. Shiren, K. Nakajima, S. Nomura, S. Nakatsuka, K. Kinoshita, J. Ni, Y. Ono, T. Ikuta, Ultrapure Blue Thermally Activated Delayed Fluorescence Molecules: Efficient HOMO–LUMO Separation by the Multiple Resonance Effect. *Adv. Mater.* **28**, 2777 (2016)

26. Y. Kondo, K. Yoshiura, S. Kitera, H. Nishi, S. Oda, H. Gotoh, Y. Sasada, M. Yanai, T. Hatakeyama, Narrowband deep-blue organic light-emitting diode featuring an organoboron-based emitter. *Nat. Photon.* **13**, 678 (2019)

27. A. Zampetti, A. Minotto, F. Cacialli, Near-Infrared (NIR) Organic Light-Emitting Diodes (OLEDs): Challenges and Opportunities. *Adv. Funct. Mater.* **29**, 1807623 (2019)

28. J. Brodeur, L. Hu, A. Malinge, E. Eizner, W. G. Skene, S. K. Cohen, Highly Efficient and Spectrally Narrow Near-Infrared Fluorescent OLEDs Using a TADF-Sensitized Cyanine Dye. *Adv. Opt. Mater.* **7**, 1901144 (2019)

29. K. T. Ly, R. W. C. Cheng, H. W. Lin, Y. J. Shiau, S. H. Liu, P. T. Chou, C. S. Tsao, Y. C. Huang, Y. Chi, Near-infrared organic light-emitting diodes with very high external quantum efficiency and radiance. *Nat. Photon.* **11**, 63 (2017)

30. K. R. Graham. Y. Yang, J. R. Sommer, A. H. Shelton, K. S. Schanze, J. Xue, J. R. Reynolds, Extended Conjugation Platinum(II) Porphyrins for use in Near-Infrared Emitting Organic Light Emitting Diodes. *Chem. Mater.* **23**, 5305 (2011)

31. S. Wang, X. Yan, Z. Cheng, H. Zhang, Y. Liu, Y. Wang, Highly Efficient Near-Infrared Delayed Fluorescence Organic Light Emitting Diodes Using a Phenanthrene-Based Charge-Transfer Compound. *Angew. Chem. Int. Ed.* **127**, 13260 (2015)

32. J. Xue, Q. Liang, R. Wang, J. Hou, W. Li, Q. Peng, Z. Shuai, J. Qiao, Highly Efficient Thermally Activated Delayed Fluorescence via J-Aggregates with Strong Intermolecular Charge Transfer. *Adv. Mater.* **31**, 1808242 (2019)

33. C. Li, R. Duan, B. Liang, G. Han, S. Wang, K. Ye, Y. Liu, Y. Yi, Y. Wang, Deep-Red to Near-Infrared Thermally Activated Delayed Fluorescence in Organic Solid Films and Electroluminescent Devices. *Angew. Chem. Int. Ed.* **56**, 11525 (2017)

34. J. Kumsampao, C. Chaiwai, P. Chasing, T. Chawanpunyawat, S. Namuangruk, T. Sudyoadsuk, V. Promarak, A Simple and Strong Electron-Deficient 5,6-Dicyano[2,1,3]benzothiadiazole-Cored Donor-Acceptor-Donor Compound for Efficient Near Infrared Thermally Activated Delayed Fluorescence. *Chem. Asian J.* **15**, 3029 (2020)

35. D. H. Kim, A. D'Aléo, X. K. Chen, A. D. S. Sandanayaka, D. Yao, L. Zhao, T. Komino, E. Zaborova, G. Canard, Y. Tsuchiya, E. Choi, J. W. Wu, F. Fages, J. L. Bredas, J. C. Ribierre, C. Adachi, High-efficiency electroluminescence and amplified spontaneous emission from a thermally activated delayed fluorescent near-infrared emitter. *Nat. Photon.* **12**, 98 (2018)

36. H. Noda, H. Nakanotani, C. Adachi, Excited state engineering for efficient reverse intersystem crossing. *Sci. Adv.* **4**, eaao6910 (2018)

37. K. Masui, H. Nakanotani, C. Adachi, Analysis of exciton annihilation in high-efficiency sky-blue organic light-emitting diodes with thermally activated delayed fluorescence. *Org. Electron.* **14**, 2721 (2013)

38. C. Murawski, K. Leo, M. C. Gather, Efficiency Roll-Off in Organic Light-Emitting Diodes. *Adv. Mater.* **25**, 6801 (2013)

39. T. Furukawa, H. Nakanotani, M. Inoue, C. Adachi, Dual enhancement of electroluminescence efficiency and operational stability by rapid upconversion of triplet excitons in OLEDs. *Sci. Rep.* **5**, 8429 (2015)

40. T. Yamanaka, H. Nakanotani, S. Hara, T. Hirohata, C. Adachi, Near-infrared organic light-emitting diodes for biosensing with high operating stability. *Appl. Phys. Express.* **10**, 074101 (2017)

41. J. Lee, C. Jeong, T. Batagoda, C. Coburn, M. E. Thompson, S. R. Forrest, Hot excited state management for long-lived blue phosphorescent organic light-emitting diodes. *Nat. Commun.* **8**, 15566 (2017)

42. H. Nakanotani, T. Higuchi, T. Furukawa, K. Masui, K. Morimoto, M. Numata, H. Tanaka, Y. Sagara, T. Yasuda, C. Adachi, High-efficiency organic light-emitting diodes with fluorescent emitters. *Nat. Commun.* **5**, 4016 (2014)

43. M. B. Smith, J. Michl, Singlet Fission. *Chem. Rev.* **110**, 6891 (2010)

44. S. R. Yost, J. Lee, M. W. B. Wilson, T. Wu, D. P. McMahon, R. R. Parkhurst, N. J. Thompson, D. N. Congreve, A. Rao, K. Johnson, M. Y. Sfeir, M. G. Bawendi, T. M. Swager, R. H. Friend, M. A. Baldo, T. V. Voorhis, A Transferable model for singlet-fission kinetics. *Nat. Chem.* **6**, 492 (2014)

45. C. E. Swenberg, W. T. Stacy, Bimolecular radiationless transitions in crystalline tetracene. *Chem. Phys. Lett.* **2**, 327 (1968)

46. P. Martin, J. Klein, R. Voltz, Autoionization as an Effective Decay Channel for Highly Excited States in Molecular Crystals. *Phys. Scr.* **35**, 575 (1987)

47. H. Rademaker, A. J. Hoff, R. V. Grondelle, L. N. M. Duysens, Carotenoid triplet yields in normal and deuterated Rhodospirillum rubrum. *Biochim. Biophys. Acta* **592**, 240 (1980)

48. N. V. Korovina, S. Das, Z. Nett, X. Feng, J. Joy, R. Haiges, A. I. Krylov, S. E. Bradforth, M. E. Thompson, Singlet fission in a covalently linked cofacial alkynyltetracene dimer. *J. Am. Chem. Soc.* **138**, 617 (2016)

49. S. Singh, W. J. Jones, W. Siebrand, B. P. Stoicheff, W. G. Schneider, Laser Generation of Excitons and Fluorescence in Anthracene Crystals. *J. Chem. Phys.* **42**, 330 (1965)

50. N. Geacintov, M. Pope, F. Vogel, Effect of Magnetic Field on the Fluorescence of Tetracene Crystals: Exciton Fission. *Phys. Rev. Lett.* **22**, 593 (1969)

51. R. E. Merrifield, P. Avakian, R. P. Groff, Fission of singlet excitons into pairs of triplet excitons in tetracence crystals. *Chem. Phys. Lett.* **3**, 386 (1969)

52. R. H. Austin, G. L. Baker, S. Etemad, R. Thompson, Magnetic field effects on triplet exciton fission and fusion in a polydiacetylene. *J. Chem. Phys.* **90**, 6642440 (1989)

53. M. C. Hanna, A. J. Nozik, Solar conversion efficiency of photovoltaic and photoelectrolysis cells with carrier multiplication absorbers. *J. Appl. Phys.* **100**, 074510 (2006)

54. W. Shockley, H. J. Queisser, Detailed Balance Limit of Efficiency of *p-n* Junction Solar Cells. *J. Appl. Phys.* **32**, 510 (1961)

55. D. N. Congreve, J. Lee, N. J. Thompson, E. Hontz, S. R. Yost, P. D. Reusswig, M. E. Bahlke, S. Reineke, T. V. Voorhis, M. A. Baldo, External Quantum Efficiency Above 100% in a Singlet-Exciton-Fission–Based Organic Photovoltaic Cell. *Science* **340**, 331 (2013)

56. M. Tabachnyk, B. Ehrler, S. Gélinas, M. L. Böhm, B. J. Walker, K. P. Musselman, N. C. Greenham, R. H. Friend, A. Rao, Resonant energy transfer of triplet excitons from pentacene to PbSe nanocrystals. *Nat. Mater.* **13**, 1033 (2014)

57. N. J. Thompson, M. W. B. Wilson, D. N. Congreve, P. R. Brown, J. M. Scherer, T. S. Bischof, M. Wu, N. Geva, M. Welborn, T. V. Voorhis, V. Bulovic, M. G. Bawendi, M. A. Baldo, Energy harvesting of non-emissive triplet excitons in tetracene by emissive PbS nanocrystals. *Nat. Mater.* **13**, 1039 (2014)

58. M. Inoue, T. Matsushima, C. Adachi, Low amplified spontaneous emission threshold and suppression of electroluminescence efficiency roll-off in layers doped with ter(9,9′-spirobifluorene). *Appl. Phys. Lett.* **108**, 133302 (2016)

59. W. Siebrand, Radiationless Transitions in Polyatomic Molecules. I. Calculation of Franck—Condon Factors. *J. Chem. Phys.* **46**, 440 (1967)

60. W. Siebrand, Radiationless Transitions in Polyatomic Molecules. II. Triplet-Ground-State Transitions in Aromatic Hydrocarbons. *J. Chem. Phys.* **47**, 2411 (1967)

61. W. Siebrand, D. F. Williams, Radiationless Transitions in Polyatomic Molecules. III. Anharmonicity, Isotope Effects, and Singlet-to-Ground-State Transitions in Aromatic Hydrocarbons. *J. Chem. Phys.* **49**, 1860 (1968)

62. R. Englman, J. Jortner, The energy gap law for radiationless transition in large molecules. *Mol. Phys.* **18**, 145 (1970)

63. W. C. Chen, P. T. Chou, Y. C. Cheng, Low Internal Reorganization Energy of the Metal-Metal-to-Ligand Charge Transfer Emission in Dimeric Pt(II) Complexes. *J. Phys. Chem. C* **123**, 10225 (2019)

64. Y. Hasegawa, K. Murakoshi, Y. Wada, S. Yanagida, J. H. kim, N. Nakashima, T. Yamanaka, Enhancement of luminescence of Nd^{3+} complexes with deuterated hexafluoroacetylacetonato ligands in organic solvent. *Chem. Phys. Lett.* **248**, 8 (1996)

Chapter 2

Harvesting of triplet exciton using bipolar TADF host matrix

R. Nagata, H. Nakanotani, C. Adachi, *Adv. Mater.* **29**, 1604265 (2017)

Abstract

A sixfold improvement in the η_{EQE} of NIR electrophosphorescence is demonstrated compared to devices with conventional fluorescent materials as host, by applying the concept of TADF host matrix to achieve an emitter layer capable of efficient spin conversion and simultaneous bipolar charge-transporting. This device architecture can maximize the performance of an organic-semiconductor-based NIR light source.

2.1 Introduction

Achieving an ideal η_γ of unity in an OLED requires the efficient harvesting of electrically generated exciton formed in triplet states, and this can be achieved through RISC of triplet states to singlet states in materials with a very small ΔE_{ST}, *i.e.*, TADF materials [1–4]. In fact, internal quantum efficiency (η_{int}) of nearly 100% in visible OLEDs utilizing such molecules as emissive centers have been already demonstrated [1,5]. Furthermore, the η_{int} for NIR-OLEDs is improving rapidly by the development of highly emissive NIR phosphors such as not only platinum-based phosphorescent emitters but also TADF emitters, resulting in the demonstration of η_{EQE} over 5% [6,7]. However, η_{EQE} is still low level for EL at wavelengths over 1 μm [8–11]. and the enhancement of η_{EQE} for emission over 1 μm is still a challenging research topic. The low efficiency for NIR emission arises from not only low values of φ_{PL} but also the narrow bandgaps of NIR phosphors. Since NIR phosphors usually act as strong carrier trapping sites in host–guest systems, which are required to suppress concentration quenching between neighboring phosphors, the carrier balance of holes and electrons inside the EML is also greatly disrupted. Therefore, the circumspect design of a host–guest system that suppresses direct carrier recombination on NIR phosphors and can transfer not only singlet but also triplet energy generated through charge carrier recombination on recombination centers, *i.e.*, host molecules, to NIR phosphors is important to realize highly efficient NIR-OLEDs. Recently, our and other groups proposed a triplet-harvesting pathway for realizing high-performance fluorescence OLEDs by using a TADF system as an energy source for conventional fluorescent emitters [12–14]. In this process, triplet excitons created on TADF molecules under electrical excitation are upconverted from the T_1 to the S_1 through RISC, and the singlet excitons on the TADF molecules are then transferred via a Förster process to fluorescent emitters, leading to efficient radiative decay from S_1 of the fluorescent emitters. Thus, TADF-based upconversion systems is a promising architecture to develop high performance fluorescent OLEDs with high η_{EQE}. However, no studies have been reported about the utilization of these systems for the development of highly efficient NIR-OLEDs emitting at over 1 μm.

In this work, I demonstrate the efficient harvesting of triplet energy by NIR phosphors via RISC in a TADF host layer also functioning as carrier recombination center, resulting in the nearly complete utilization of electrically generated exciton energy for NIR-EL. Here, I used 2-phenoxazine-4,6-diphenyl-1,3,5-triazine (PXZ-TRZ) as a host matrix capable of efficient RISC [15] and copper phthalocyanine (CuPc) and platinum phthalocyanine (PtPc) as NIR phosphors (**Figure 2-1a**) [16]. Since the energy level differences between HOMO and LUMO of PXZ-TRZ and those of the Pc derivatives are rather small compared to those for the Pc derivatives and other green TADF emitters (*e.g.*, (4s,6s)-2,4,5,6-tetra(9H-carbazol-9-yl)isophthalonitrile (4CzIPN), HOMO = −5.8 eV, LUMO = −3.4 eV) [1], I chose PXZ-TRZ as the host matrix in this study to avoid the effect of direct carrier trap on the Pc derivatives. The conventional fluorescent material tris(8-hydroxyquinolinato)aluminum (Alq_3) and 5,6,11,12-tetraphenylnaphthacene (Rubrene) were also used as reference hosts to confirm the effects of RISC on the device performance.

2.2 Results and discussion

2.2.1 Fundamental photophysical properties

The ground-state absorption spectra of the Pc derivatives and the PL spectra of the host molecules are shown in **Figure 2-1b**. Because of the large overlap between the host emission spectra and the Pc absorption spectra, the emission intensity from host molecules in solid films was dramatically reduced when doped with 1mol%-CuPc or PtPc, resulting in a φ_{PL} in the visible region ($\varphi_{PL\ (vis)}$) of below 2% for co-deposited PXZ-TRZ film compared to 49% for the neat film. The large decrease in PXZ-TRZ emission corresponds to energy transfer from S_1 of the donor (S_1_PXZ-TRZ) to S_1 of the acceptor

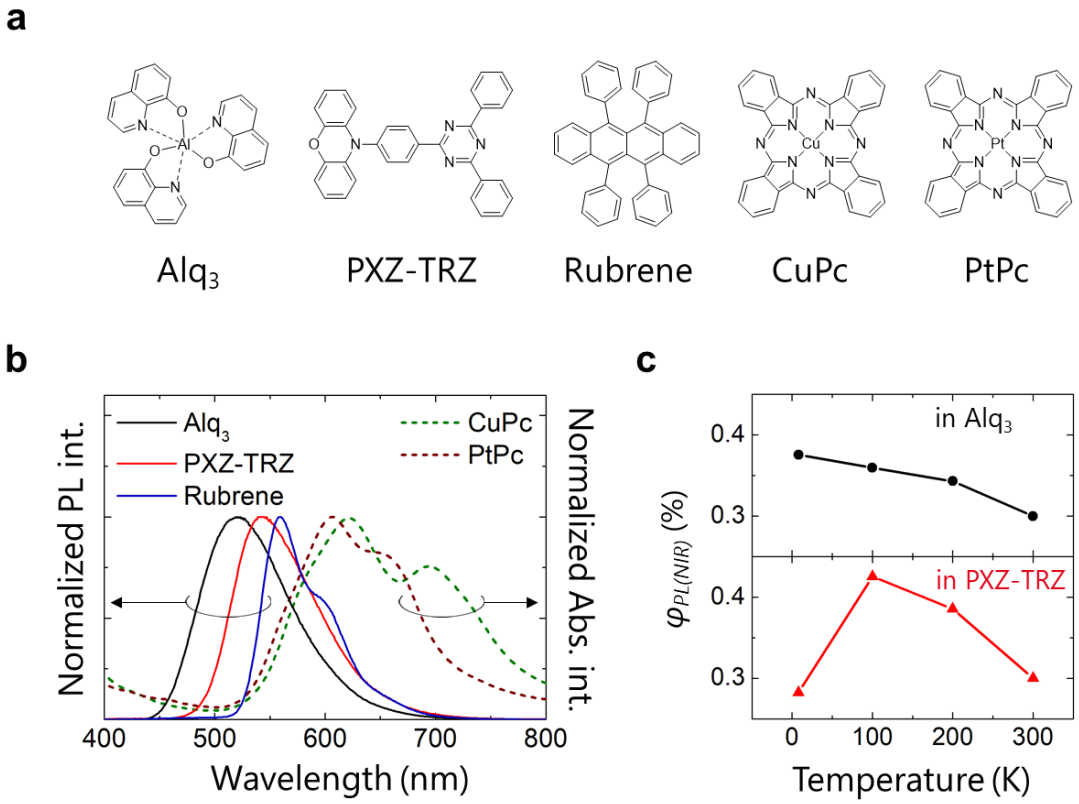

Fig. 2-1. a) Chemical structures of host and guest molecules. b) Absorption spectra of Pc derivatives and PL spectra of host molecules. c) The temperature dependence of the PL quantum yield of NIR emission for a 1mol%-PtPc-Alq_3 (top) and a 1mol%-PtPc-PXZ-TRZ (bottom) co-deposited film.

(S_1_Pc) with an efficiency of over 95%, and similar PL quenching of host emission was observed with Alq_3 or Rubrene as host with an energy transfer efficiency of nearly 90%. Therefore, I confirmed that the energy transfer efficiency is nearly the same in these co-deposited films.

Although the φ_{PL} of NIR emission ($\varphi_{PL\ (NIR)}$) in 1mol%-PtPc doped matrix was comparable for both hosts (0.3 ± 0.05%), the temperature dependences of $\varphi_{PL\ (NIR)}$ were pronouncedly different as shown in **Figure 2-1c** for 1mol%-PtPc-Alq_3 and 1mol%- PtPc-PXZ-TRZ co-deposited films. In the 1mol%-PtPc-Alq_3 film, $\varphi_{PL\ (NIR)}$ gradually increases with decreasing temperature and reaches 0.38% at 8 K, indicating the suppression of non-radiative decay from the lowest triplet state (T_1_PtPc) to the ground state in PtPc molecules. On the other hand, $\varphi_{PL\ (NIR)}$ for the matrix with PXZ-TRZ as host gradually increased with decreasing temperature before suddenly decreasing for temperatures below 100 K. Since the emission from PXZ-TRZ includes a delayed component originating from thermal

activated RISC that also contributes to $\varphi_{PL\ (NIR)}$ [15], the observed temperature dependence of $\varphi_{PL\ (NIR)}$ in the 1mol%-PtPc-PXZ-TRZ co-deposited film clearly indicates that triplet excitons from PXZ-TRZ molecules play a crucial role in NIR emission. This occurs because PXZ-TRZ triplets can upconvert to S_1_PXZ-TRZ by RISC and then resonantly transfer to an S_1_PtPc state, which undergoes ISC to T_1_PtPc before decaying radiatively. Namely, the increase of $\varphi_{PL\ (NIR)}$ from 5 to 100 K and the decrease from 100 to 300 K can be ascribed to the activation of the TADF and the increase of internal deactivation of PtPc, respectively. Since spin statics dictates that the number of triplet excitons generated upon recombination of holes and electrons in organic semiconductors is three times that of singlet excitons [17], the contribution of host triplet excitons to radiative decay from T_1_PtPc through RISC and energy transfer will be larger during electrical excitation.

2.2.2 OLED properties

To demonstrate the triplet harvesting ability in electrical excitation, I fabricated NIR-OLEDs described by the corresponding energy level diagram in **Figure 2-2a**. In the OLEDs with PXZ-TRZ as host, intense NIR electrophosphorescence with emission peaks at 970 nm for PtPc and 1.1 μm for CuPc as an emitter was observed as shown in **Figure 2-2b**. Although the η_{EQE} in the CuPc-OLED with Alq_3 or Rubrene as host was quite low ($< 5 \times 10^{-3}$%), changing the host to PXZ-TRZ increased η_{EQE} nearly six times to 0.03% (**Figure 2-2c**). This η_{EQE} (0.03%) is also about five times that of a previously reported CuPc-based OLED utilizing a fluorescent molecule as host matrix [8]. The PtPc-OLEDs exhibited an even more intense NIR emission and a similar host dependence, with an η_{EQE} for PXZ-TRZ as host (0.1%) that is three times that with Alq_3 as host (0.03%). Here I note the effect of doping concentration of Pc derivatives on the device performance. In the OLEDs with an EML consisting of 0.5, 1.0, 2.0 mol%-CuPc-PXZ-TRZ, although the η_{EQE} increases with CuPc concentration for low concentrations (0.5 to 1.0 mol%), a reduction of η_{EQE} was observed with further increase of the CuPc concentration, as shown in **Figure 2-3**. A similar dependence of doping

concentration on device performances was observed in the PtPc-based OLEDs. Thus, I set the doping concentration of the Pc derivatives to 1.0 mol%.

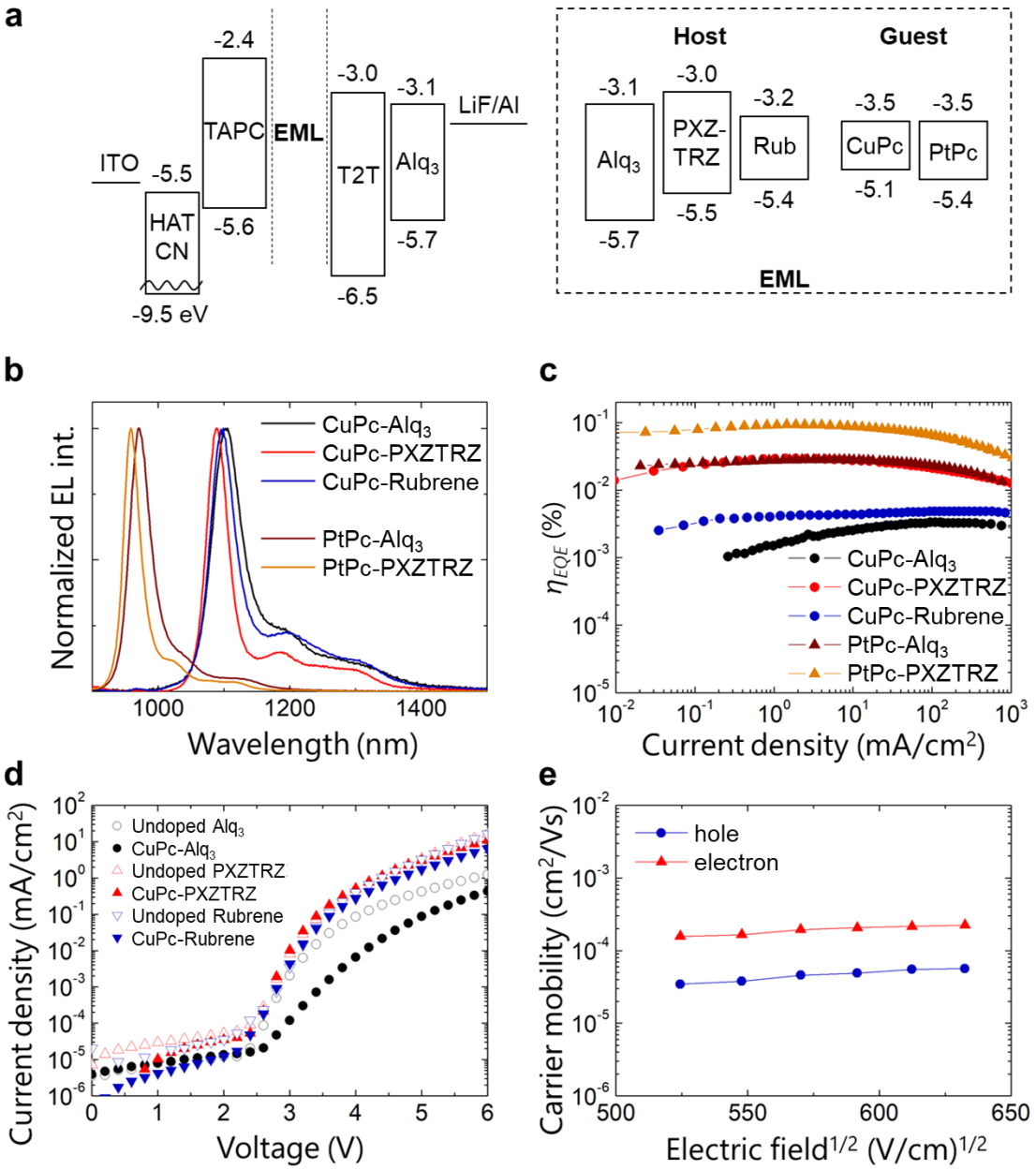

Fig. 2-2. a) Energy-level diagrams of the device structure used for the tested OLEDs. b) NIR-EL spectra of the OLEDs at a current density of 10 mA cm^{-2}. c) External EL quantum efficiency–current density characteristics for the NIR of the OLEDs. d) Current density–voltage characteristics of the OLEDs. The filled and open symbols indicate the characteristics of doped and undoped devices. e) The electrical field dependence of the hole (circles) and electron (triangles) mobilities of the PXZ-TRZ neat film.

The current density (J)–voltage (V) characteristics of the tested OLEDs are shown in **Figure 2-2d**. Doping CuPc into the OLED with an Alq_3 host matrix caused a significant increase of driving voltage compared to that of the corresponding undoped OLED, indicating that CuPc molecules in the Alq_3 matrix act as strong hole trapping sites that lead to an imbalance of charge recombination due to the deeper HOMO level for CuPc (−5.1 eV) than for Alq_3 (−5.7 eV). On the other hand, the driving voltages of the OLEDs with PXZ-TRZ or Rubrene as host are nearly the same regardless of whether CuPc guest molecules are doped in the EML, indicating an absence of carrier trapping sites in the EML and the direct creation of singlet and triplet excitons on the PXZ-TRZ or Rubrene molecules.

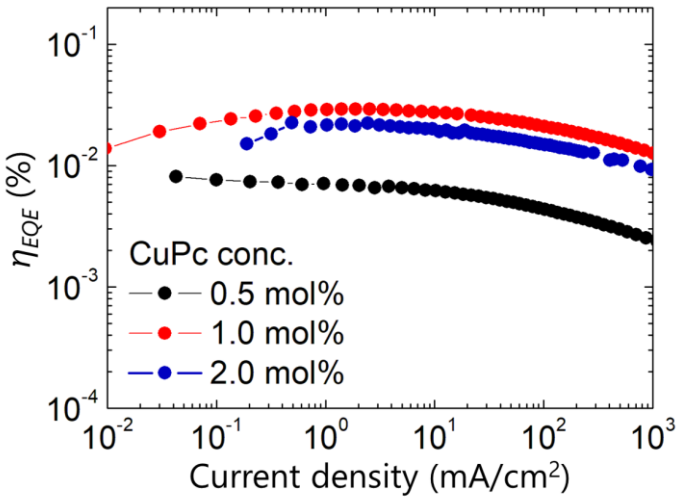

Fig. 2-3. External EL quantum efficiency–current density characteristics of the OLEDs with different doping concentration of CuPc.

Time-of-flight (TOF) measurements were performed to investigate the charge-carrier-transport properties of the PXZ-TRZ matrix and revealed that the PXZ-TRZ molecules have a bipolar charge transport ability with carrier mobilities on the order of $\mu_h \approx 10^{-5}$ cm^2 V^{-1} s^{-1} for holes and $\mu_e \approx 10^{-4}$ cm^2 V^{-1} s^{-1} for electrons. This hole mobility is slightly higher than the field-effect hole mobility reported for a phenoxazine-based polymer ($\mu_h = 10^{-6}$–10^{-5} cm^2 V^{-1} s^{-1}) [18], while the electron mobility is comparable to those of common electron-transport materials (ETMs) such as 1,3,5-triazine derivatives [19] and about 100 times higher than that of the conventional ETM of Alq_3 [20]. Interestingly, the introduction of the phenoxazine unit does not appear to significantly hinder the electron-transport ability of the 1,3,5-triazine unit. Since the large dihedral angle (74.9°) between the phenoxazine unit and the phenyl ring connecting to the triazine unit breaks the conjugation between the electron-donating and electron-accepting units, the HOMO and the LUMO are localized on the phenoxazine and the triazine moieties, respectively. This separation facilitates spatially separated

carrier-transport channels on the PXZ-TRZ molecules, so 1,3,5-triazine is likely to play a principle role in electron transport in the TADF host. Because of the separated channels for hole and electron transport, the PXZ-TRZ matrix can act as a well-balanced bipolar carrier-transport host, making it useful in OLEDs as a bipolar host matrix with triplet harvesting ability. Since weak electric field dependences with similar slopes for electron and hole mobilities were observed (**Figure 2-2e**), well-balanced carrier-transport is expected over the applied range of electrical fields. On the other hand, since Alq_3 provides only electron transport with $\mu_e \approx 10^{-5}$ cm^2 V^{-1} s^{-1} and no μ_h, holes are easily trapped by dopants, leading to the direct formation of excitons on them. Although Alq_3-host-based OLEDs show unipolar charge transport properties, Rubrene molecules intrinsically possess bipolar charge transport ability even in thin films [21,22], suggesting a well-balanced carrier-transport during device operation. However, despite the J–V characteristics indicating that carrier recombination occurs on the Rubrene host, the OLED with Rubrene as host shows a much lower η_{EQE} (5×10^{-3}%) compared with that of the OLED with PXZ-TRZ as host. These results indicate that the harvesting of electrically generated triplet excitons by the TADF host through RISC, *i.e.*, TADF-sensitized phosphorescence, is the key to the large improvement of efficiency in the NIR-phosphorescent OLEDs.

Finally, I discuss the energy transfer mechanism of the TADF sensitized electrophosphorescence. Two possible routes for the transfer of triplet energy from S_1 (or T_1) of PXZ-TRZ molecules to S_1 (or T_1) of Pc molecules exist: Förster resonance energy transfer (S_1_PXZTRZ → S_1_CuPc) and Dexter energy transfer (T_1_PXZTRZ → T_1_CuPc). Although the Förster mechanism is well known as a long-

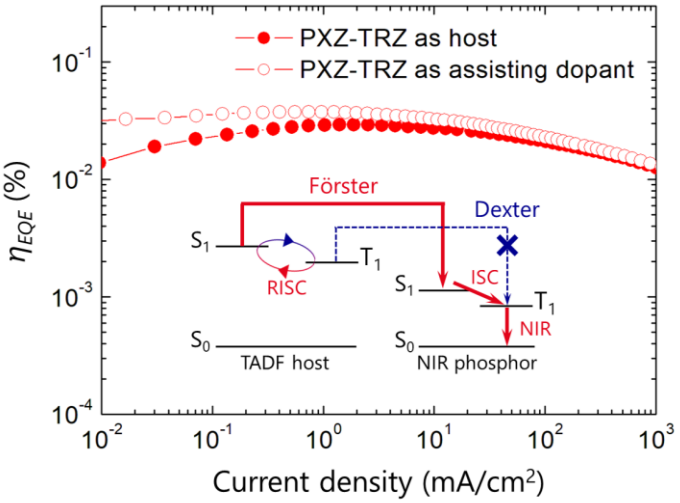

Fig. 2-4. External EL quantum efficiency–current density characteristics of the OLEDs. Inset shows a schematic illustration of EL process.

range interaction process, *i.e.*, a critical distance for energy transfer of ≈ 10 nm, Dexter-type energy transfer is a short-range interaction process because it requires electron exchange between the energy donor (D) and acceptor (A) molecules. Therefore, the average distance between D and A molecules significantly affects the energy transfer efficiency of the Dexter mechanism. To investigate the energy transfer process from TADF molecules to Pc molecules, I examined a TADF assisted fluorescence (TAF)-OLED using PXZ-TRZ as an assistant dopant [12]. **Figure 2-4** shows the η_{EQE}–J characteristics of an OLED with 3,3-di(9H-carbazol-9-yl)biphenyl (mCBP) as host doped with 1mol%-CuPc and 45mol%-PXZ-TRZ as emitter and assistant dopant, respectively, along with the characteristics of the OLED with PXZ-TRZ as a host doped with CuPc as emitter. In the EML with PXZ-TRZ as assistant dopant, the average distance between PXZ-TRZ and Pc is well separated compared to that of the host–guest system, suggesting the suppression of the Dexter channel. The OLED with PXZ-TRZ as assistant dopant exhibited an η_{EQE} (0.037%) that is almost the same as that of the OLED with PXZ-TRZ as host, suggesting that the contribution of direct energy transfer from T_1_PXZTRZ to T_1_CuPc to the total EL intensity would be small even in the OLED with PXZ-TRZ as a host. This would be due to not only the large separation between the triplet energy levels, *i.e.*, T_1_PXZTRZ − T_1_CuPc ≈ 1.10 eV but also the rather short triplet exciton diffusion length of TADF molecules [23]. Thus, I suppose that the main triplet energy transfer route from PXZ-TRZ to Pc derivatives is Förster resonance energy transfer after RISC, *i.e.*, T_1_PXZTRZ → S_1_PXZTRZ → S_1_CuPc. In summary, I revealed that the utilization of the TADF molecule PXZ-TRZ as not only host matrix but also triplet sensitizer provides us an ideal η_γ in NIR-TADF-OLEDs according to the balanced bipolar carrier-transport properties of PXZ-TRZ molecules with hole and electron mobilities on the order of 10^{-5} and 10^{-4} cm^2 V^{-1} s^{-1}. These results indicate that a TADF-based host matrix can provide not only triplet harvesting ability but also balanced carrier-transport properties according to the spatially separated HOMO and LUMO distributions. Although the relatively low phosphorescence yield of the Pc derivatives (< 1%) [16] is still a barrier to further boosting the η_{EQE} of NIR-OLEDs with Pc derivatives as NIR phosphors, this can be overcome by the introduction of the heavy metal effect in a TADF-sensitized electrophosphorescence system or the utilization of

highly emissive NIR-phosphors. Therefore, I believe our proposed TADF-sensitized electrophosphorescence system is the most promising way to maximize the performance of NIR emitters and realize highly efficient NIR-OLEDs emitting at over 1 μm.

2.3 Materials and Methods

Materials

The materials Rubrene, CuPc, PtPc, and TAPC were purchased from Luminescence Technology Corp. The host Alq_3 was used as received from Nippon Steel Chemical Co., Ltd. The OLED materials PXZ-TRZ and T2T were synthesized in house. Before fabrication of samples, the crude powder of Rubrene was purified by train sublimation with a thermal gradient under a base pressure of less than 5×10^{-3} Pa; this procedure was repeated three times to obtain highly pure compounds.

Sample preparation and characterization of PL characteristics

For each optical measurement, samples with thicknesses of 100 nm were deposited onto clean quartz substrates under high vacuum condition of $< 10^{-4}$ Pa. PL quantum yields were measured with separate absolute PL quantum yield measurement systems for the visible region (C11347-01, Hamamatsu Photonics) and NIR region (C13534-21, Hamamatsu Photonics) under the flow of Ar gas with an excitation wavelength of 340 nm for Alq_3 and 400 nm for PXZ-TRZ. The UV/VIS absorption spectra of the films were taken using a spectrophotometer (LAMBDA 950-PKA, PerkinElmer). The emission spectra in the visible region were measured using a spectrofluorometer (FluoroMax-4, Horiba Jobin–Yvon) with an excitation wavelength of 337 nm. The emission spectra and the temperature dependences of NIR emission were obtained under vacuum conditions using a spectrometer (C9913GC, Hamamatsu Photonics), a He–Cd laser (Kimmon Koha) as an excitation source with an excitation wavelength of 325 nm, and a cryostat (CNA-11, Sumitomo Heavy Industries).

OLED fabrication and performance characterization

OLEDs with active areas of 1 mm^2 were fabricated by thermal deposition onto clean indium-tin-oxide (ITO)-coated glass substrates under high vacuum conditions of $< 10^{-4}$ Pa. After fabrication, the OLEDs were immediately encapsulated with a glass lid using epoxy glue in a N_2-filled glove box. The current–density–voltage (J–V) characteristics and external-quantum-efficiency–current density (η_{EQE}–J) characteristics were measured using a semiconductor parameter analyzer (E5273A, Agilent Technologies) and a calibrated InGaAs photodetector (818-IG-L, Newport) connected to an optical power meter (Newport). EL spectra of the OLEDs were also measured using a spectrometer (C9913GC, Hamamatsu Photonics).

TOF measurements

TOF measurements were performed to evaluate the hole and electron mobilities of PXZ-TRZ films at room temperature. The device structure of ITO (110 nm)/Al (5 nm)/PXZ-TRZ (10 μm)/Al (200 nm) with an active area of 2 mm × 2 mm was used. The absorption coefficient of PXZ-TRZ at a wavelength of 337 nm is 6.23×10^4 cm^{-1}, indicating that the incident light is completely absorbed by the organic layer within 1 μm thick from the surface. A N_2 gas laser with a pulse width of 4 ns at a wavelength of 337 nm was used for carrier generation, and terminal resistors between 1 and 10 kΩ were connected in series to the samples. From the transit times, τ_T, determined from the intersection between the two slopes in the photocurrent profile, carrier mobilities were determined using $\mu = d/\tau_T E$.

References

1. H. Uoyama, K. Goushi, K. Shizu, H. Nomura, C. Adachi, Highly efficient organic light-emitting diodes from delayed fluorescence. *Nature* **492**, 234 (2012)

2. Q. Zhang, B. Li, S. Huang, H. Nomura, H. Tanaka, C. Adachi, Efficient blue organic light-emitting diodes employing thermally activated delayed fluorescence. *Nat. Photon.* **8**, 326 (2014)

3. H. Wang, L. Xie, Q. Peng, L. Meng, Y. Wang, Y. Yi, P. Wang, Novel Thermally Activated Delayed Fluorescence Materials–Thioxanthone Derivatives and Their Applications for Highly Efficient OLEDs. *Adv. Mater.* **26**, 5198 (2014)

4. S. Hirata, Y. Sakai, K. Masui, H. Tanaka, S. Y. Lee, H. Nomura, N. Nakamura, M. Yasumatsu, H. Nakanotani, Q. Zhang, K. Shizu, H. Miyazaki, C. Adachi, Highly efficient blue electroluminescence based on thermally activated delayed fluorescence. *Nat. Mater.* **14**, 330 (2015)

5. C. Adachi, M. A. Baldo, M. E. Thompson, S. R. Forrest, Nearly 100% internal phosphorescence efficiency in an organic light-emitting device. *J. Appl. Phys.* **90**, 5048 (2001)

6. C. Borek, K. Hanson, P. I. Djurovich, M. E. Thompson, K. Aznavour, R. Bau, Y. Sun, S. R. Forrest, J. Brooks, L. Michalski, J. Brown, Highly Efficient, Near-Infrared Electrophosphorescence from a Pt–Metalloporphyrin Complex. *Angew. Chem. Int. Ed.* **46**, 1109 (2007)

7. S. Wang, X. Yan, Z. Cheng, H. Zhang, Y. Liu, Y. Wang, Highly Efficient Near-Infrared Delayed Fluorescence Organic Light Emitting Diodes Using a Phenanthrene-Based Charge-Transfer Compound. *Angew. Chem. Int. Ed.* **54**, 13068 (2015)

8. C. H. Cheng, Z. Q. Fan, S. K. Yu, W. H. Jiang, X. Wang, 1.1 μm near-infrared electrophosphorescence from organic light-emitting diodes based on copper phthalocyanine. *Appl. Phys. Lett.* **88**, 213505 (2006)

9. F. Yan, W. L. Li, B. Chu, T. L. Li, W. M. Su, Z. S. Su, J. Z. Zhu, D. F. Yang, G. Zhang, D. F. Bi, L. L. Han, Sensitized electrophosphorescence of infrared emission diode based on copper phthalocyanine by an ytterbium complex. *Appl. Phys. Lett.* **91**, 203512 (2007)

10. T. C. Rosenow, K. Walzer, K. Leo, Near-infrared organic light emitting diodes based on heavy metal phthalocyanines. *J. Appl. Phys.* **103**, 043105 (2008)

11. F. Yan, W. Li, B. Chu, H. Liu, G. Zhang, Z. Su, J. Zhu, L. Han, T. Li, Y. Chen, C. H. Cheng, Z. Q. Fan, G. T. Du, Sensitized infrared electrophosphorescence based on divalent copper complex by an iridium(III) complex. *Org. Electron.* **10**, 1408 (2009)

12. H. Nakanotani, T. Higuchi, T. Furukawa, K. Masui, K. Morimoto, M. Numata, H. Tanaka, Y. Sagara, T. Yasuda, C. Adachi, High-efficiency organic light-emitting diodes with fluorescent emitters. *Nat. Commun.* **5**, 4016 (2014)

13. D. Zhang, L. Duan, C. Li, Y. Li, H. Li, D. Zhang, Y. Qiu, High-Efficiency Fluorescent Organic Light-Emitting Devices Using Sensitizing Hosts with a Small Singlet–Triplet Exchange Energy. *Adv. Mater.* **26**, 5050 (2014)

14. X. K. Liu, Z. Chen, C. J. Zheng, M. Chen, W. Liu, X. H. Zhang, C. S. Lee, Nearly 100% Triplet Harvesting in Conventional Fluorescent Dopant-Based Organic Light-Emitting Devices Through Energy Transfer from Exciplex. *Adv. Mater.* **27**, 2025 (2015)

15. H. Tanaka, K. Shizu, H. Miyazaki, C. Adachi, Efficient green thermally activated delayed fluorescence (TADF) from a phenoxazine–triphenyltriazine (PXZ–TRZ) derivative. *Chem. Commun.* **48**, 11392 (2012)

16. P. S. Vincett, E. M. Voigt, K. E. Rieckhoff, Phosphorescence and Fluorescence of Phthalocyanines. *J. Chem. Phys.* **55**, 4131 (1971)

17. M. A. Baldo, D. F. O'Brien. M. E. Thompson, S. R. Forrest, Excitonic singlet-triplet ratio in a semiconducting organic thin film. *Phys. Rev. B* **60**, 14422 (1999)

18. Y. Zhu, A. Babel, S. A. Jenekhe, Phenoxazine-Based Conjugated Polymers: A New Class of Organic Semiconductors for Field-Effect Transistors. *Macromolecules* **38**, 7983 (2005)

19. H. F. Chen, S. J. Yang, Z. H. Tsai, W. Y. Hung, T. C. Wang, K. T. Wong, 1,3,5-Triazine derivatives as new electron transport–type host materials for highly efficient green phosphorescent OLEDs. *J. Mater. Chem.* **19**, 8112 (2009)

20. R. G. Kepler, P. M. Beeson, S. J. Jacobs, R. A. Anderson, M. B. Sinclair, V. S. Valencia, P. A. Cahill, Electron and hole mobility in *tris*(8-hydroxyquinolinolato-N1,O8) aluminum. *Appl. Phys. Lett.* **66**, 3618 (1995)

21. S. Seo, B. N. Park, P. G. Evans, Ambipolar rubrene thin film transistors. *Appl. Phys. Lett.* **88**, 232114 (2006)

22. B. Park, I. In, P. Gopalan, P. G. Evans, S. King, P. F. Lyman, Enhanced hole mobility in ambipolar rubrene thin film transistors on polystyrene. *Appl. Phys. Lett.* **92**, 133302 (2008)

23. S. M. Menke, R. J. Holmes, Exciton Transport in an Organic Semiconductor Exhibiting Thermally Activated Delayed Fluorescence. *J. Phys. Chem. C* **120**, 8502 (2016)

Chapter 3

Exploiting of singlet fission for exciton multiplication in OLEDs

R. Nagata, H. Nakanotani, W. J. Potscavage Jr., C. Adachi,

Adv. Mater. **30**, 1801484 (2018)

Abstract

The exciton generation efficiency, η_γ, in an OLED has been theoretically limited to 100% of the electron–hole pairs. Here, breaking of this limit by exploiting singlet fission in an OLED is reported. Based on the dependence of EL intensity on an applied magnetic field, it is confirmed that triplets produced by singlet fission in host matrix are emitted as intense NIR-EL from NIR phosphor. EL employing singlet fission provides a route toward developing high-intensity NIR light sources, which are of particular interest for sensing, optical communications, and medical applications.

3.1 Introduction

At present, OLEDs with η_γ of nearly 100% are some of the most promising for next-generation displays and lighting applications. According to the rules of spin statistics in organic semiconductors, the recombination of four holes and electrons will yield one singlet exciton and three triplet excitons [1]. Thus, the utilization of both singlet and triplet excitons is necessary to achieve η_γ approaching 100%, and this has been accomplished with phosphorescence [2,3] and TADF [4,5]. However, the realization of η_γ greater than the theoretical limit of 100% could lead to light sources with high intensities surpassing those of current cutting-edge OLEDs. One path to breaking the η_γ limit is singlet fission, in which two triplet excitons are created from one singlet exciton when the energetics of the organic semiconductor are favorable (E_{S1} (singlet energy) > 2 × E_{T1} (triplet energy)) [6]. While singlet-fission sensitizers—organic molecules that exhibit efficient singlet fission—have been used to overcome the Shockley–Queisser limit in single-junction photovoltaics [7] and achieve the excitonic energy transfer of "dark" triplet excitons from molecules to emissive inorganic nanocrystals [8,9], the exploitation of singlet fission for EL in OLEDs has not yet been realized. To harvest the triplet excitons created via singlet fission, energy-accepting molecules having a triplet energy level lower than that of the singlet-fission sensitizers are required. Since the triplet energies of well-known singlet-fission sensitizers such as tetracene, Rubrene, and pentacene lie close to the NIR-regime (< 1.5 eV) [6], NIR phosphors are suitable as energy acceptors. For example, inorganic nanocrystals such as lead selenide (PbSe) and lead sulfide (PbS) can receive triplet excitons from singlet-fission sensitizers because of their low energy bandgaps [8,9]. Alternatively, erbium-based complexes, which have been used in OLEDs exhibiting NIR emission originating from the intra-4f shell transition between the excited state ($^4I_{13/2}$) and the ground state ($^4I_{15/2}$) of the erbium(III) ion [10–13], also have the potential to receive triplet exciton energy from singlet-fission sensitizers. Here, I show that erbium(III) tris(8-hydroxyquinoline) (ErQ_3) can harvest triplet excitons that are produced when the singlet-fission sensitizer Rubrene is excited not only optically but also electrically, and I exploit this process in an OLED to surpass the classical limitation of η_γ for the first time. This work offers a path

toward the development of low-cost, flexible, and highly efficient OLEDs emitting in the NIR, which would open a range of new applications in sensors, optical communications, and medicine.

3.2 Results and discussion

3.2.1 Fundamental photophysical properties

Figure 3-1a shows the ground-state absorption spectrum of ErQ_3 dissolved in DMSO-d_6 along with the fluorescence spectrum of a neat film of Rubrene. The lack of clear spectral overlap between the absorption spectrum of the energy acceptor (ErQ_3) and the emission spectrum of the energy donor (Rubrene) indicates that dipole–dipole resonance energy transfer, *i.e.*, Förster-type energy transfer, from the singlet state of Rubrene to the singlet state of the ErQ_3 can be neglected. When Rubrene molecules are excited optically, singlet excitons are initially created, and the singlet excitons undergo singlet fission rather than ISC ($S_1 \rightarrow T_1$), leading to the generation of "dark" triplet excitons with high yields approaching over 180% even in amorphous Rubrene films at room temperature [14]. Since the singlet-fission process competes with bimolecular triplet fusion, *i.e.*, $T_1 + T_1 \rightarrow S_1 + S_0$, some triplet excitons can up-convert to "bright" singlet states, which can be observed as delayed fluorescence. In our Rubrene thin films, I confirmed φ_{PL} of 5%, indicating that over 90% of optically

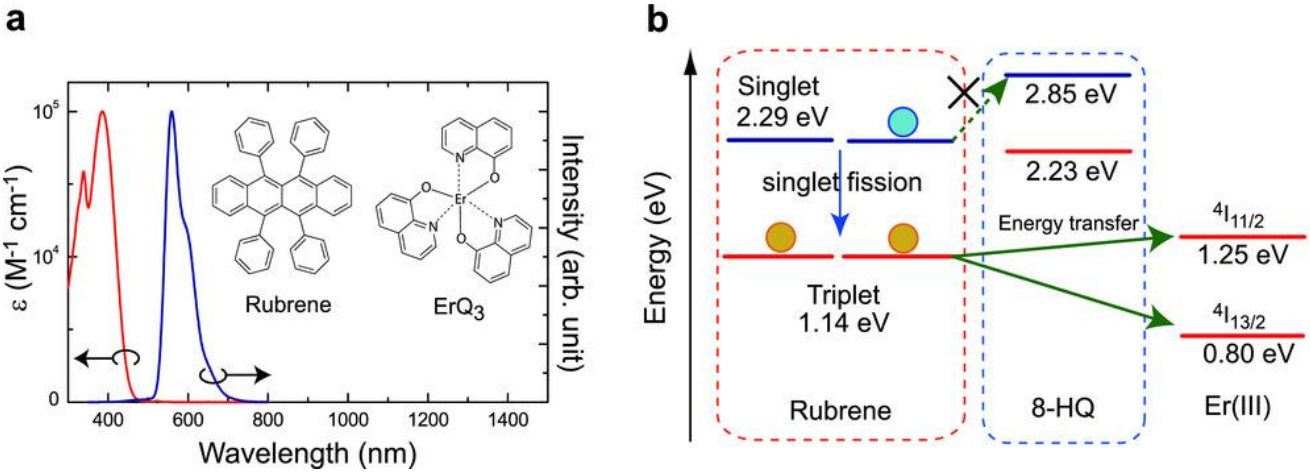

Fig. 3-1. a) The absorption spectrum of ErQ_3 in solution (red) and the PL spectrum of a Rubrene film (blue). b) Jablonski diagram for harvesting of triplets produced by singlet fission in Rubrene.

created singlet excitons underwent non-radiative decay processes such as singlet fission. The delayed component was observably decreased when 2mol%- ErQ_3 was doped into the Rubrene matrix (**Figure 3-2**), indicating the presence of additional decay pathways from the triplet level. The T_1 energy level of Rubrene (1.14 eV) is much lower than that of the 8-hydroxyquinoline (8-HQ: 2.23 eV) [15] but relatively close to the $^4I_{13/2}$ (0.80 eV) or $^4I_{11/2}$ (1.25 eV) levels of Er^{3+} ions, so the reduction of triplet fusion strongly suggests that triplet energy is directly transferred from the T_1 of Rubrene to the center Er^{3+} ion of ErQ_3 via Dexter-type energy transfer, as shown in **Figure 3-1b**.

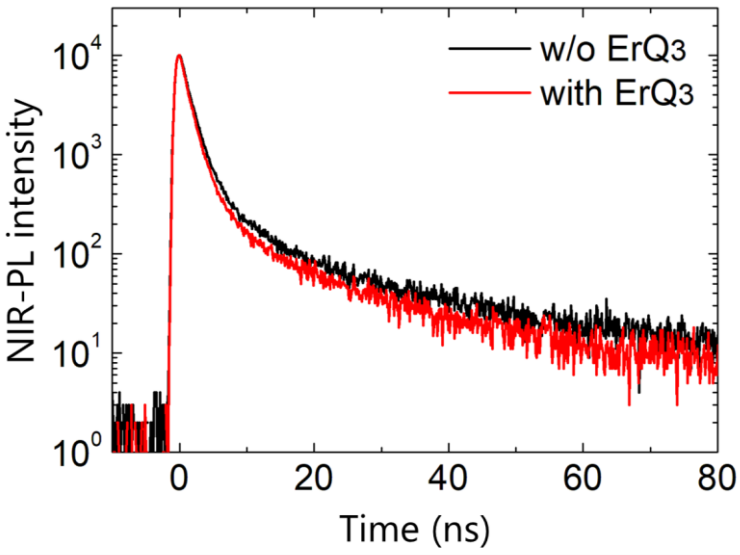

Fig. 3-2. Transient PL decay in Rubrene film with and without ErQ_3 dopant.

The 2mol%-ErQ_3-doped Rubrene films exhibited NIR emission with an emission peak wavelength of 1.53 μm (**Figure 3-3**), which corresponds to the transition from $^4I_{13/2}$ to $^4I_{15/2}$ for Er^{3+} ions, when excited at a wavelength of 515 nm. On the other hand, a 2mol%-ErQ_3-doped 4,4′-bis(N-carbazolyl)-1,1′-biphenyl (CBP) film did not exhibit any NIR emission when using the same pumping conditions. Because the CBP matrix does not have an absorption band at the pump wavelength, this indicates that Er^{3+} is not directly excited by the 515 nm excitation. In addition, the transient NIR emission decay profile of the 2mol%-ErQ_3-doped Rubrene film showed a biexponential curve with decay lifetimes of 2.1 and 22 μs (**Figure 3-4**). The observed transient

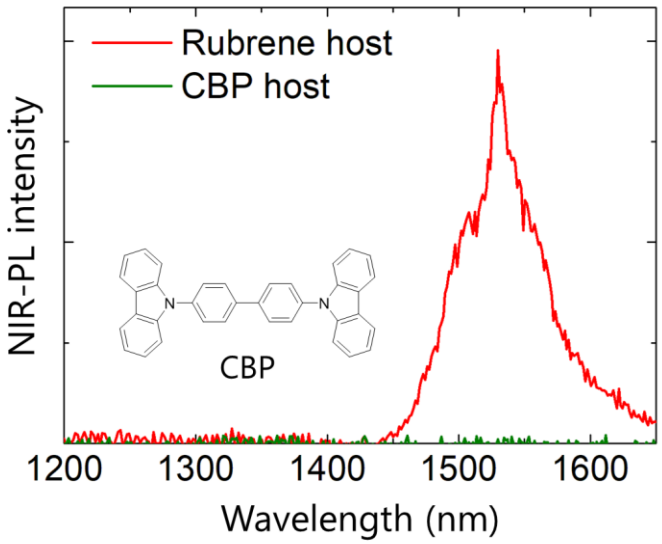

Fig. 3-3. NIR emission spectrum of ErQ_3 in a Rubrene (red line) or CBP host matrix (green line). Inset: chemical structure of CBP.

lifetimes are much longer than those of ErQ_3 in a polycarbonate blend film (0.21 and 0.75 μs) [16], indicating that the NIR emission reflects the long exciton lifetimes of triplets in Rubrene. Furthermore, extremely weak NIR emission was confirmed in a 2mol% ErQ_3-10mol%-Rubrene-CBP co-deposited film (**Figure 3-5**). Thus, I conclude that the NIR emission in the ErQ_3-Rubrene co-deposited films originates not from direct excitation of ErQ_3 but from triplet energy transfer from the energy donor Rubrene to the energy acceptor ErQ_3.

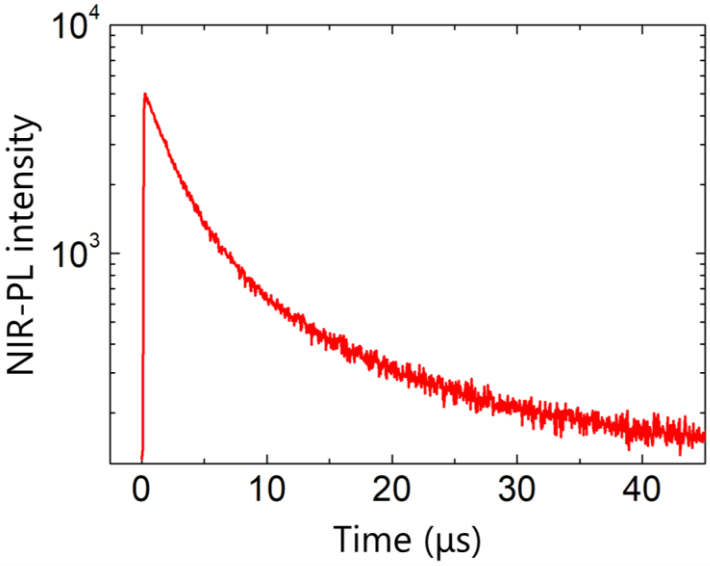

Fig. 3-4. Transient NIR-emission decay profile of 2mol%-ErQ_3-Rubrene film monitored at a wavelength of 1.53 μm with an excitation wavelength of 532 nm.

To further assess the effect of the singlet-fission-sensitizer host on the NIR emission efficiency of ErQ_3, I also characterized ErQ_3-doped films with a host matrix of 2,8-di-tert-butyl-5,11-bis(4-tert-butylphenyl)-6,12-diphenyltetracene (TBRb) [17]. I chose TBRb because even though its emission spectrum and absorption coefficients are similar to those of Rubrene (**Figure 3-6**), its four tertiary-butyl groups reduce intermolecular interactions between neighboring host molecules. Since the intermolecular electronic coupling between neighboring molecules is critical to a singlet fission process [18,19], the reduced intermolecular interactions for TBRb compared with Rubrene should decrease the singlet-fission efficiency. In 2mol%-ErQ_3-TBRb co-deposited films, NIR emission weaker than that from the

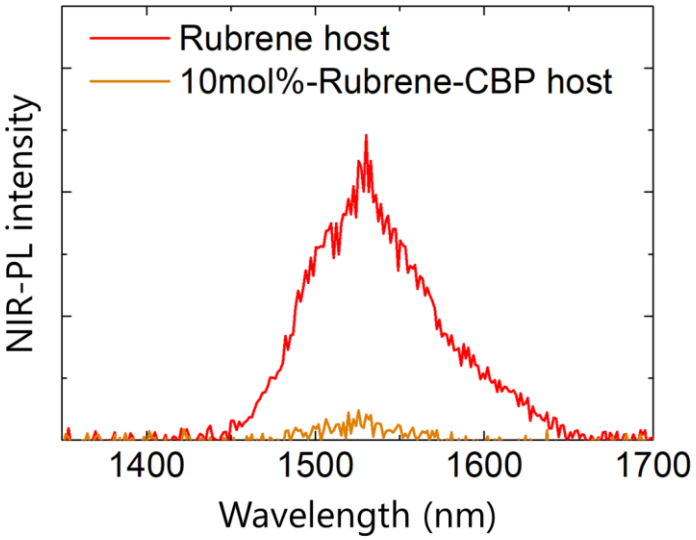

Fig. 3-5. NIR emission spectrum of ErQ_3 in a Rubrene (red line) or 10mol%-Rubrene-CBP host matrix (orange line).

Rubrene-based films was observed (**Figure 3-7a**). Although I cannot completely exclude the effect of vibrational deactivation of excited Er^{3+} ions by high-energy oscillations, such as of C-H bonds, in TBRb on NIR emission intensity, the triplet exciton density must be lower than that of the Rubrene matrix because of a lower singlet-fission efficiency. Therefore, the total number of generated triplets, which can contribute to NIR emission from ErQ_3, should be decreased compared with the Rubrene matrix, leading to a weaker NIR emission intensity. In addition, φ_{PL} in the NIR of the 2mol%-ErQ_3-Rubrene co-deposited films (0.007%) was about 1.75 times higher than that for the TBRb matrix, strongly indicating that triplets are more efficiently produced by singlet fission when Rubrene is used as the singlet-fission-sensitizer matrix.

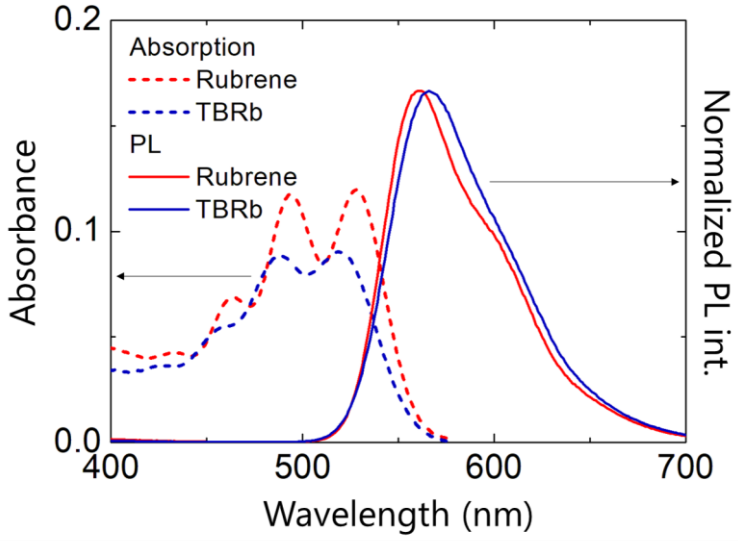

Fig. 3-6. Absorption and PL spectra of 100 nm-thick Rubrene (red) or TBRb (blue) neat films.

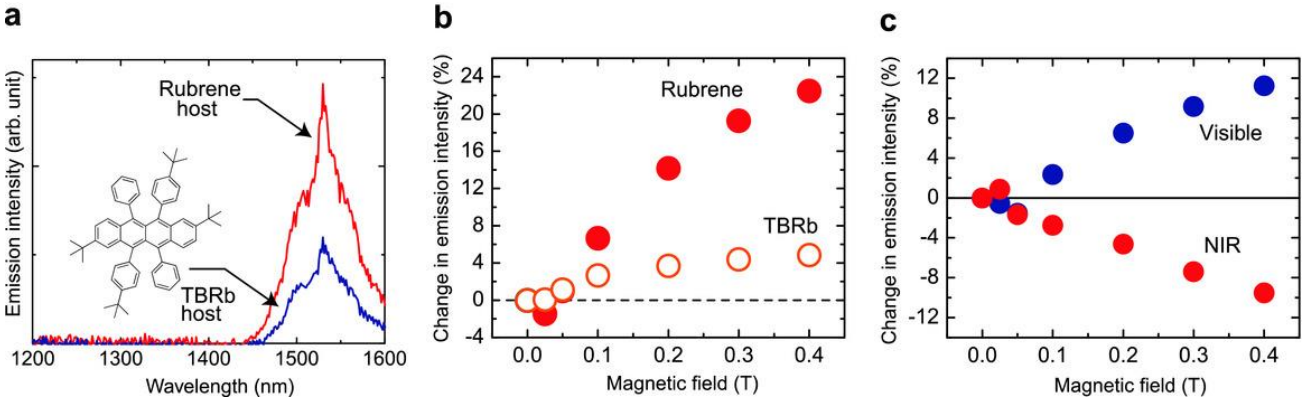

Fig. 3-7. a) The NIR emission spectra of ErQ_3 in Rubrene (red) and TBRb (blue) host matrices. b) The steady-state change in fluorescence intensity from a Rubrene neat film (red) and a TBRb neat film (orange) as a function of external magnetic field. c) The steady-state change in fluorescence intensity (blue) and NIR emission intensity (red) from a 2wt%-ErQ_3-Rubrene film as a function of external magnetic field.

I studied the steady-state magnetic field dependence of singlet fission to further investigate the emission mechanism. The steady-state change in fluorescence intensity (ΔI_{PL}) was calculated as ΔI_{PL}

= 100% × ($I_H - I_0$)/I_0, where I_H is the emission intensity with an applied magnetic field and I_0 is that without an applied magnetic field. In both Rubrene and TBRb neat films, a positive change in fluorescence intensity (**Figure 3-7b**) was observed in the high magnetic field regime above 0.05 T. This behavior is consistent with the presence of singlet fission, because the increasing magnetic field should decrease the number of correlated triplet-pair states with singlet character ^{1}(TT) [14]. which mediate the dissociation into two triplet excitons, *i.e.*, $^1(TT) \rightarrow T_1 + T_1$. Although ΔI_{PL} reaches +22.5% at 0.4 T in the Rubrene films, the ΔI_{PL} in the TBRb films is limited to only +4.8% at 0.4 T. The reduced singlet fission for TBRb compared with Rubrene is due to the reduction of intermolecular interaction by the bulky tertiary-butyl groups of TBRb [20] and is consistent with higher φ_{PL} in the TBRb neat film (46%) and weaker NIR emission intensity in ErQ_3-doped TBRb.

The steady-state intensity changes for visible ($\Delta I_{PL\text{-}vis}$) and NIR ($\Delta I_{PL\text{-}NIR}$) emission from a 2mol%-ErQ_3-Rubrene co-deposited film as a function of magnetic field (**Figure 3-7c**) exhibit complementary behavior ($\Delta I_{PL\text{-}vis}$ = +11.3% and $\Delta I_{PL\text{-}NIR}$ = −9.5% at 0.4 T). The negative sign of $\Delta I_{PL\text{-}NIR}$ indicates the reduction of emission intensity from triplet excitons according to the reduction of the probability of singlet fission in the Rubrene matrix [9]. Thus, this observation is conclusive evidence of triplets generated by singlet fission being transferred from optically excited Rubrene to ErQ_3. Since I simultaneously observed $\Delta I_{PL\text{-}vis}$ and $\Delta I_{PL\text{-}NIR}$, the triplet exciton production efficiency in the 2mol%-ErQ_3-Rubrene system under optical pumping can be obtained using **Eq. 3-1** (Derivation in **Section 3.3**).

$$\varphi_{PL-T} = 2\varphi_{SF} = \frac{2}{1-\left(\Delta I_{PL-NIR}/\Delta I_{PL-vis}\right)} \qquad \text{(Eq. 3-1)}$$

In this equation, $\varphi_{PL\text{-}T}$ is the triplet exciton production efficiency under photoluminescence (PL), *i.e.*, the number of excitons that ultimately end up in the triplet state represented as a percentage of the initially generated excitons, and φ_{SF} is the singlet-fission efficiency, *i.e.*, the fraction of singlets that undergo singlet fission. I also note that the efficiency of the energy transfer process has already been considered in the equation of $\Delta I_{PL\text{-}NIR}$. Thus, a $\varphi_{PL\text{-}T}$ of 108.6% is achieved in our system based on a calculated φ_{SF} of 54.3% for the intensity changes at 0.4 T. In this way, singlet fission can be evaluated

using simple measurement systems based on straightforward assumptions. The estimated φ_{SF} value is lower than that of a pure Rubrene film [14], suggesting that doping with ErQ_3 molecules, even at low concentrations, affects the singlet-fission efficiency.

When another erbium(III) complex, *i.e.*, 5,10,15,20-tetraphenylporphinato(2,2,6,6-tetramethyl-3,5-heptanedionato)erbium(III) (Er(TPP)TMHD), was used as NIR emitter, an Er(TPP)TMHD-Rubrene film also exhibited NIR emission corresponding to the transition from $^4I_{13/2}$ to $^4I_{15/2}$ for Er^{3+} ions (**Figure 3-8a**). In contrast to the ErQ_3-Rubrene film, however, the Er(TPP)TMHD-Rubrene film did not exhibit a magnetic field dependence in emission intensity (**Figure 3-8b**), indicating the absence of singlet fission. This result can be rationalized by the presence of a strong π-π^* absorption band in Er(TPP)TMHD that is in resonance with the emission band of Rubrene (**Figure 3-8c**), leading to efficient Förster resonance energy transfer (FRET) from S_1_Rubrene to S_1_Er(TPP)TMHD with a FRET radius of ≈ 5.5 nm. Moreover, the singlet fission process in Rubrene is a slightly endothermic process and is limited to a rate in the range of 10^9–10^{10} s^{-1} [21]. indicating that the FRET process is dominant in the Er(TPP)TMHD-Rubrene film. This claim is further supported by the reduction of the prompt PL component in transient PL measurements (**Figure 3-8d**).

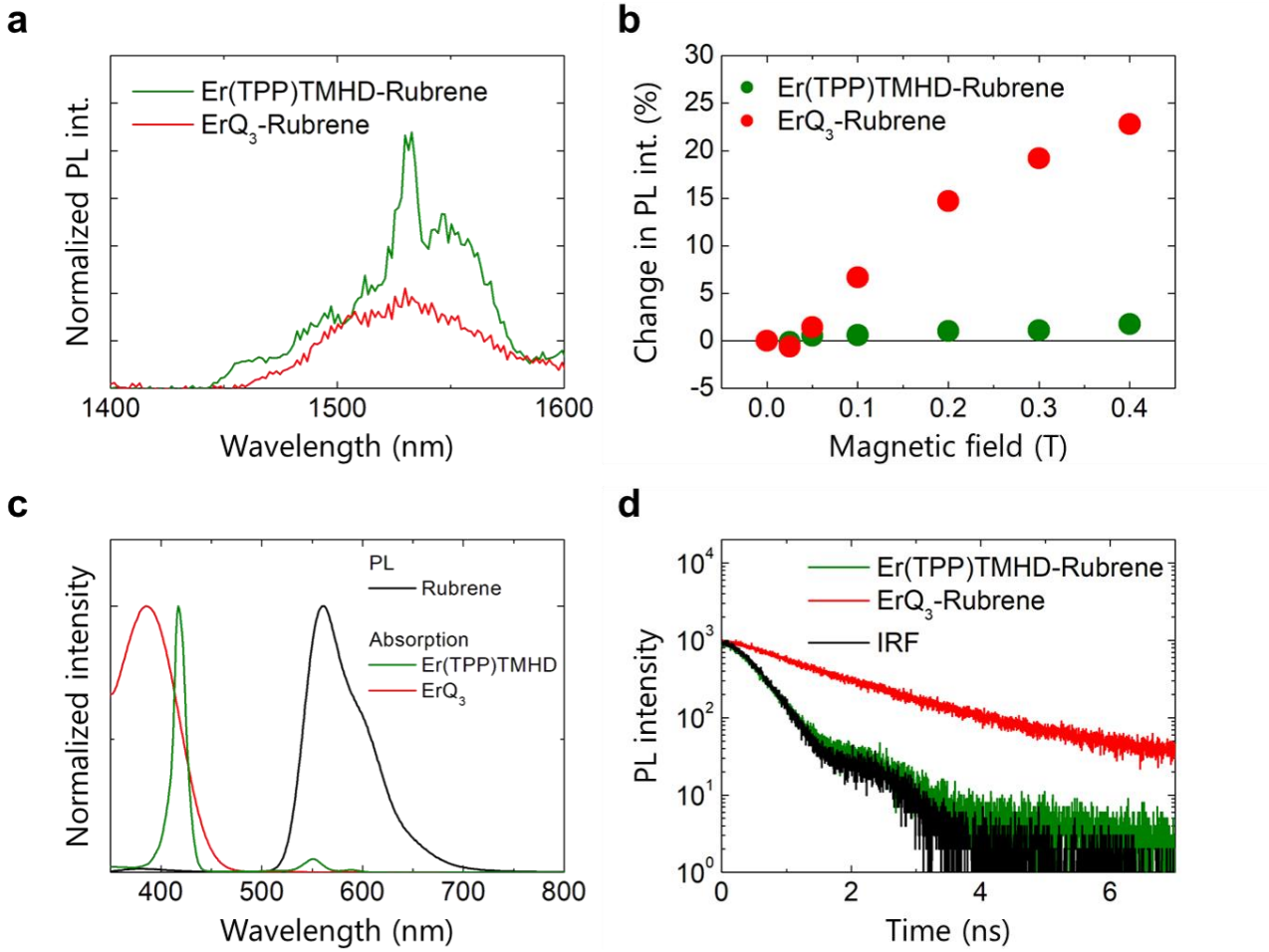

Fig. 3-8. a) The NIR emission spectra of Er(TPP)TMHD (green line) or ErQ_3 (red line) in a Rubrene host matrix. b) The steady-state change in fluorescence intensity from Er(TPP)TMHD (green filled circles) or ErQ_3 (red filled circles) in a Rubrene host matrix as a function of external magnetic field under optical excitation with an excitation wavelength of 515 nm. c) PL spectrum of Rubrene neat film (black line) and ground-state absorption spectrum of Er(TPP)TMHD (green line) or ErQ_3 (red line) in solution (10^{-5} M in DMSO-d_6) and. d) PL transient decay characteristics of Er(TPP)TMHD-Rubrene (green line) or ErQ_3-Rubrene (red line) co-deposited films.

3.2.2 OLED properties

As thermally evaporated co-deposited ErQ_3-Rubrene films are amorphous (**Figure 3-9**), they are expected to be electrically suitable as an EML. Thus, to harvest electrically generated singlets as EL via singlet fission, I designed an OLED (**Figure 3-10a**) with a 2mol%-ErQ_3-Rubrene film as the emitting layer (EML). Since the triplet energies of the 4,4′-cyclohexylidenebis[N,N-bis(4-methylphenyl)benzenamine] (TAPC: 2.87 eV) and 2,4,6-tris(biphenyl-3-yl)-1,3,5-triazine (T2T: 2.68

eV) [22] carrier blocking layers are dramatically higher than that of Rubrene (1.14 eV), the triplet excitons generated on Rubrene molecules should be effectively confined within the 30 nm-thick EML during electrical pumping.

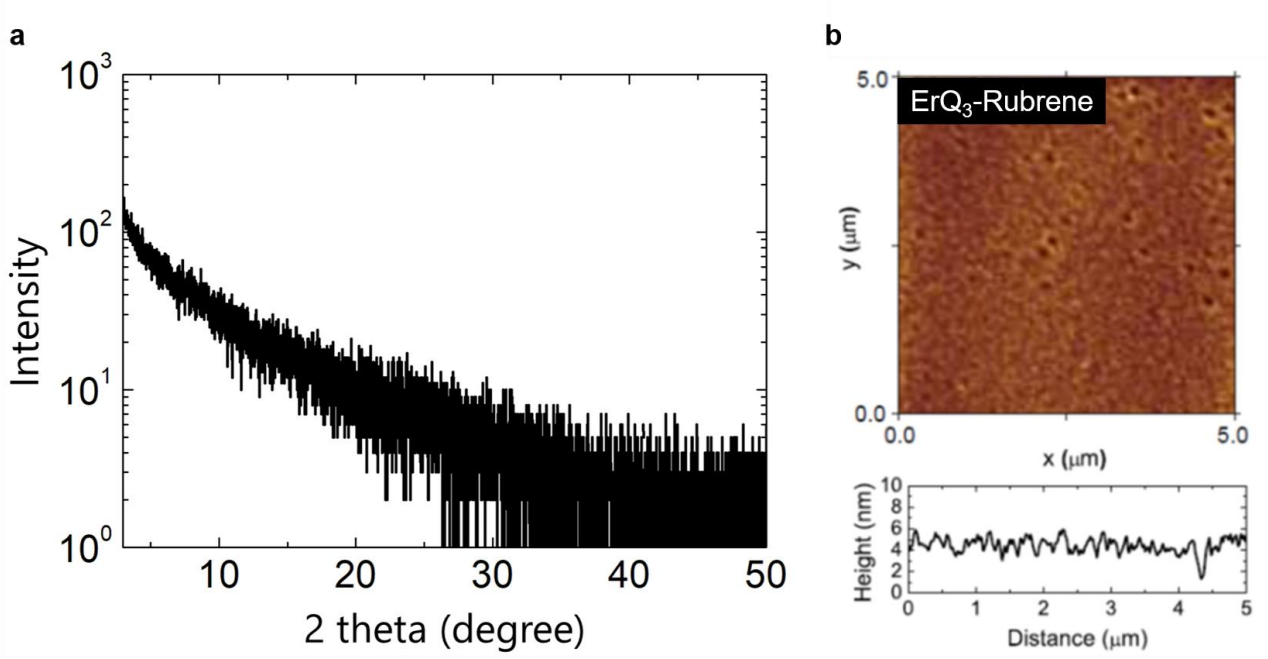

Fig. 3-9. Surface morphology of the thermally evaporated 2mol%-ErQ_3-Rubrene co-deposited film. a) X-ray diffraction profile. b) Atomic force microscope image. The root-mean-square roughness was calculated to be 0.58 nm.

Figure 3-10b shows the current density (J)–voltage (V) characteristics of the fabricated OLEDs. The driving voltage of the OLEDs is nearly the same regardless of whether ErQ_3 is doped in the Rubrene matrix. This indicates that ErQ_3 does not act as a strong carrier trapping site, which is likely due to the large energy bandgap of the 8-HQ ligands. Furthermore, this suggests that the creation of excitons through carrier recombination mainly occurs on the Rubrene molecules. After carrier recombination, the electrically generated singlet excitons undergo singlet fission or radiative decay as prompt electrofluorescence, and the created triplet excitons are harvested by ErQ_3 through Dexter energy transfer, leading to NIR-EL (**Figure 3-10c**). The singlet fission process is just like that occurring under optical excitation, as the NIR emission spectrum is very similar for both optical and electrical pumping. The integrated intensity of NIR-EL in the OLED with Rubrene as host was about

1.2–1.3 times higher than that of an OLED with TBRb as host at any given current density (**Figure 3-10c inset**), indicating a higher NIR-EL efficiency in the Rubrene-based OLED, which can be attributed to the enhancement of φ_{PL} for NIR emission in the 2mol%-ErQ_3-Rubrene system. I note here that the absolute quantum efficiency of the device cannot be measured due to the quite low φ_{PL} of the 2mol%-ErQ_3-Rubrene system ($\varphi_{PL} \approx 10^{-3}$%).

At 50 mA cm^{-2} in the OLED with ErQ_3-doped Rubrene as the EML, the steady-state change in EL intensity (I_{EL}) with magnetic field was positive in the visible regime and negative in the NIR regime, as shown in **Figure 3-10d**. This complementary behavior is consistent with singlet fission

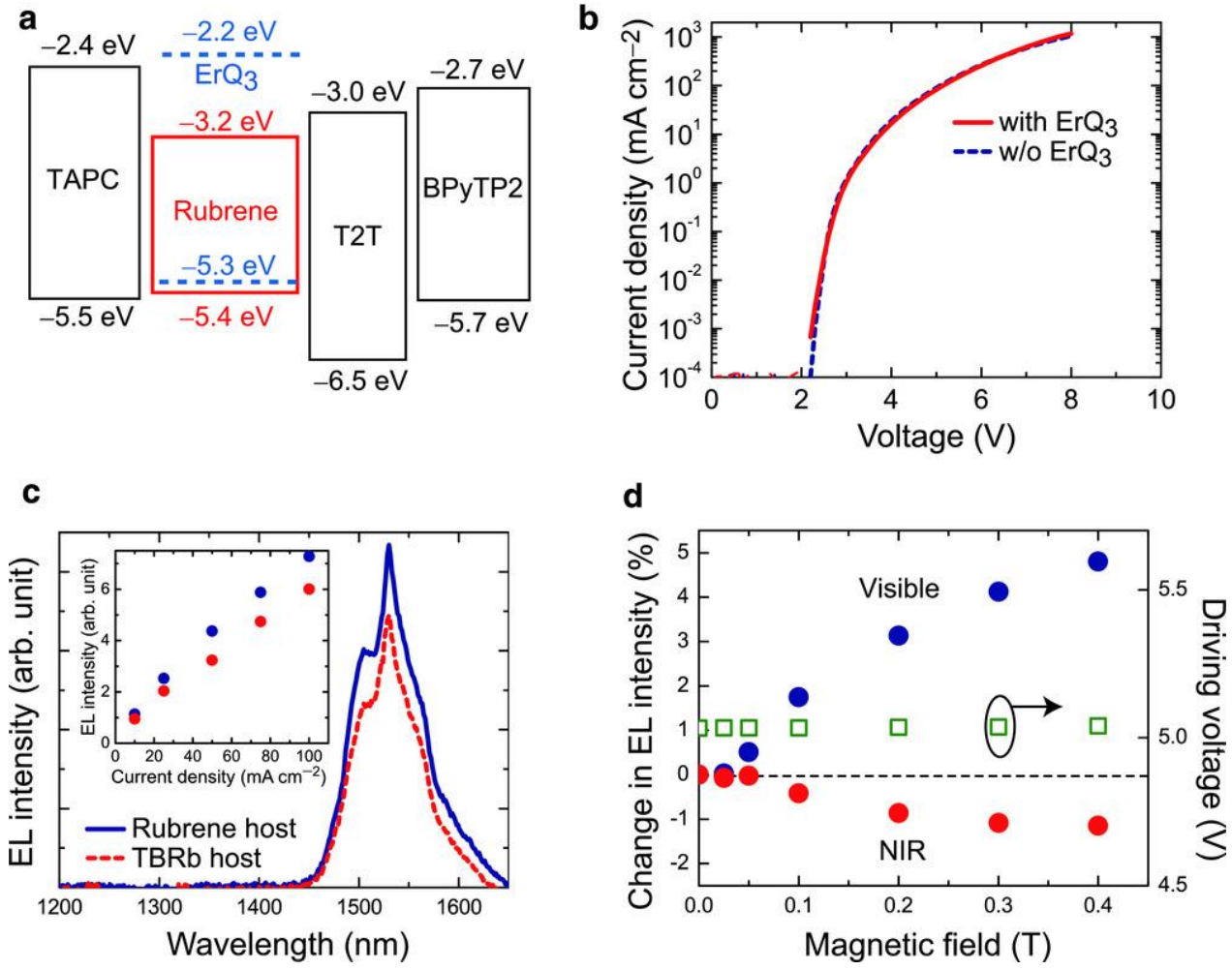

Fig. 3-10. a) Energy level diagram of the designed OLEDs. The OLEDs employed a 100 nm thick ITO layer as anode (work function, WF: −5.2 eV) and a 15 nm thick MgAg alloy as cathode (WF: −3.7 eV). b) Current density as a function of applied voltage for the OLEDs with and without ErQ_3 dopant. c) The NIR-EL spectrum of ErQ_3 in Rubrene (blue line) and TBRb (red line) host matrices. d) The steady-state change in fluorescence intensity (blue circles) and NIR emission intensity (red circles) from a 2mol%-ErQ_3-Rubrene based OLED as a function of external magnetic field with the change in driving voltage (green square).

contributing to the EL. The driving voltage did not change during the magneto-EL measurements (**Figure 3-10d**), indicating that the applied external magnetic field does not affect the electrical conduction in the OLEDs. In addition, I did not observe any change in EL intensity in the visible region with magnetic field in the OLED with ErQ_3-doped TBRb as the EML (**Figure 3-11**).

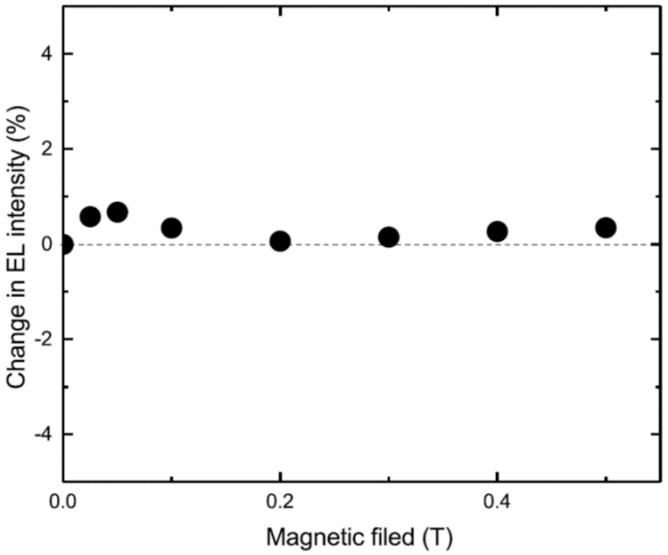

Fig. 3-11. The steady-state change in fluorescence intensity from a 2mol%-ErQ_3-TBRb based OLED as a function of external magnetic field.

Although the absolute values of ΔI_{PL} for the NIR and visible are similar, the absolute values of ΔI_{EL} are higher in the visible region than the NIR region. This difference under electrical pumping is due to spin-statistics rules during carrier recombination. Since 75% of electrically generated excitons are directly formed as triplets and 25% as singlets, the fraction of excitons that can undergo singlet fission is lower than that of the optical pumping. Thus, the triplet production yield under EL ($\varphi_{EL\text{-}T}$) is expressed by **Eq. 3-2** (Derivation in **Section 3.3**).

$$\varphi_{EL-T} = 2\varphi_{SF}S_0 + T_0 = \frac{2\left(\Delta I_{EL-vis}/\Delta I_{EL-NIR}\right)+3}{\left(\Delta I_{EL-vis}/\Delta I_{EL-NIR}\right)-1}S_0 + T_0 \qquad \text{(Eq. 3-2)}$$

Here, S_0 and T_0 are the fractions of initially generated singlets and triplets under electrical pumping, 25% and 75%, respectively. Using the experimentally obtained values, the φ_{SF} under electrical pumping is calculated to be 51.6% in the 2mol%-ErQ_3-Rubrene-based OLED, which agrees well with that of a film under optical pumping. Thus, a triplet production yield before Dexter energy transfer, $\varphi_{EL\text{-}T}$, of 100.8% was achieved in the OLED, emphasizing the potential of a singlet fission-sensitized OLED: the classical limitation of η_γ can be broken by utilizing singlet fission even under electrical excitation.

I demonstrated the harvesting of triplets produced by singlet fission under electrical excitation as NIR emission, leading to an enhancement of the quantum efficiency of the device. Currently, the low φ_{PL} of ErQ_3 (on the order of 10^{-3}%) limits the EL radiant flux in the NIR even with the increased exciton generation from singlet fission, but the φ_{PL} of Er complexes can be further enhanced through careful design of ligands that suppress non-radiative decay arising from molecular vibrations [23]. Also, the number of candidates for singlet-fission sensitizers is, at the present, rather limited. Well-known molecules exhibiting efficient singlet fission, such as tetracene, pentacene, and TIPS-pentacene, are impractical because their crystalline morphologies are electrically unsuitable for application in evaporated OLEDs, and doping of emissive molecules into an amorphous matrix exhibiting intermolecular singlet fission, such as Rubrene, detrimentally effects singlet fission because of reduced intermolecular interactions. However, intramolecular singlet fission with a high yield has recently been demonstrated [24], and I think further development of efficient intramolecular-singlet-fission sensitizers that are amorphous even when evaporated to form thin films will greatly expand the utility of our approach. The present approach, unfortunately, cannot achieve the maximum possible power efficiency for an ideal OLED, which would require the energy difference between injected holes and electrons to be similar to either the energy of the emitted photons or, if all excitons underwent fission, twice the energy of the emitted photons. Nonetheless, our approach can slightly enhance the power efficiency relative to present Er complex-based OLEDs because exciton formation occurs on the singlet-fission sensitizer instead of the wider-energy-gap ligands of the complex, resulting in a lower energy loss when excitons are transferred to the low-energy emissive state of the erbium (III) ion. Development of ways to further increase the number of singlets available for undergoing singlet fission would greatly improve the power efficiency.

3.3 Materials and methods

Materials

The materials Rubrene, TBRb, TAPC, and 8-hydroxyquinolinato-lithium (Liq) were purchased from Luminescence Technology Corp. ErQ_3 was purchased from Sigma Aldrich Co. LLC. The host CBP was used as received from Nippon Steel Chemical Co., Ltd. The OLED materials T2T, 2,7-bis(2,2′-bipyridine-5-yl)triphenylene (BPy-TP2) and Er(TPP)TMHD were synthesized in house (see below). Before fabrication of samples, the crude powders of Rubrene and ErQ_3 were purified by train sublimation with a thermal gradient under a base pressure of less than 5×10^{-3} Pa; this procedure was repeated three times to obtain highly pure compounds.

Synthesis of Er(TPP)TMHD

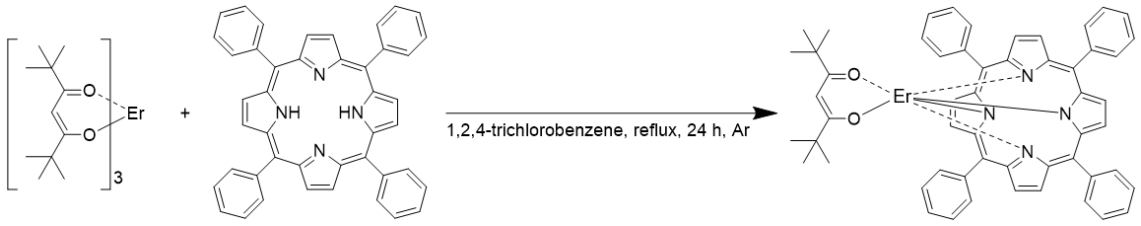

Er(TPP)TMHD was synthesized according to the reported procedure [25].

Sample preparation

Organic solid-state films with a thickness of 100 nm for PL measurements were grown on quartz substrates by thermal evaporation. Organic deposition was performed under vacuum at pressures of below 5×10^{-5} Pa. For OLED fabrication, glass substrates with a pre-patterned, 100 nm thick tin-doped indium oxide (ITO) coating as anode were used. Substrates were washed by sequential ultrasonication in neutral detergent, distilled water, acetone, and isopropanol and then exposed to UV–ozone (NL-UV253, Nippon Laser & Electronics Lab.) to remove adsorbed organic species. After pre-cleaning the substrates, effective device areas of 4 mm^2 were defined on the patterned-ITO substrates by a polyimide insulation layer using a conventional photolithography technique. Organic layers were formed by thermal evaporation. The structure of OLEDs with a singlet-fission sensitizer

and a singlet-fission harvester was as follows: TAPC (50 nm)/2mol%-ErQ_3-Rubrene (30 nm)/T2T (10 nm)/BPy-TP2 (55 nm)/Liq (2 nm)/MgAg (15 nm). After the fabrication, devices were immediately encapsulated with glass lids using epoxy glue in a nitrogen-filled glove box (O_2 < 0.1 ppm, H_2O < 0.1 ppm). Commercial calcium oxide desiccant (Dynic Co.) was included in each encapsulated package.

Optical characterization of organic thin films

The steady-state visible PL spectra and intensities were measured using a multichannel spectrophotometer (PMA-12, Hamamatsu Photonics), and the steady-state NIR-PL spectra of samples were measured using a spectrophotometer (C9913GC, Hamamatsu Photonics). The NIR emission intensities were detected through an optical fiber using a thermoelectrically cooled NIR-PMT unit (C9913GC, Hamamatsu Photonics). PL quantum yield for visible and NIR emission was measured using an absolute PL quantum yield measurement system (Quantaurus-QY Plus, Hamamatsu Photonics) under the flow of argon gas with an excitation wavelength of 515 nm.

Characterization of OLEDs

The current density–voltage–radiant flux characteristics of the OLEDs were measured using a semiconductor parameter analyzer (E5273A, Agilent Technologies) and a calibrated InGaAs photodetector (818-IG-L, Newport) connected to an optical power meter. NIR-EL spectra of the OLEDs were also measured using a spectrometer (C9913GC, Hamamatsu Photonics). All measurements were performed in ambient atmosphere at room temperature.

Characterization of magnetoluminescence

The change in steady-state emission intensity from the samples under an applied external magnetic field was characterized using an electromagnet system. The samples were mounted between the pole pieces of an electromagnet. For magneto-PL measurement, the samples were excited using a continuous-wave semiconductor laser (SAPPHIRE 514–50 CW CDRH, Coherent, Inc.) with an output wavelength of 515 nm, and the emission from the samples was collected through two optical fibers, which were connected to a multichannel spectrophotometer (PMA-12, Hamamatsu Photonics) and an NIR-PMT (C9913GC, Hamamatsu Photonics). The excitation power was fixed at 5 mW. For magneto-EL measurements, the mounted OLEDs were operated using a source meter (Keithley 2400, Keithley Instruments Inc.), and the EL was collected in the same way as for the magneto-PL measurements. All the measurements were performed in ambient atmosphere at room temperature.

The theoretical treatment of magnetoluminescence

1) Optical pumping

The steady-state change in emission intensity (ΔI_{PL}) is defined as $\Delta I_{PL} = 100\% \times (I_H - I_0) / I_0$, where I_H is the emission intensity with an applied magnetic field and I_0 is that without an applied magnetic field. I note that these emission intensity reflects the influence of energy transfer efficiency from Rubrene to ErQ_3 via Dexter type energy transfer. For the steady-state change in visible emission intensity under optical pumping, the number of singlet excitons remaining after singlet fission under an external magnetic field ($S_{PL(B)}$) is described as $S_{PL(B)} = S_0 \times (1 - \gamma_B \times \varphi_{SF})$, where S_0 is the number of initially created singlets before singlet fission, φ_{SF} is the singlet fission efficiency, and γ_B is the magnetic field effect coefficient for singlet fission ($0 < \gamma_B < 1$). Here, $\gamma_B = 1$ corresponds to no change in singlet fission and $\gamma_B = 0$ corresponds to a complete quenching of singlet fission under the magnetic field. Defining $S_{PL(0)}$ as the number of singlet excitons remaining after singlet fission without an external magnetic field, $\Delta I_{PL\text{-}vis}$ can then described by the following equation:

$$\Delta I_{PL-vis} = \frac{I_H - I_0}{I_0} = \frac{S_{PL(B)} - S_{PL(0)}}{S_{PL(0)}} = \frac{(1-\gamma_B\varphi_{SF})S_0 - (1-\varphi_{SF})S_0}{(1-\varphi_{SF})S_0} = \frac{(1-\gamma_B)\varphi_{SF}}{1-\varphi_{SF}} \qquad \text{(Eq. 1)}$$

In the same manner, the number of triplets produced by singlet fission with and without an external magnetic field are defined as $T_{PL(B)} = 2 \times S_0 \times \gamma_B \times \varphi_{SF}$ and $T_{PL(0)} = 2 \times S_0 \times \varphi_{SF}$, respectively. Thus, $\Delta I_{PL\text{-}NIR}$ is described by following equation:

$$\Delta I_{PL-NIR} = \frac{I_H - I_0}{I_0} = \frac{T_{PL(B)} - T_{PL(0)}}{T_{PL(0)}} = \frac{2\gamma_B \varphi_{SF} S_0 - 2\varphi_{SF} S_0}{2\varphi_{SF} S_0} = \gamma_B - 1 \qquad \text{(Eq. 2)}$$

Here, I assume that the PL quantum yield of the NIR emitter and the energy transfer efficiency from Rubrene to ErQ_3 do not exhibit a magnetic field dependence. From Eq. 1 and 2, I get Eq. 3 which can be rearranged to arrive at Eq. 3-1.

$$\frac{\Delta I_{PL-vis}}{\Delta I_{PL-NIR}} = \frac{\varphi_{SF}}{\varphi_{SF} - 1} \qquad \text{(Eq. 3)}$$

2) Electrical pumping

Under electrical pumping, the $\Delta I_{EL\text{-}vis}$ will be described by a formula similar to Eq. 1:

$$\Delta I_{EL-vis} = \frac{I_H - I_0}{I_0} = \frac{S_{EL(B)} - S_{EL(0)}}{S_{EL(0)}} = \frac{(1-\gamma_B \varphi_{SF}) - (1-\varphi_{SF})}{1-\varphi_{SF}} = \frac{(1-\gamma_B)\varphi_{SF}}{1-\varphi_{SF}} \qquad \text{(Eq. 4)}$$

However, since 75% of all electrically generated excitons are directly formed as triplets states, the number of triplets with and without the presence of an external magnetic field under electrical pumping include an additional value for the number of initially generated triplets (T_0) and are defined as $T_{EL(B)} = T_0 + 2 \times S_0 \times \gamma_B \times \varphi_{SF}$ and $T_{EL(0)} = T_0 + 2 \times S_0 \times \varphi_{SF}$, respectively. Thus, $\Delta I_{EL\text{-}NIR}$ is describe by following equation:

$$\Delta I_{EL-NIR} = \frac{I_H - I_0}{I_0} = \frac{T_{EL(B)} - T_{EL(0)}}{T_{EL(0)}} = \frac{(T_0 + 2\gamma_B \varphi_{SF} S_0) - (T_0 + 2\varphi_{SF} S_0)}{T_0 + 2\varphi_{SF} S_0} \qquad \text{(Eq. 5)}$$

Because spin statistics states that three triplets are generated for each singlet under electrical excitation, I can write that $T_0 = 3 \times S_0$. Plugging this into Eq. 5, I get

$$\Delta I_{EL-NIR} = \frac{(3S_0 + 2\gamma_B \varphi_{SF} S_0) - (3S_0 + 2\varphi_{SF} S_0)}{3S_0 + 2\varphi_{SF} S_0} = \frac{\varphi_{SF}(\gamma_B - 1)}{1.5 + \varphi_{SF}} \qquad \text{(Eq. 6)}$$

Using Eq. 4 and 6, I obtain Eq. 7 which can be rearranged to arrive at Eq. 3-2.

$$\frac{\Delta I_{EL-vis}}{\Delta I_{EL-NIR}} = \frac{1.5+\varphi_{SF}}{\varphi_{SF}-1} \qquad \text{(Eq. 7)}$$

References

1. M. A. Baldo, D. F. O'Brien, M. E. Thompson, S. R. Forrest, Excitonic singlet-triplet ratio in a semiconducting organic thin film. *Phys. Rev. B* **60**, 14422 (1999)

2. C. Adachi, M. A. Baldo, M. E. Thompson, S. R. Forrest, Nearly 100% internal phosphorescence efficiency in an organic light-emitting device. *J. Appl. Phys.* **90**, 5048 (2001)

3. S. O. Jeon, S. E. Jang, H. S. Son, J. Y. Lee, External Quantum Efficiency Above 20% in Deep Blue Phosphorescent Organic Light-Emitting Diodes. *Adv. Mater.* **23**, 1436 (2011)

4. H. Uoyama, K. Goushi, K. Shizu, H. Nomura, C. Adachi, Highly efficient organic light-emitting diodes from delayed fluorescence. *Nature* **492**, 234 (2012)

5. S. Hirata, Y. Sakai, K. Masui, H. Tanaka, S. Y. Lee, H. Nomura, N. Nakamura, M. Yasumatsu, H. Nakanotani, Q. Zhang, K. Shizu, H. Miyazaki, C. Adachi, Highly efficient blue electroluminescence based on thermally activated delayed fluorescence. *Nat. Mater.* **14**, 330 (2015)

6. M. B. Smith, J. Michl, Singlet Fission. *Chem. Rev.* **110**, 6891 (2010)

7. D. N. Congreve, J. Lee, N. J. Thompson, E. Hontz, S. R. Yost, P. D. Reusswig, M. E. Bahlke, S. Reineke, T. V. Voorhis, M. A. Baldo, External Quantum Efficiency Above 100% in a Singlet-Exciton-Fission–Based Organic Photovoltaic Cell. *Science* **340**, 331 (2013)

8. M. Tabachnyk, B. Ehrler, S. Gélinas, M. L. Böhm, B. J. Walker, K. P. Musselman, N. C. Greenham, R. H. Friend, A. Rao, Resonant energy transfer of triplet excitons from pentacene to PbSe nanocrystals. *Nat. Mater.* **13**, 1033 (2014)

9. N. J. Thompson, M. W. B. Wilson, D. N. Congreve, P. R. Brown, J. M. Scherer, T. S. Bischof, M. Wu, N. Geva, M. Welborn, T. V. Voorhis, V. Bulovic, M. G. Bawendi, M. A. Baldo, Energy harvesting of non-emissive triplet excitons in tetracene by emissive PbS nanocrystals. *Nat. Mater.* **13**, 1039 (2014)

10. W. P. Gillin, R. J. Curry, Erbium (III) tris(8-hydroxyquinoline) (ErQ): A potential material for silicon compatible 1.5 μm emitters. *Appl. Phys. Lett.* **74**, 798 (1999)

11. R. J. Curry, W. P. Gillin, Silicon-based organic light-emitting diode operating at a wavelength of 1.5 μm. *Appl. Phys. Lett.* **77**, 2271 (2000)

12. P. M. Ramos, M. R. Silva, C. Coya, C. Zaldo, Á. L. Álvarez, S. Á. García, A. M. M. Beja, J. M. Gil, Novel erbium(III) fluorinated β-diketonate complexes with *N*,*N*-donors for optoelectronics: from synthesis to solution-processed devices. *J. Mater. Chem. C* **1**, 2725 (2013)

13. F. Artizzu, F. Quochi, L. Marchiò, E. Sessini, M. Saba, A. Serpe, A. Mura, M. L. Mercuri, G. Bongiovanni, P. Deplano, Fully Efficient Direct Yb-to-Er Energy Transfer at Molecular Level in a Near-Infrared Emitting Heterometallic Trinuclear Quinolinolato Complex. *J. Phys. Chem. Lett.* **4**, 3062 (2013)

14. G. B. Piland, J. J. Burdett, D. Kurunthu, C. J. Bardeen, Magnetic Field Effects on Singlet Fission and Fluorescence Decay Dynamics in Amorphous Rubrene. *J. Phys. Chem. C* **117**, 1224 (2013)

15. R. V. Deun, P. Fias, K. Driesen, K. Binnemans, C. G. Walrand, Halogen substitution as an efficient tool to increase the near-infrared photoluminescence intensity of erbium(iii) quinolinates in non-deuterated DMSO. *Phys. Chem. Chem. Phys.* **5**, 2754 (2003)

16. S. W. Magennis, A. J. Ferguson, T. Bryden, T. S. Jones, A. Beeby, I. D. W. Samuel, Time-dependence of erbium(III) tris(8-hydroxyquinolate) near-infrared photoluminescence: implications for organic light-emitting diode efficiency. *Synth. Met.* **138**, 463 (2003)

17. Y. S. Wu, T. H. Liu, H. H. Chen, C. H. Chen, A new yellow fluorescent dopant for high-efficiency organic light-emitting devices. *Thin Solid Films* **496**, 626 (2006)

18. C. Sutton, N. R. Tummala, D. Beljonne, J. L. Brédas, Singlet Fission in Rubrene Derivatives: Impact of Molecular Packing. *Chem. Mater.* **29**, 2777 (2017)

19. W. Jia, Q. Chen, L. Chen, D. Yuan, J. Xiang, Y. Chen, Z. Xiong, Molecular Spacing Modulated Conversion of Singlet Fission to Triplet Fusion in Rubrene-Based Organic Light-Emitting Diodes at Ambient Temperature. *J. Phys. Chem. C* **120**, 8380 (2016)

20. H. H. Fong, S. K. So, W. Y. Sham, C. F. Lo, Y. S. Wu, C. H. Chen, Effects of tertiary butyl substitution on the charge transporting properties of rubrene-based films. *Chem. Phys.* **298**, 119 (2004)

21. S. R. Yost, J. Lee, M. W. B. Wilson, T. Wu, D. P. McMahon, R. R. Parkhurst, N. J. Thompson, D. N. Congreve, A. Rao, K. Johnson, M. Y. Sfeir, M. G. Bawendi, T. M. Swager, R. H. Friend, M. A. Baldo, T. V. Voorhis, A transferable model for singlet-fission kinetics. *Nat. Chem.* **6**, 492 (2014)

22. H. Nakanotani, K. Masui, J. Nishide, T. Shibata, C. Adachi, Promising operational stability of high-efficiency organic light-emitting diodes based on thermally activated delayed fluorescence. *Sci. Rep.* **3**, 2127 (2013)

23. G. Mancino, A. J. Ferguson, A. Beeby, N. J. Long, T. S. Jones, Dramatic Increases in the Lifetime of the Er^{3+} Ion in a Molecular Complex Using a Perfluorinated Imidodiphosphinate Sensitizing Ligand. *J. Am. Chem. Soc.* **127**, 524 (2005)

24. J. Xia, S. N. Sanders, W. Cheng, J. Z. Low, J. Liu, L. M. Campos, T. Sun, Singlet Fission: Progress and Prospects in Solar Cells. *Adv. Mater.* **29**, 1601652 (2017)

25. W. D. Horrocks Jr., C. P. Wong, Lanthanide Porphyrin Complexes. Evaluation of Nuclear Magnetic Resonance Dipolar Probe and Shift Reagent Capabilities. *J. Am. Chem. Soc.* **98**, 7157 (1976)

Chapter 4

Development of highly efficient NIR-TADF molecule

U. Balijapalli*, **R. Nagata***, N. Yamada, H. Nakanotani, M. Tanaka, A. D'Aléo, V. Placide, M. Mamada, Y. Tsuchiya C. Adachi, *Angew. Chem. Int. Ed.* (accepted).
(*Equal contribution)

Abstract

The rather low η_{EQE} of NIR-OLEDs has been a critical obstacle for the potential applications. Here, I demonstrate a highly efficient NIR emitter exhibiting TADF and its application to NIR-OLEDs. The designed NIR-TADF emitter, TPA-PZTCN, has a high φ_{PL} of over 40% with a peak wavelength at 729 nm even in a highly doped co-deposited film. The EL peak wavelength of the NIR-OLED is 734 nm with an η_{EQE} of 13.4%, which is unprecedented among rare-metal-free NIR-OLEDs in this spectral range. Further, TPA-PZTCN can sensitize a deep NIR fluorophore to achieve a peak wavelength of approximately 900 nm, resulting in an η_{EQE} of over 1% in a TADF-sensitized NIR-OLED with high operational device durability (LT95 > 600 hr.).

4.1 Introduction

As discussed in **Chapter 2**, to maximize the η_{EQE} of NIR-OLEDs, harvesting of low-energy dark triplet excitons as EL before non-radiative decay is required because triplet excitons in organic emitters are directly generated in every charge carrier recombination event [1]. In fact, room-temperature phosphorescent-based NIR-OLEDs based on platinum-complexes have an almost ideal η_{EQE} of 24% at an EL wavelength of 740 nm [2] and a high η_{EQE} of 3.8% even at 900 nm [3]. Another possible pathway is the use of pure organic compounds that exhibit TADF, which enables harvesting of triplet excited state energy as delayed fluorescence without using any precious noble metals [4].

Recently, there has been a great deal of interest in NIR-TADF-OLEDs. Considerable progress has been made in the field of NIR-TADF emitters, *e.g.*, pyrazinophenanthrene [5,6,7], pyrazinoacenaphthene [8,9,10,11], dibenzophenazine [12], quinoxaline [13,14], benzothiadiazole [15], and boron-curcuminoid [16,17,18] derivatives (**Figure 4-1**), and η_{EQE} > 10% at wavelengths beyond 700 nm is achieved in NIR-TADF-OLEDs [9]. However, NIR-OLEDs suffer from a high η_{EQE} roll-off in the high current region. This effect might be attributed to the small k_{RISC}: ~10^4 s^{-1} [9,12]. In addition, although operational device stability is critical for practical use, few reports have mentioned the operational device stability of NIR-OLEDs, implying that the considerable challenges remain to achieving both highly efficient and operationally durable devices.

Here, I show that our well-thought-out electron donor (D) – electron acceptor (A) type TADF molecule, 11,12-bis(4-(diphenylamino)phenyl)dibenzo[a,c]phenazine-2,3,6,7-tetracarbonitrile (TPA-PZTCN), exhibits intense NIR-EL ($\eta_{EQE(max)}$: 13.4% ± 0.8%) at the peak wavelength of 734 nm by harvesting triplet excitons as delayed fluorescence with a well suppressed η_{EQE} roll off behavior (η_{EQE} > 10% at 1 mA cm^{-2}) against that of the previously reported NIR-TADF-OLEDs (η_{EQE} < 6% at 1 mA/cm^2) [5,8,9,10,11,13,15,16,17]. Importantly, it has unveiled that NIR-OLEDs possess high device durability (LT95 = 168 h under constant current density operation of 10 mA/cm^2). These features of TPA-PZTCN based NIR-OLEDs originate mainly from an enhancement of k_{RISC} (~10^5 s^{-1}) compared to that of previous NIR-TADF molecules (k_{RISC}: ~10^4 s^{-1}) [9,12]. Moreover, TPA-PZTCN

can effectively serve as an energy sensitizer for NIR fluorophores that have deeper NIR emission at 900 nm, providing a high maximum η_{EQE} of 1.1% ± 0.2% with a peak EL wavelength of 901 nm in a TADF-assisted-fluorescence (TAF) NIR-OLED. According to an efficient singlet energy transfer from TPA-PZTCN to the NIR fluorophore, a promising device operational lifetime of LT95 > 600 h was also achieved in the TAF NIR-OLED. This work thus offers a promising strategy for developing low-cost, flexible, and efficient dual-band NIR-OLEDs, which would be critical for highly sensitive sensing applications.

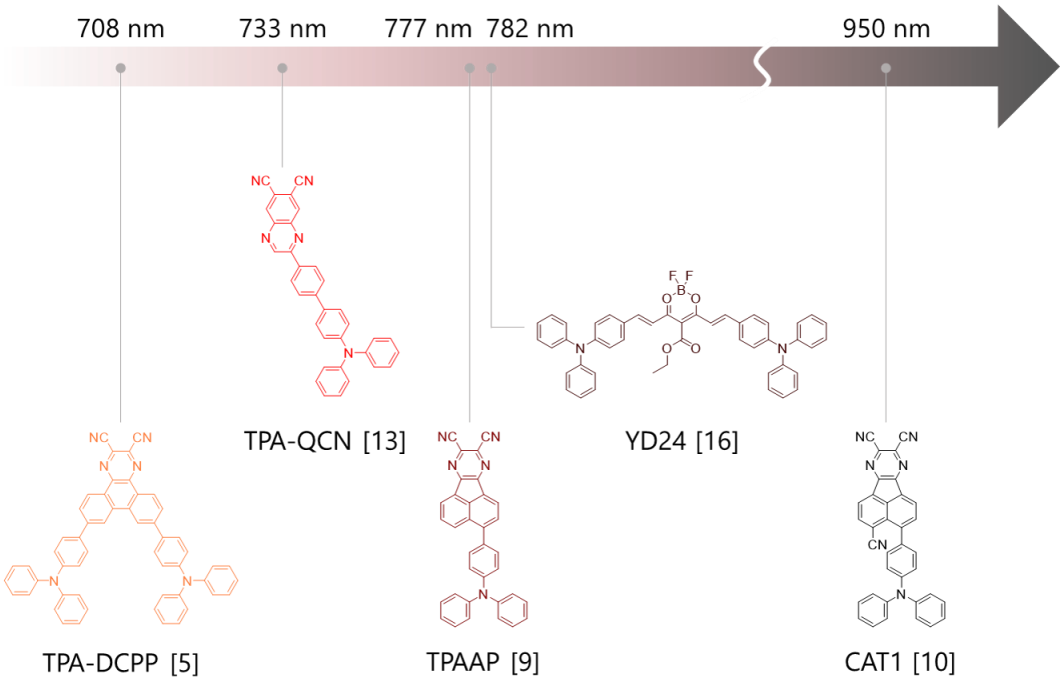

Fig. 4-1. Molecular structures of state-of-the-art NIR-TADF materials against their lowest-energy reported PL wavelength.

4.2 Results and discussion

4.2.1 Molecular design

The molecular structure of the designed NIR-TADF emitter is illustrated in **Figure 4-2a**. A dibenzo[a,c]phenazine-2,3,6,7-tetracarbonitrile (PZTCN) unit that has high molecular rigidity is used as a novel electron accepting moiety, and two triphenylamine (TPA) units are attached in the sterically hindered 11,12-positions as electron-donating moieties to afford efficient NIR-TADF behavior. To support our molecular design rules for NIR-TADF emitters, a computational study based on time-dependent density functional theory (TD-DFT) was performed with the B3LYP functional and the 6-311G+(d) basis. The optimized geometry in the ground-state revealed a twisted structure between the electron-donating TPA units and the electron-withdrawing PZTCN unit with a dihedral angle of 48.5°. This twisting led to a spatial separation of HOMO and LUMO, as shown in **Figure 4-2b**. Therefore, I expect that this spatial orbital separation affords a small ΔE_{ST} through a small electron exchange integral in a charge-transfer (CT) excited state [4], resulting in the ΔE_{ST} = 0.14 eV.

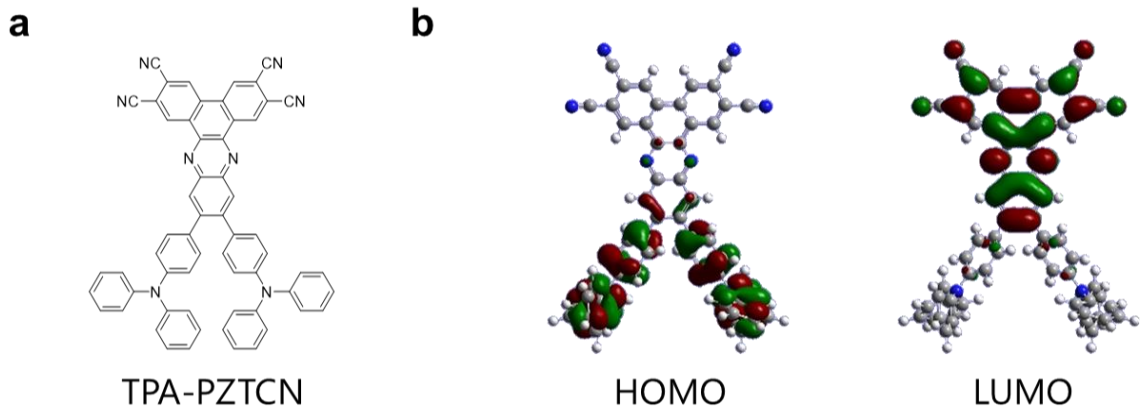

Fig. 4-2. a) The chemical structure of TPA-PZTCN. b) HOMO, LUMO distribution of TPA-PZTCN.

Furthermore, the reorganization energy in fluorescent process of TPA-PZTCN was investigated using S_0 and S_1 optimized geometry. Since the non-radiative decay rate (k_{nr}) depends not only on the energy gap between S_0 and S_1 but also on the reorganization energy in luminescent process [19], suppression of structural relaxation is expected to enhance φ_{PL}. In fact, a recent study on platinum-based phosphorescent material revealed a clear relationship between the reorganization energy and

φ_{PL} [20]. As shown in **Figure 4-3a**, the reorganization energy (λ_M) in TPA-PZTCN was calculated to be 185 meV, which is significantly smaller than those calculated for conventional NIR-TADF materials, *e.g.*, YD24: 245 meV, indicating suppressed k_{nr} in TPA-PZTCN due to the introduction of a rigid PZTCN moiety and sterically hindered TPA units. The rigidity of TPA-PZTCN is further supported by the significant change in S_0 energy with the varied C-C angle between TPA and PZTCN units (**Figure 4-3b**).

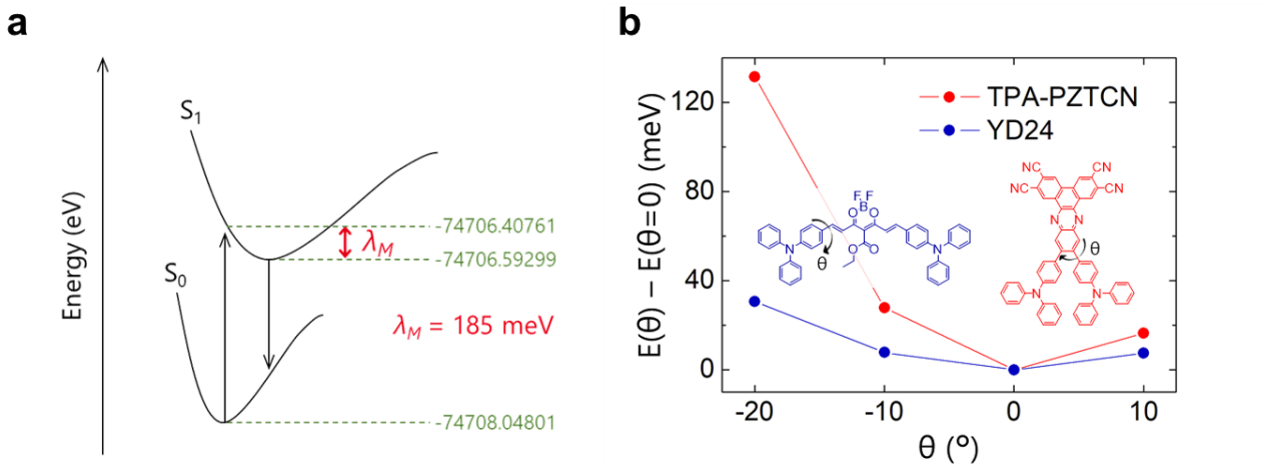

Fig. 4-3. a) Calculated reorganization energy during fluorescence process in TPA-PZTCN. b) Calculated S_0 energy against different C-C angle (θ) between TPA and acceptor units in TPA-PZTCN (red) and YD24 (blue). θ=0 corresponds to the C-C angle in S_0-optimized structure.

4.2.2 Electrochemical and thermal properties

TPA-PZTCN was synthesized by a condensation reaction between N^4,N^4,$N^{4\prime\prime}$,$N^{4\prime\prime}$-tetraphenyl-[1,1′:2′,1″-terphenyl]-4,4′,4″,5′-tetraamine and 3,6-dibromo-2,7-diiodophenanthrene-9,10-dione followed by a substitution reaction with CuCN (detail synthesis procedure in **Section 4.3**). As shown in **Figure 4-4**, Thermogravimetric differential thermal analysis (TG-DTA) reveals the high thermal stability of TPA-PZTCN, *i.e.*, a high decomposition temperature of 562 °C, which permits the use of vacuum deposition techniques in the fabrication of high-quality OLEDs.

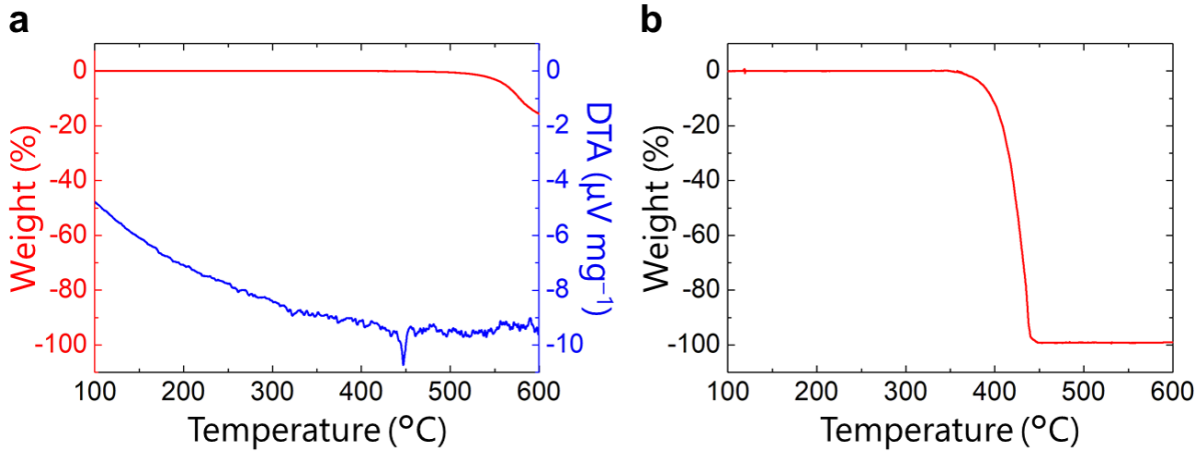

Fig. 4-4. TG-DTA curves of TPA-PZTCN. a) TG (red) - DTA (blue) curves at 1 atm. The 5 wt% loss point indicates decomposition temperature of 562 °C. b) TG curve at 1 Pa. The 5 wt% loss point indicates sublimation temperature of 386 °C.

In addition, cyclic voltammetry measurements show reversible curves both for oxidation and reduction, indicating the high electrochemical stability of TPA-PZTCN (**Figure 4-5**). Here, the HOMO and LUMO levels of TPA-PZTCN are calculated to be –5.66 and –3.84 eV, respectively, leading to a narrow electrochemical bandgap of 1.82 eV as expected from theoretical calculations.

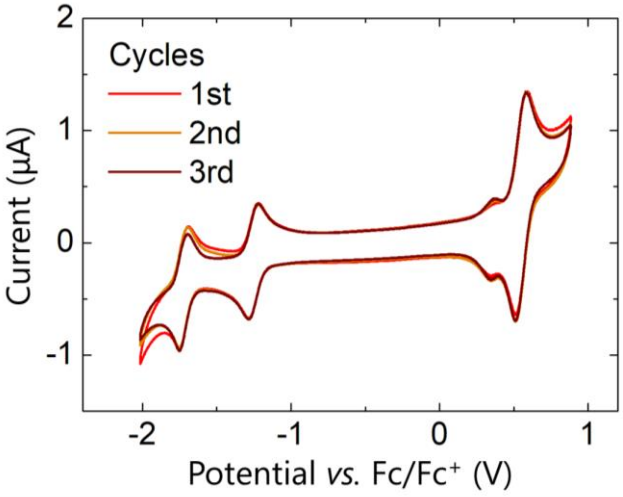

Fig. 4-5. Cyclic voltammetry curves of TPA-PZTCN in dichloromethane with $TBAPF_6$ as the supporting electrolyte.

4.2.3 Fundamental photophysical properties

The absorption spectrum of TPA-PZTCN in toluene (10^{-5} M), the PL spectra of TPA-PZTCN in toluene and in a 3,3-di(9H-carbazol-9-yl)-1,1-biphenyl (mCBP) host matrix are shown in **Figure 4-6a**, and **Table 4-1** summarizes their related photophysical data. TPA-PZTCN in toluene has an absorption maximum at 550 nm and a PL maximum at 674 nm with a PL quantum yield (φ_{PL}) of 77.7% ± 0.5%. The spectra of TPA-PZTCN are considerably redshifted from those of state-of-the-art NIR-TADF molecules such as TPA-PZCN (Abs: 488 nm, PL: 585 nm) [12] and TPAAP (Abs: 487

nm, PL: 609 nm) [9], indicating the stronger electron-withdrawing ability of the PZTCN moiety than that of dibenzo[a,c]phenazine-3,6-dicarbonitrile (PZCN) acenaphthopyrazine (AP) moiety. The 1wt%-TPA-PZTCN-mCBP film also had PL at a peak wavelength of 672 nm with a φ_{PL} of 78.1% ± 0.3%. Notably, the solid-state films exhibited a greater redshift of their emission as the doping concentration of TPA-PZTCN was increased. A moderately high φ_{PL} of 40.8% ± 0.1% at a PL maximum of 729 nm was maintained even in a 10wt%-TPA-PZTCN-mCBP film, exhibiting over 100 nm redshifted PL from that of a 10wt%-TPA-PZCN doped film [12].

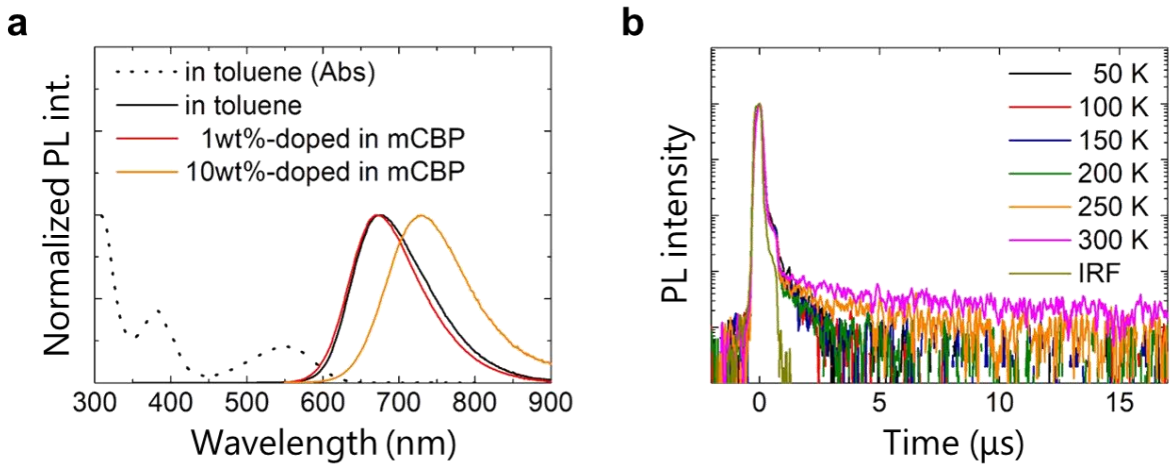

Fig. 4-6. a) PL spectra of TPA-PZTCN in dilute toluene solution (black), 1wt%-doped in mCBP film (red), and 10wt%-doped in mCBP film (orange). Black dashed line indicates the absorption spectrum of TPA-PZTCN solution. b) Temperature-dependent transient PL decay curves of a 10wt%-TPA-PZTCN-mCBP film.

Table 4-1. Fundamental PL properties of TPA-PZTCN

Sample type	Absorption [nm]	PL [nm]	PLQY prompt/delay [%]	τ_d [μs]	k_r [10^7 s^{-1}]	k_{ISC} [10^8 s^{-1}]	k_{RISC} [10^5 s^{-1}]	k_{nr}^T [10^4 s^{-1}]
10^{-5} M in toluene	550	674	77.7	-	-	-	-	-
1wt%-doped in mCBP	-	672	32.5/45.6	19.2	3.3	0.7	1.1	1.7
10wt%-doped in mCBP	-	729	19.1/21.7	18.6	2.6	1.1	0.8	3.9

To get insight into the triplet-harvesting ability of TPA-PZTCN, I performed a temperature-dependent transient PL measurement for the 10wt%-TPA-PZTCN-mCBP film. As shown in **Figure 4-6b**, the appearance of the temperature-dependent delayed fluorescence components (delayed

fluorescence lifetime: τ_d = 18.6 μs at 300 K) at the high temperature region (200–300 K) clearly indicates the presence of a RISC process from the T_1 to the S_1 followed by TADF in TPA-PZTCN. Here I note that the energy gap between the S_1 (1.95 eV) and T_1 (1.85 eV) of TPA–PZTCN was estimated to be 0.1 eV (**Figure 4-7**). Remarkably, the k_{RISC} is calculated to be 1.1 × 10^5 s^{-1} (1wt%-doped in mCBP) and 7.6 × 10^4 s^{-1} (10wt%-doped in mCBP) at 300 K. The k_{RISC} values for TPA-PZTCN observed in films are one order of magnitude higher than previously reported values of NIR-TADF materials such as TPA-PZCN (9.2 × 10^3 s^{-1}) [12] and TPAAP (8.3 × 10^3 s^{-1}) [9]. In addition, it is confirmed that TPA-PZTCN has a slightly smaller experimental ΔE_{ST} value of 0.10 eV (**Figure 4-7**) than 0.13 eV of TPA-PZCN [12].

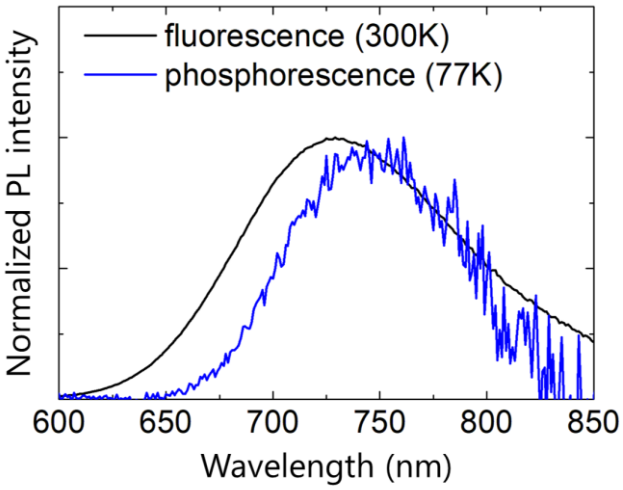

Fig. 4-7. Fluorescence (black line) and phosphorescence (blue line) spectrum of the 10wt%-TPA-PZTCN-mCBP film. Phosphorescence spectra were collected 10 ms after turn-off the excitation light at 77K.

In order to further evaluate the fast RISC process in TPA-PZTCN, natural transition orbital (NTO) simulation was performed on the excited states in TPA-PZTCN (**Figure 4-8**). TD-DFT calculation predicted the existence of a T_2 state (1.59 eV) that neighbors both the S_1 (1.64 eV) and the T_1 (1.50 eV) states, and the both states are assigned as a CT excited state because the highest occupied NTO (HONTO) and the

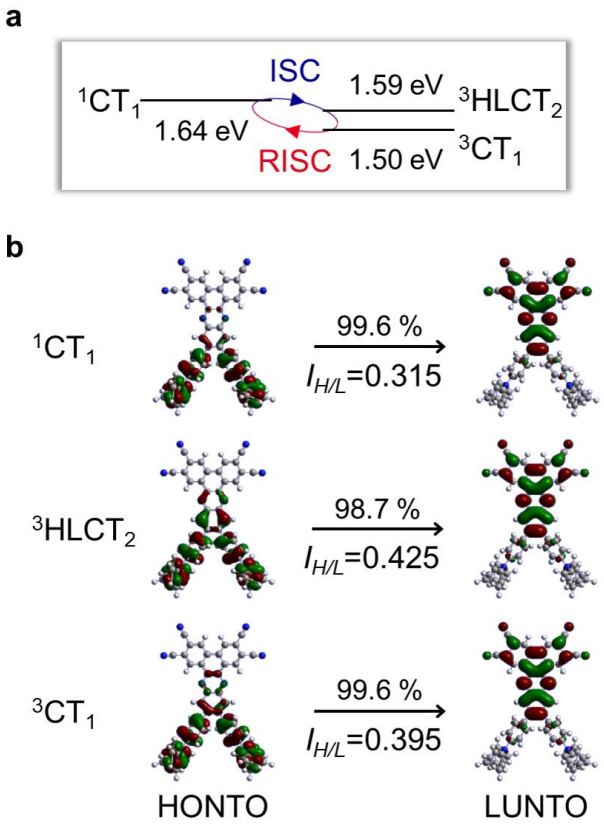

Fig. 4-8. a) Schematic illustration of $^1CT_1$, $^3CT_1$, and $^3HLCT_2$ energy level alignment for RISC in TPA-PZTCN. b) HONTO and LUNTO distribution, and the overlap integral ($I_{H/L}$) for the excited states in TPA-PZTCN.

lowest unoccupied NTO (LUNTO) are spatially separated. In fact, the phosphorescence spectrum of TPA-PZTCN in the 10wt%-TPA-PZTCN-mCBP film had a structureless Gaussian shape (**Figure 4-7**). Furthermore, the prompt fluorescence spectrum of TPA-PZTCN had a notable positive solvatochromic trend with increasing solvent polarity (**Figure 4-9**). These results indicate the strong CT character of the S_1 state. Conversely, an increase in the overlap integral ($I_{H/L}$) between HONTO and LUNTO was observed in the T_2 state, *i.e.*, S_1: $I_{H/L}$ = 0.315 → T_2: $I_{H/L}$ = 0.425, indicating the T_2 state obtains a hybrid local-CT character (^{3}HLCT$_2$). Since a spin-orbit coupling matrix element should become large when there is a large difference in excitation character between the initial state and the final state, [21,22,23] this result strongly suggests that spin-flip events are effectively mediated not only by small ΔE_{ST} but also by the energetically closed T_2 state in TPA-PZTCN, leading to high k_{RISC}.

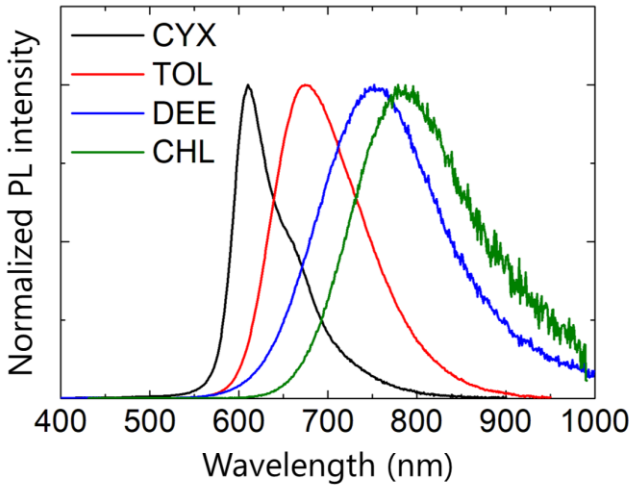

Fig. 4-9. The PL spectra of TPA-PZTCN in solution (10^{-5} M^{-1}). CYX: cyclohexane, TOL: toluene, DEE: diethyl ether, CHL: chloroform.

While TPA-PZTCN has highly efficient NIR-PL in the spectral range of ~750 nm, over 60 nm redshifted from those of reported high-performance NIR-TADF materials [9,12], efficient NIR-TADF-OLEDs with an EL peak beyond 900 nm are mainly limited because of the lack of NIR fluorophores that have a high φ_{PL} and triplet-harvesting ability. Fortunately, the high φ_{PL} and the large k_{RISC} of TPA-PZTCN contributes to efficient energy transfer of both excited singlet and triplet energies to deeper-NIR-fluorophores.

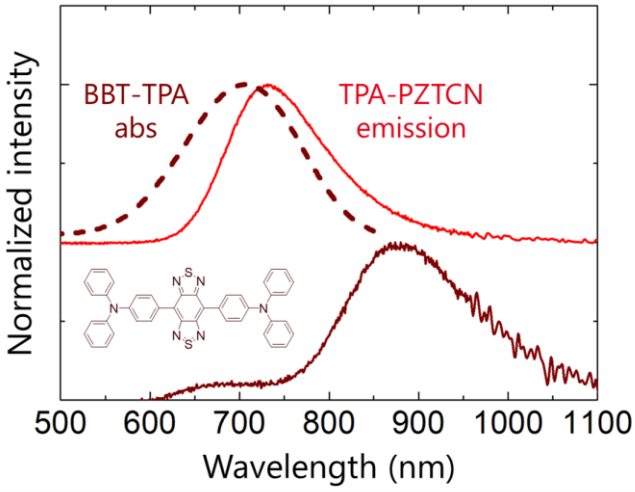

Fig. 4-10. PL spectrum of the 10wt%-TPA-PZTCN-mCBP film (red solid line), absorption spectrum of BBT-TPA in dilute toluene solution (dashed brown line) and PL spectrum of the 1wt%-BBT-TPA-10wt%-TPA-PZTCN-mCBP film (brown solid line). Chemical structure of BBT-TPA is also shown.

To demonstrate proof-of-concept of the deep-NIR sensitizing, TPA-PZTCN was used as an energy sensitizer for a deeper-NIR-fluorophore, namely BBT-TPA that had a relatively high φ_{PL} of 7.4% in solution but no TADF activity [24,25]. **Figure 4-10** shows the PL spectrum of the 10wt%-TPA-PZTCN in an mCBP host matrix and an absorption spectrum of the BBT-TPA toluene solution (10^{-5} M). The large overlap between the PL spectrum and the absorption spectrum is attributed to an efficient Förster-type dipole-dipole energy transfer (FRET) from the S_1 of TPA-PZTCN to the S_1 of BBT-TPA with a large FRET radius (10.1 nm). This result leads to sufficient singlet excited energy transfer even when the BBT-TPA is doped at a very dilute concentration, which is critical to avoid aggregation-induced quenching of the deep-NIR-fluorophore. In fact, the 1wt%-BBT-TPA-10wt%-TPA-PZTCN-mCBP film had a deep-NIR-PL with a peak wavelength of 874 nm that mainly originates from BBT-TPA. The φ_{PL} of the 1wt%-BBT-TPA-10wt%-TPA-PZTCN-mCBP film is 12.9 ± 0.1%. This value is slightly higher than the φ_{PL} of BBT-TPA in solution, indicating the presence of an efficient FRET process and suppression of the vibration-induced exciton quenching in the host-guest film. The efficient FRET in the BBT-TPA-TPA-PZTCN system thus enables fabrication of highly efficient TAF-OLEDs [26].

4.2.4 OLED properties

To demonstrate the triplet-harvesting and the energy-sensitizing ability of TPA-PZTCN under electrical excitation, I fabricated both types of the NIR-OLEDs, *i.e.*, TADF-OLED (without BBT-TPA) and TAF-OLED (with BBT-TPA as the terminal emitter). The corresponding energy diagram of the OLED and the chemical structures of materials used in the OLEDs are shown in **Section 4.3**. **Figure 4-11** and **Table 4-2** summarizes the fundamental OLED performances. As shown in **Figure 4-11a**, our NIR-OLEDs exhibited intense NIR-EL with an EL peak at 734 nm in TADF-OLED and at 901 nm in TAF-OLED. Note that these EL spectra match well with the difference in the extinction coefficient between reduced hemoglobin and oxyhemoglobin [27]. Because both wavelengths were

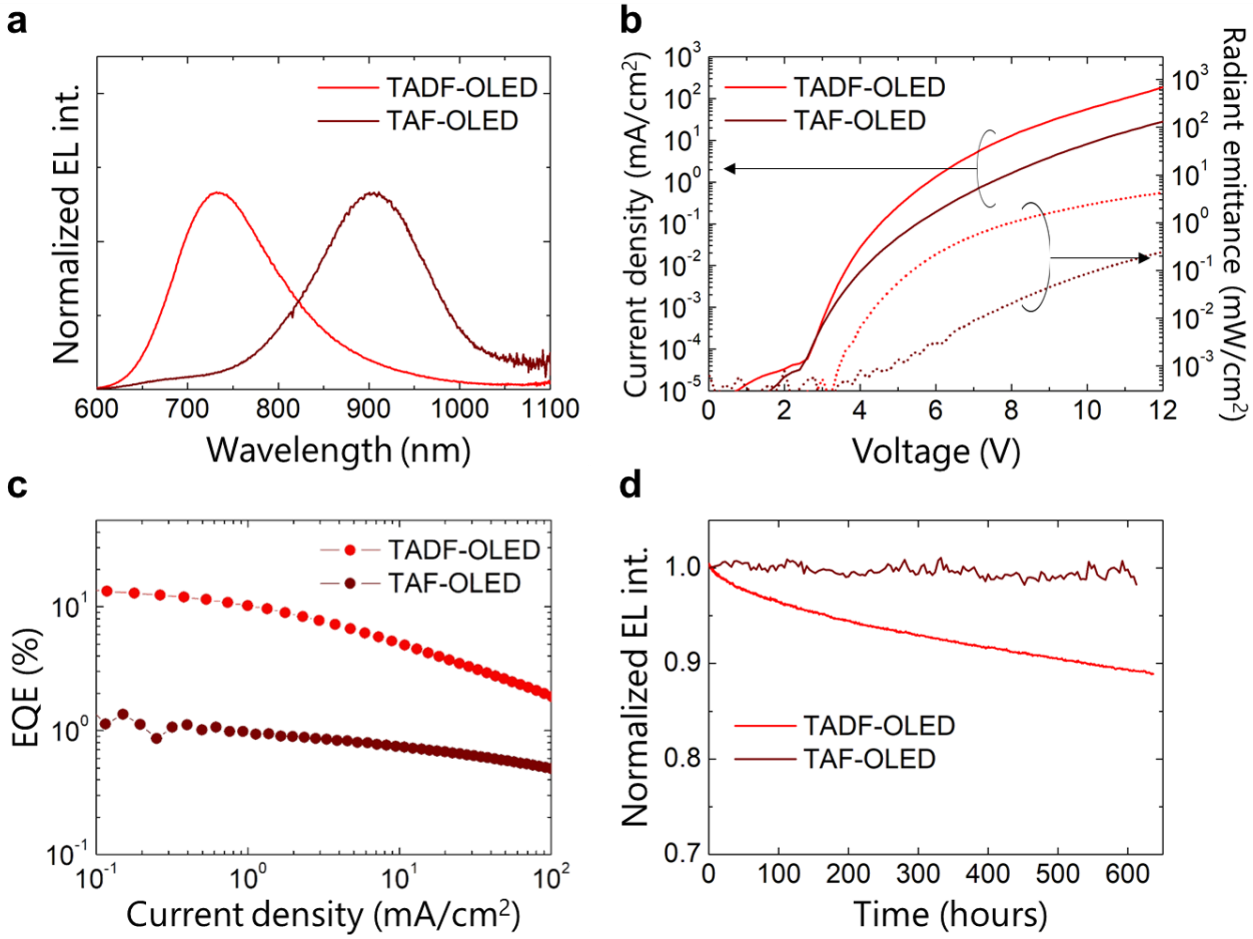

Fig. 4-11. a) EL spectra of TADF-OLED (red) and TAF-OLED (brown) at a current density of 10 mA/cm^2. b) Current density-radiant emittance-voltage characteristics of tested devices. c) External EL quantum efficiency as a function of current density for tested devices. d) Normalized EL intensity of tested devices as a function of operating time at 10 mA/cm^2.

Table 4-2. EL properties of tested NIR-OLEDs

OLED type	EL [nm][a)]	EQE_{max} [%]	EQE [%][a)]	EQE [%][b)]	Voltage [V][b)]	Output power [mW/cm^2][b)]	LT95 [hours][b)]
TADF	734	13.4	10.2	4.9	7.6	0.9	168
TAF	901	1.1	1.0	0.8	10.4	0.1	>600

[a)] Measured at 1 mA/cm^2; [b)] Measured at 10 mA/cm^2.

obtained by merely adding BBT-TPA as the terminal emitter, this strategy is advantageous for reducing the fabrication cost of sensors, which might be used in applications such as a pulse-oximetry.

Remarkably, these NIR-OLEDs have unprecedented $\eta_{EQE(max)}$ values among rare-metal-free NIR-OLEDs, *i.e.*, $\eta_{EQE(max)}$ of 13.4% ± 0.8% in the TADF-OLED and $\eta_{EQE(max)}$ of 1.1% ± 0.2% in the TAF-OLED (**Figure 4-11c**). Notably, the η_{EQE} of the TADF-OLED partially originates from a high light-

outcoupling efficiency (calculated value: 34.5%) owing to horizontal orientation of the transition dipole moment (TDM) of TPA-PZTCN in the co-deposited film (**Figure 4-12**). The spontaneous orientation of the TDM relates to the high aspect ratio of the molecular structure of TPA-PZTCN [28]. Here, I note that TADF-OLEDs employing 1,3,6wt%-TPA-PZTCN-mCBP as an emitting layer also showed significant EL performance in deep-red to NIR region, *i.e.*, $\eta_{EQE(max)}$: 19.3% (EL: 651 nm), $\eta_{EQE(max)}$: 17.7% (EL: 671 nm), and $\eta_{EQE(max)}$: 15.8% (EL: 712 nm), respectively (**Figure 4-13**). Importantly, our NIR-OLED had well-suppressed EL efficiency roll-off behavior compared with those in the previous reports [5,8,9,10,11,13,15,16,17], *i.e.*, η_{EQE} > 10% even at > 1 mA/cm^2. This is not only because of well-balanced charge transport in the OLED but also because of the high k_{RISC} of TPA-PZTCN, which reduces the accumulated triplet density at the high current density region and suppresses triplet-related deactivation processes such as singlet-triplet, triplet-polaron, and triplet-triplet annihilations [22,29,30,31]. Note that the η_{EQE} of TAF-OLED might still be improved. The maximum theoretically predicted η_{EQE} is 2.6%, but the experimental value was limited to 1.1%. This result might be attributed to electron trapping caused by the narrow energy gap of BBT-TPA, leading to direct carrier recombination on the BBT-TPA molecules. This result might be overcome by selection of a proper host material.

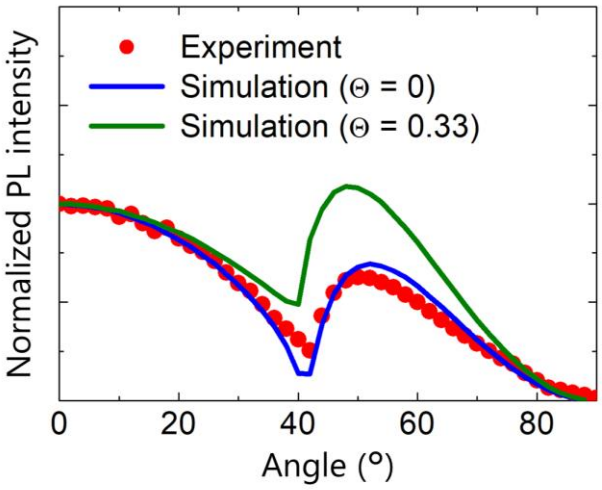

Fig. 4-12. Angle-dependent PL measurement for the 10wt%-TPA-PZTCN-mCBP film. Experimental data (red dot) is in good agreement with the simulational curve corresponding to the horizontal transition dipole orientation of TPA-PZTCN (blue solid line).

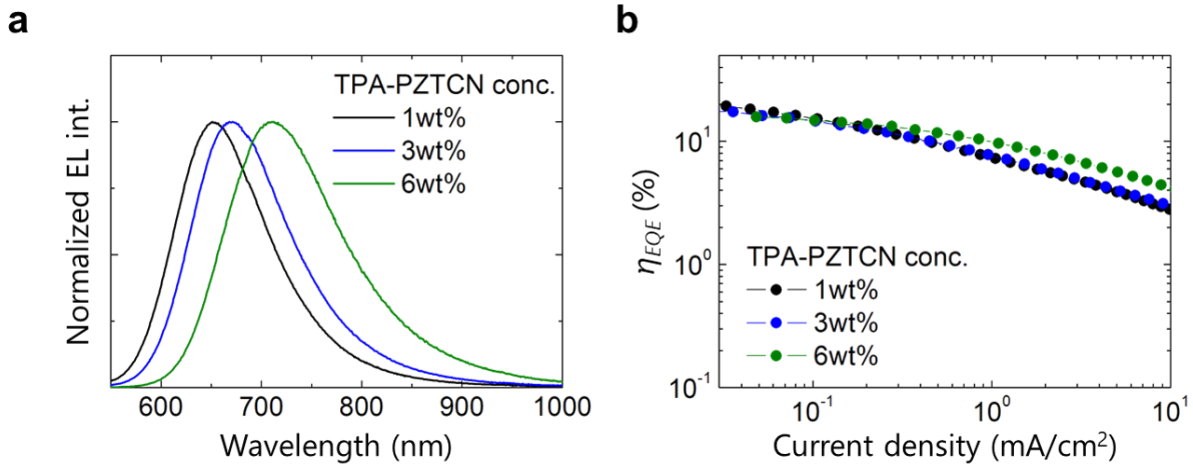

Fig. 4-13. a) EL spectra of the devices with different doping concentration of TPA-PZTCN (black: 1wt%, blue: 3wt%, green: 6wt%) at a current density of 10 mA cm^{-2}. b) External EL quantum efficiency as a function of current density.

In addition, as shown in **Figure 4-11d**, the 10wt%-TPA-PZTCN-mCBP based TADF-OLED exhibited a long device operational lifetime of LT95 = 168 h (operation current density of 10 mA/cm^2, corresponding to an output power of 0.9 mW/cm^2). This long device operational lifetime might originate from reduction of reactive higher-lying triplet excitons [32] in addition to the efficient RISC process in TPA-PZTCN. Furthermore, the 1wt%-BBT-TPA-10wt%-TPA-PZTCN-mCBP based TAF-OLED exhibited a long device operational lifetime of LT95 > 600 hours (operation current density of 10 mA/cm^2, corresponding to an output power of 0.1 mW/cm^2) owing to rapid RISC in TPA-PZTCN and efficient FRET for the fluorescent emitter with a stable aromatic skeleton, leading to a further reduction of chemically unstable triplet excitons [31].

Finally, the finger photoplethysmographic (PPG) sensing was performed using our developed NIR-TADF-OLEDs integrated with a conventional organic photodiode (OPD) [33,34] (**Figure 4-14a**). The OPD fabricated here showed a high EQE of more than 8.3% at 700 ~ 900 nm and high specific detection ability of about 10^{11} ~ 10^{12} Jones in operation at 0 V (**Figure 4-14b**, **Figure 4-14c**). As shown in **Figure 4-14d**, a change in the intensity of scattered or reflected light was observed in the case of both NIR-TADF-OLED (EL: 734 nm) and NIR-TAF-OLED (EL: 901 nm), indicating that "all-organic" PPG using dual NIR-wavelength were successfully performed.

In summary, I designed and synthesized TPA-PZTCN, which exhibits efficient TADF through the use of PZTCN as a rigid and strong electron-withdrawing core, and demonstrated its triplet-harvesting ability and the energy-sensitizing ability for deep-NIR-fluorophore. The fabricated NIR-OLEDs has one of the highest $\eta_{EQE(max)}$ of 13.4% (EL: 734 nm) and 1.1% (EL: 901 nm) among reported rare-metal-free NIR-OLEDs, with well suppressed roll-off behavior and the long device operational lifetime even in the high current operation. Furthermore, the developed NIR-OLEDs are integrated with an OPD to demonstrate the all-organic PPG sensing at dual NIR-wavelength. Thus, I believe that our proposed design strategy for this NIR-TADF molecule and its application in the deep-NIR-OLEDs will pave the way for the realization of highly sensitive and convenient health management and diagnosis in daily life.

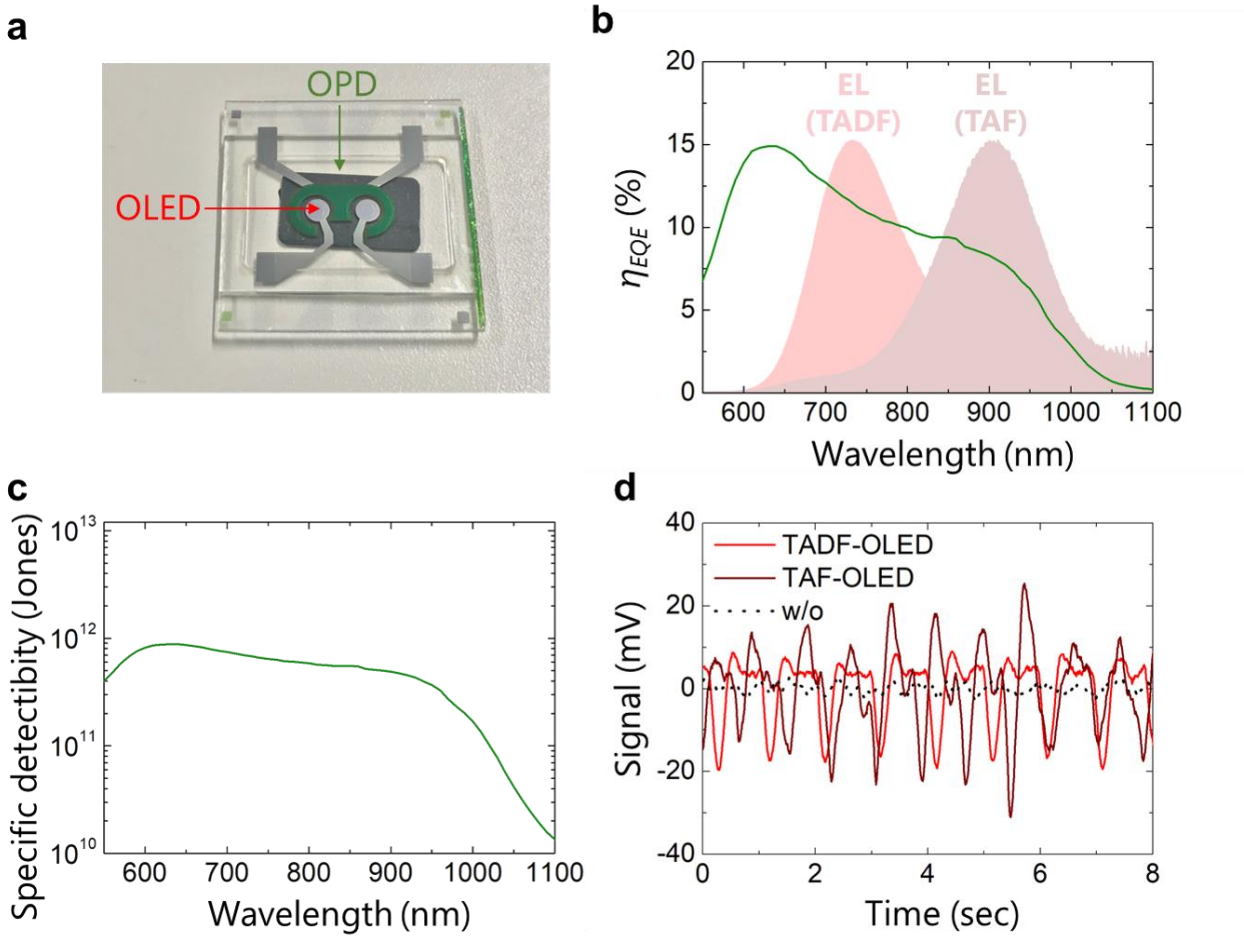

Fig. 4-14. a) Photograph of OLED (red arrow) /OPD (green arrow) integrated devices. b) EQE spectral response at 0 V for the OPD with EL spectra of the OLEDs. c) Calculated specific detectibity spectrum at 0 V for the OPD. d) Finger PPG sensing signals using OLED/OPD integrated devices (red: TADF-OLED, brown: TAF-OLED). Black dashed line indicates the dark current in the measurement system.

4.3 Materials and methods

Synthesis of TPA-PZTCN

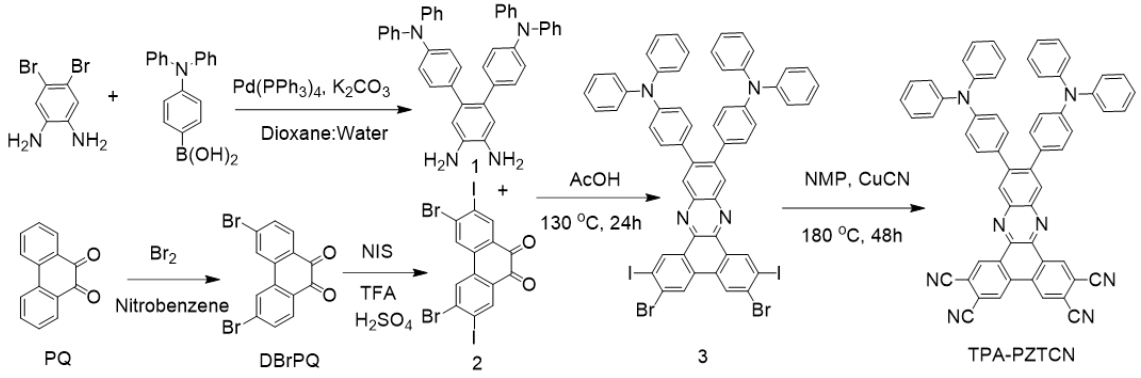

Compound 2 was synthesized according to the reported procedure [35].

N^4,N^4,$N^{4''}$,$N^{4''}$-tetraphenyl-[1,1′:2′,1″-terphenyl]-4,4′,4″,5′-tetraamine (1):

4,5-Dibromobenzene-1,2-diamine (1.33 g, 5.0 mmol) and (4-(diphenylamino)phenyl)boronic acid (3.47 g, 12 mmol), K_2CO_3 (2.76 g, 20 mmol), and $Pd(PPh_3)_4$ (116 mg, 0.1 mmol) were added in a 100 mL mixture of 1,4-dioxane and water (10/1, v/v) under nitrogen. The solution was stirred for 24 h at 90 °C, cooled down to room temperature, poured into 100 mL of water, and then extracted with dichloromethane (DCM). The obtained layer was evaporated under reduced pressure and further purified via column chromatography using n-hexane and ethyl acetate (2/1, v/v) as the eluent to afford a white solid (2.32 g, 78%). ^{1}H NMR (500 MHz, DMSO-*d*$_6$, 300 K): δ/ppm = 7.23 (dd, J = 8.0 Hz, J = 7.5 Hz, 8H), 6.99 (t, J = 7.5 Hz, 4H), 6.95 (d, J = 8.0 Hz, 8H), 6.93 (d, J = 8.5 Hz, 4H), 6.83 (d, J = 8.5 Hz, 4H), 6.58 (s, 2H), 4.61 (s, 4H; NH_2). ^{13}C NMR (125 MHz, DMSO-*d*$_6$, 300 K): δ/ppm = 147.27, 144.46, 137.35, 134.44, 130.54, 129.36, 128.56, 123.44, 123.23, 122.52, 115.94. ASAP-MS: m/z: calculated for $C_{42}H_{34}N_4$: 594.76; found: 594.56.

^{1}H NMR spectra of compound 1 (500 MHz, DMSO-d_6, 300 K)

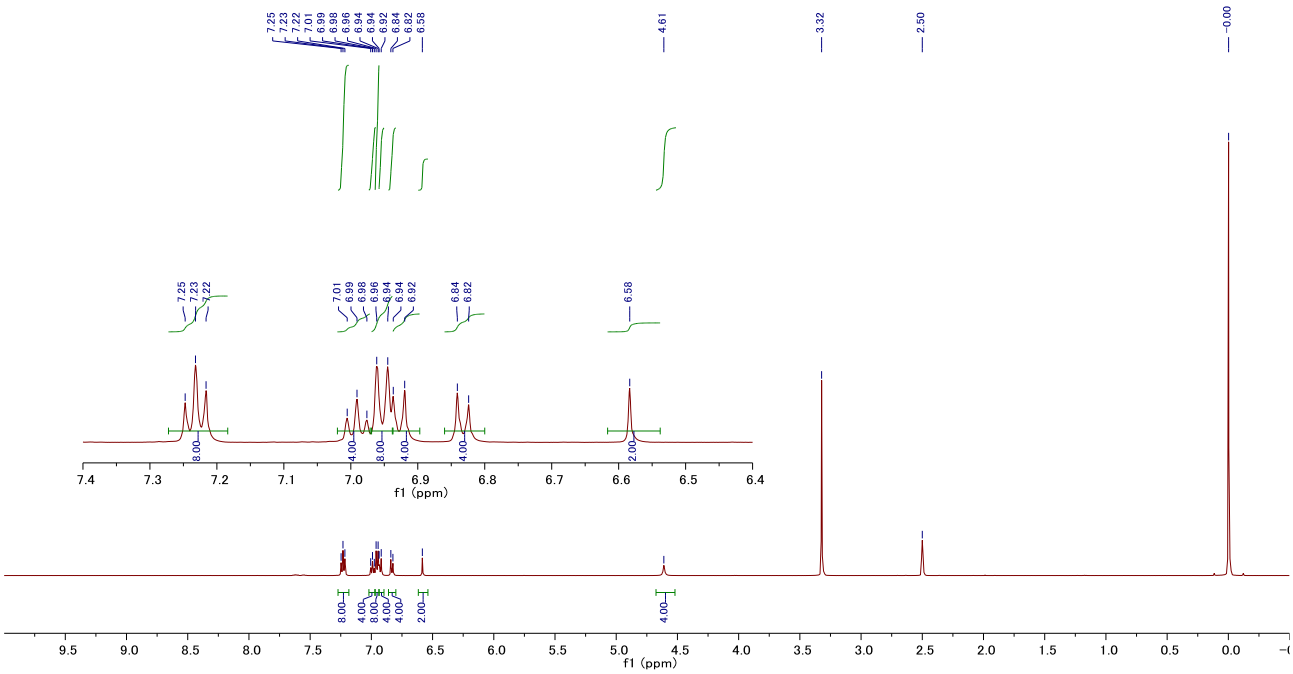

^{13}C NMR spectra of compound 1 (125 MHz, DMSO-d_6, 300 K)

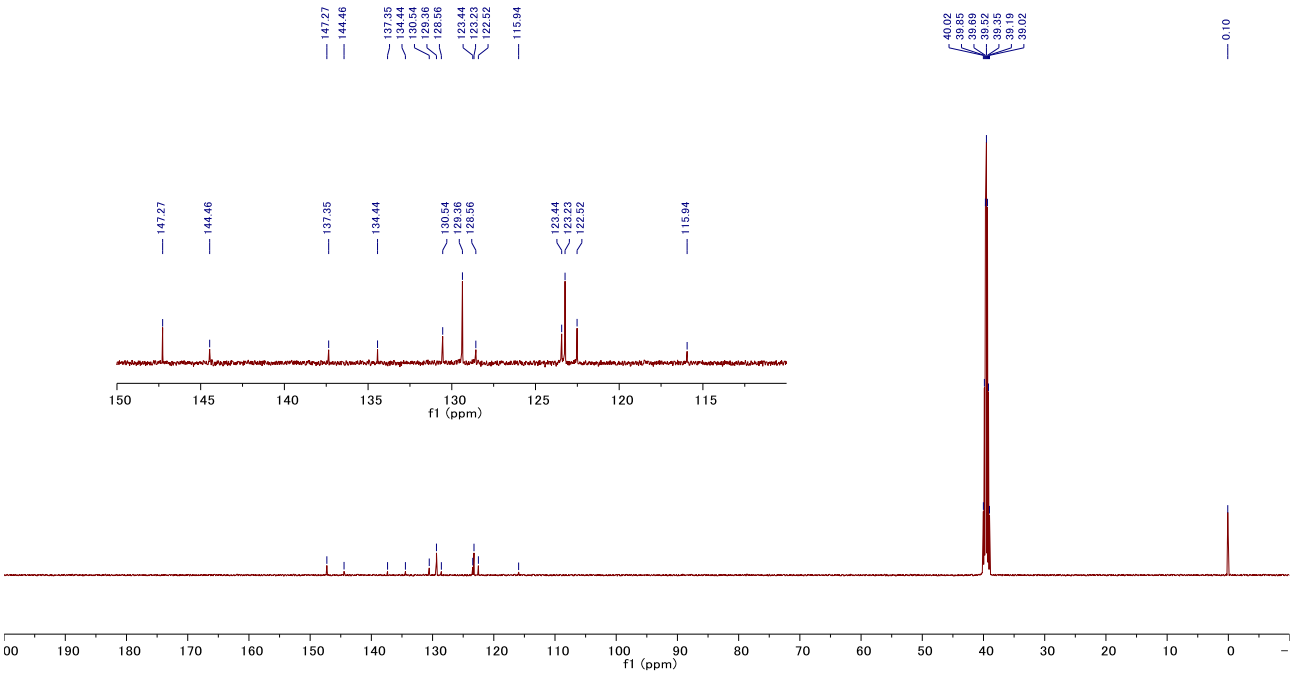

ASAP-MS spectra of compound 1

4,4′-(3,6-dibromo-2,7-diiododibenzo[a,c]phenazine-11,12-diyl)bis(N,N-diphenylaniline) (3):

Compound 1 (1.15 g, 1.94 mmol), 3,6-dibromo-2,7-diiodophenanthrene-9,10-dione (2) (1.0 g, 1.62 mmol) were added to 250 mL of AcOH under nitrogen. The solution was stirred for 24 h at 125 °C, after completion of reaction, the mixture was cooled down to room temperature, and mixed with ice water. The obtained solid was filtered under reduced pressure and washed with methanol followed by recrystallization in chloroform to obtain a deep red solid (crude: 1.71 g, 90 %). ^{1}H NMR (500 MHz, $CDCl_3$, 300 K): δ/ppm = 9.77 (s, 2H), 8.62 (s, 2H), 8.33 (s, 2H), 7.28 (dd, J = 8.0 Hz, 8H), 7.21 (d, J = 8.5 Hz, 4H), 7.14 (d, J = 8.0 Hz, 8H), 7.06 (t, J = 8.5 Hz, 4H), 7.04 (d, J = 8.0 Hz, 4H). ^{13}C NMR could not be taken due to the low solubility. MALDI-TOF-MS: m/z: calculated for $C_{56}H_{34}Br_2I_2N_4$: 1176.53; found: 1177.05.

^{1}H NMR spectra of compound 3 (500 MHz, $CDCl_3$, 300 K)

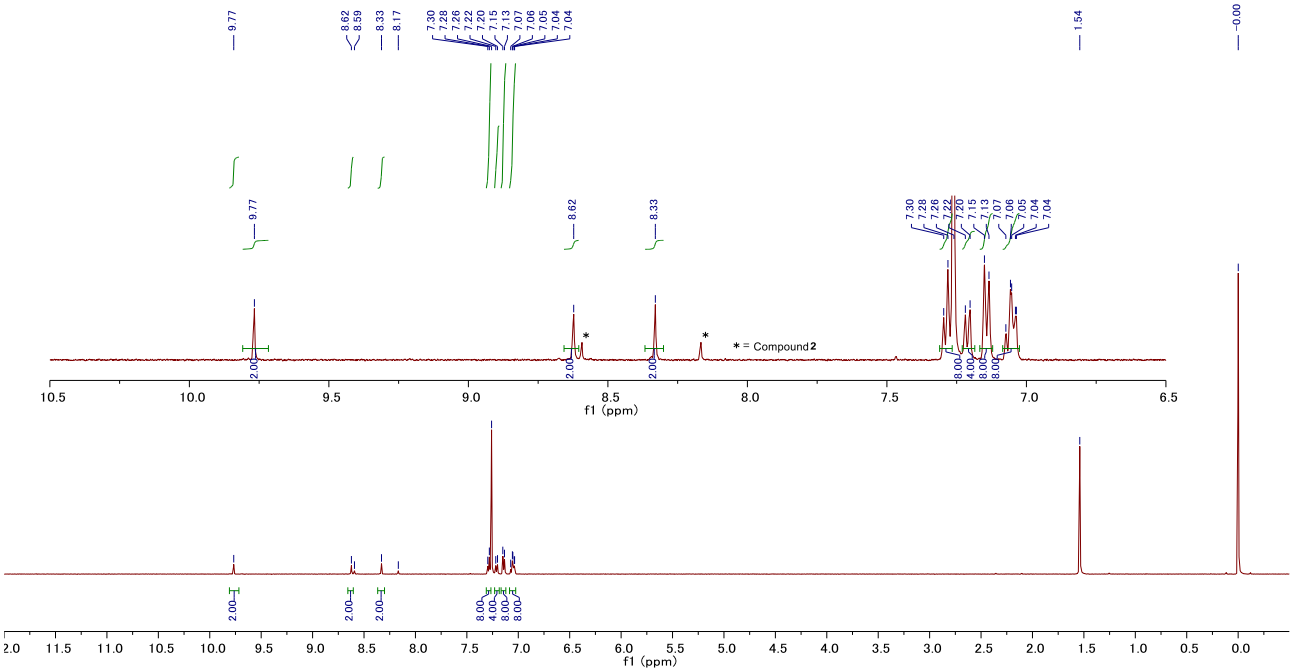

MALDI-TOF-MS spectra of compound 3

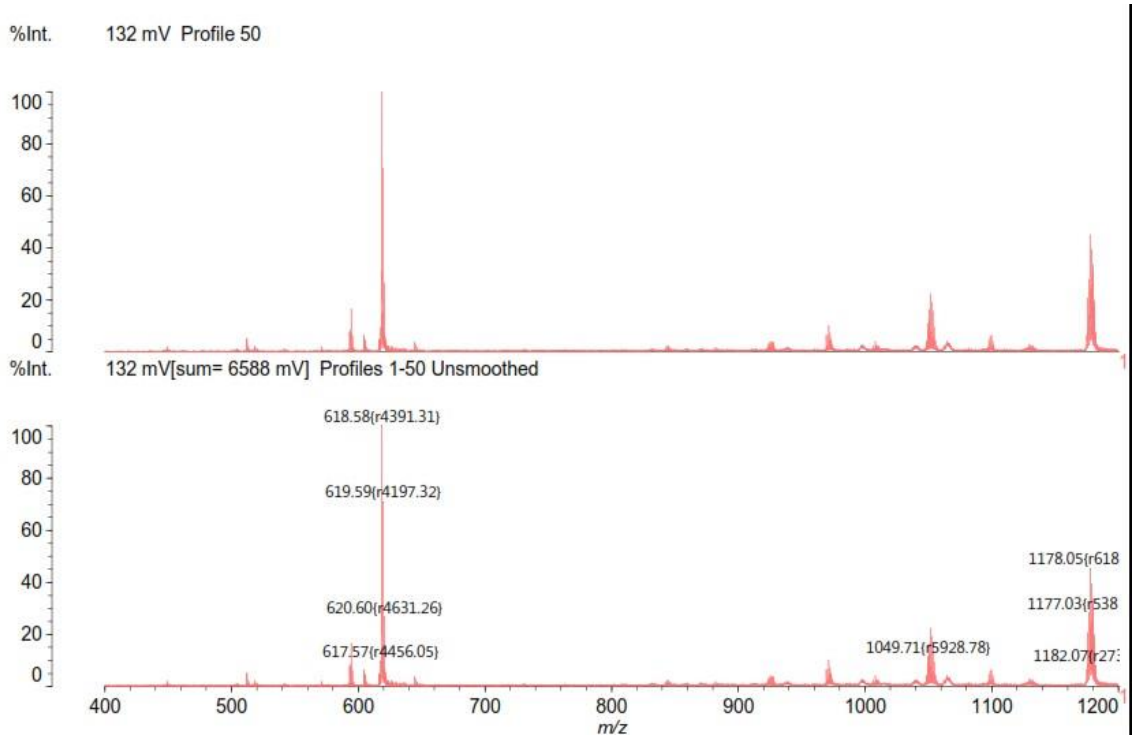

11,12-bis(4-(diphenylamino)phenyl)dibenzo[a,c]phenazine-2,3,6,7-tetracarbonitrile (TPA-PZTCN):

Compound 3 (1.5 g, 1.25 mmol) and CuCN (1.12 g, 12.5 mmol) were added into 150 mL of anhydrous NMP under argon. The mixture was heated at 180 °C for 48 h, the progress of the reaction was monitored by TLC. After the completion of reaction, the mixture was cooled to room temperature, added 500 ml of 2% aqueous ammonia solution followed by extraction with 150 ml of Toluene (3 × 50 mL), washed by water, and dried over $MgSO_4$. The obtained product was further purified via column chromatography using toluene and chloroform (9/1, v/v) as the eluent to yield TPA–PZTCN as a dark blue solid (820 mg, 76 %). ^{1}H NMR (500 MHz, $CDCl_3$, 300 K): δ/ppm = 9.96 (s, 2H), 9.00 (s, 2H), 8.44 (s, 2H), 7.30 (dd, J = 7.5 Hz, 8H), 7.22 (d, J = 8.0 Hz, 4H), 7.16 (d, J = 8.0 Hz, 8H), 7.09 (t, J = 7.5 Hz, 4H), 7.06 (d, J = 8.0 Hz, 4H). ^{13}C NMR (125 MHz, $CDCl_3$, 300 K): δ/ppm = 148.15, 147.44, 147.31, 143.18, 139.37, 134.96, 132.89, 132.68, 131.43, 130.86, 129.81, 129.61, 125.15, 123.75, 122.27, 116.18, 116.04, 115.16. MALDI-TOF-MS: m/z: calculated for $C_{60}H_{34}N_8$: 866.9880; found: 867.25. Anal. calcd for $C_{60}H_{34}N_8$: C 83.12, H 3.95, N 12.92; found: C 83.04, H 3.95, N 12.84.

^{1}H NMR spectra of TPA-PZTCN (500 MHz, $CDCl_3$, 300 K)

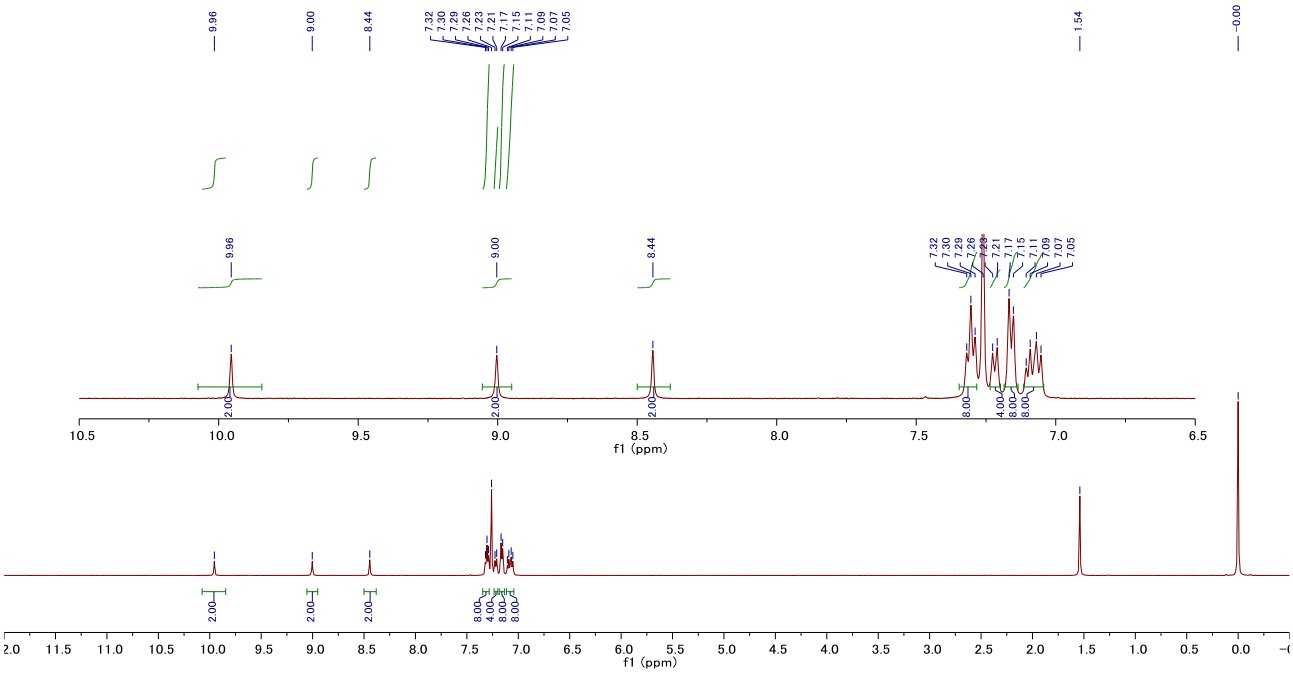

^{13}C NMR spectra of TPA-PZTCN (125 MHz, $CDCl_3$, 300 K)

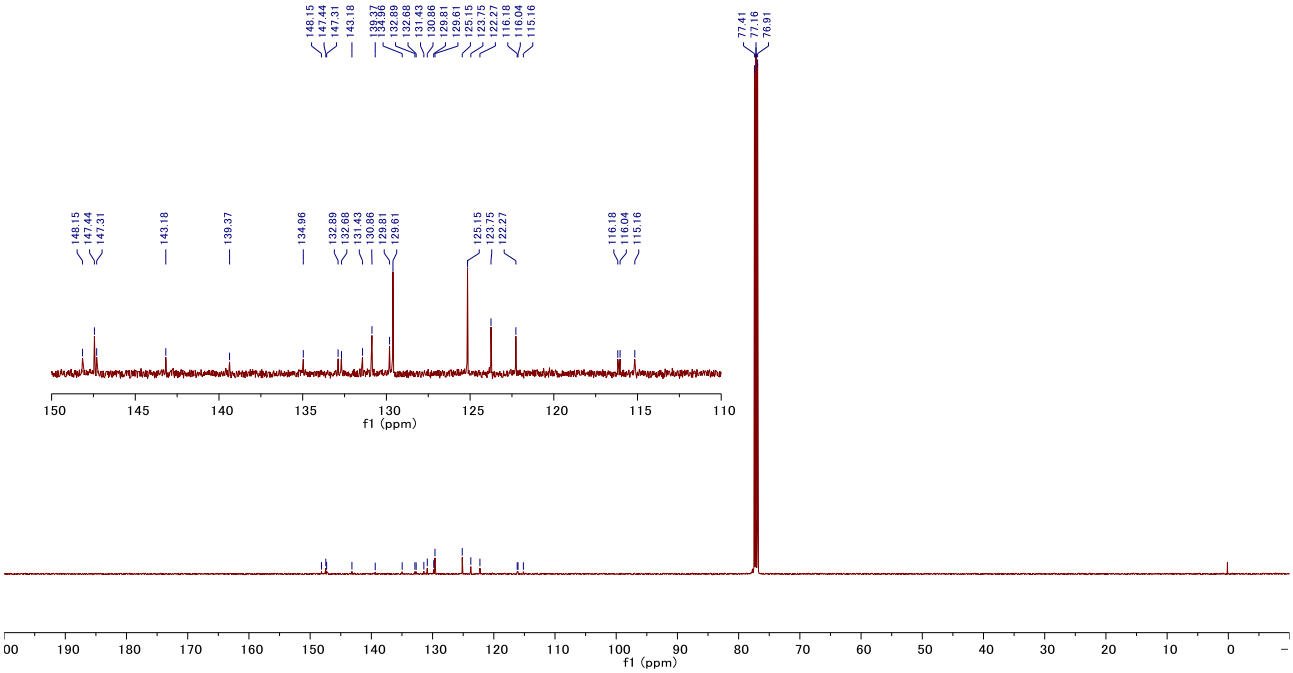

MALDI-TOF-MS spectra of TPA-PZTCN

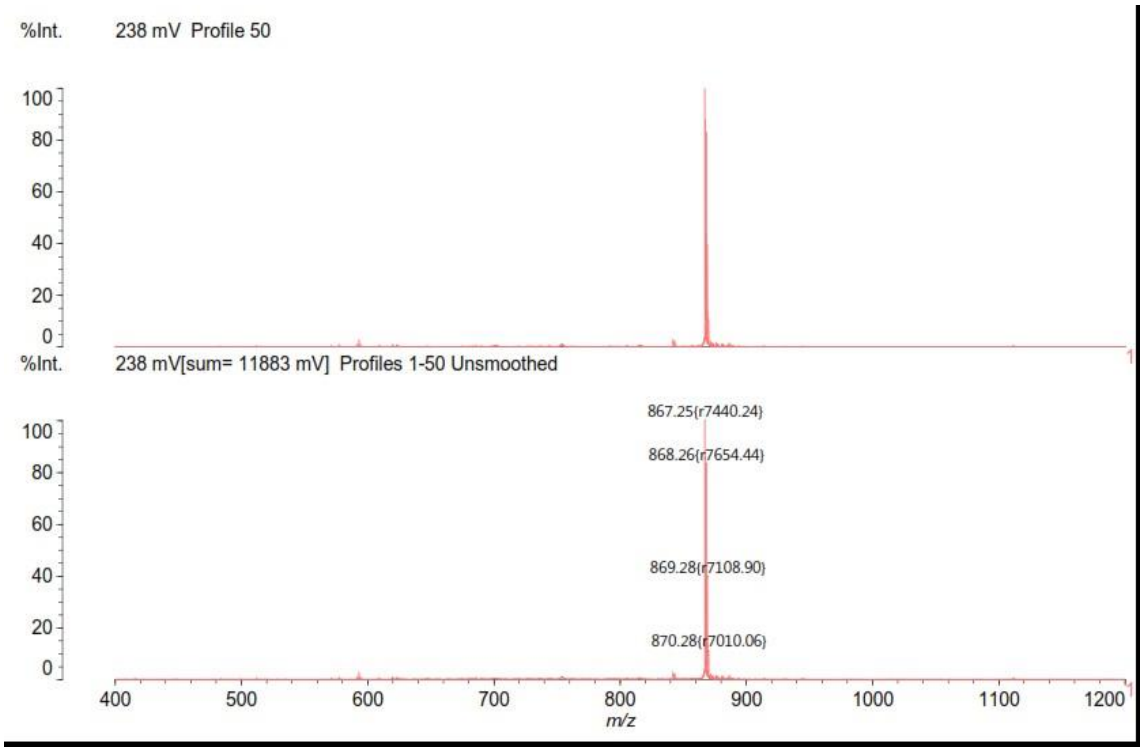

Materials

4,4'-Cyclohexylidenebis[N,N-bis(4-methylphenyl)benzenamine] (TAPC), 2,3,6,7,10,11-hexacyano-1,4,5,8,9,12-hexaazatriphenylene (HATCN), 8-hydroxyquinolinolato-lithium (Liq) and lead(II) phthalocyanine (PbPc) were purchased from Luminescence Technology Corp. Copper(I) iodide (CuI) was purchased from FUJIFILM Wako Pure Chemical Corp. Fullerene (C_{60}), and bathocuproine (BCP) were purchased from Tokyo Chemical Industry Co., Ltd. The OLED materials, 4,8-bis[4-(N,N-diphenylamino)phenyl]benzo[1,2-c:4,5-c']bis[1,2,5]thiadiazole (BBT-TPA), 3,3'-bis(9-carbazolyl)-1,1'-biphenyl (mCBP), 2,4,6-tris(biphenyl-3-yl)-1,3,5-triazine (T2T) and 2,7-bis(2,2'-bipyridine-5-yl)triphenylene (BPy-TP2) were synthesized in house. Before fabrication of the OLEDs and OPDs, each powders were purified repeatedly by a train sublimation with a thermal gradient under a base pressure of less than 5×10^{-3} Pa.

Sample preparation

Organic solid-state films with a thickness of 100 nm for PL measurements were deposited on quartz substrates by thermal evaporation. Vacuum deposition was performed under vacuum at pressures of below 5×10^{-4} Pa. For OLED fabrication, glass substrates with a pre-patterned, 100-nm-thick tin-doped indium oxide (ITO) coating as anode were used. Substrates were washed by sequential ultrasonication in neutral detergent, distilled water, acetone, and isopropanol and then exposed to UV-ozone (NL-UV253, Nippon Laser & Electronics Lab.) to remove adsorbed organic species. After pre-cleaning the substrates, effective device areas of 1 mm^2 were defined on the patterned-ITO substrates by a polyimide insulation layer using a conventional photolithography technique. Organic layers were formed by thermal evaporation. An OLED with a NIR-TADF sensitizer and a fluorescent emitter is as follows: HATCN (10 nm) / TAPC (20 nm) / 1wt%-BBT-TPA-10wt%-TPA-PZTCN-mCBP (60 nm) / T2T (10 nm) / BPy-TP2 (50 nm) / Liq (2 nm) / Al (100 nm). The corresponding energy diagram of the OLED and the chemical structures of materials used in the OLEDs are described below. For the on-chip integrated devices for PPG sensing, ITO patterns were fabricated by photolithography, polyimide insulator films were formed on the ITO patterns, and then OLEDs and an OPD were fabricated by vacuum deposition. An OPD was fabricated using a reported device structure [28] combined with hole-blocking layer [29]: CuI (4 nm) / PbPc (60 nm) / C_{60} (60 nm) / T2T (6 nm) / BCP (6 nm) / Al (100 nm). After the fabrication, devices were immediately encapsulated with glass lids using epoxy glue in a nitrogen-filled glove box ($O_2 < 0.1$ ppm, $H_2O < 0.1$ ppm). Commercial calcium oxide desiccant (Dynic Co.) was included in each encapsulated package.

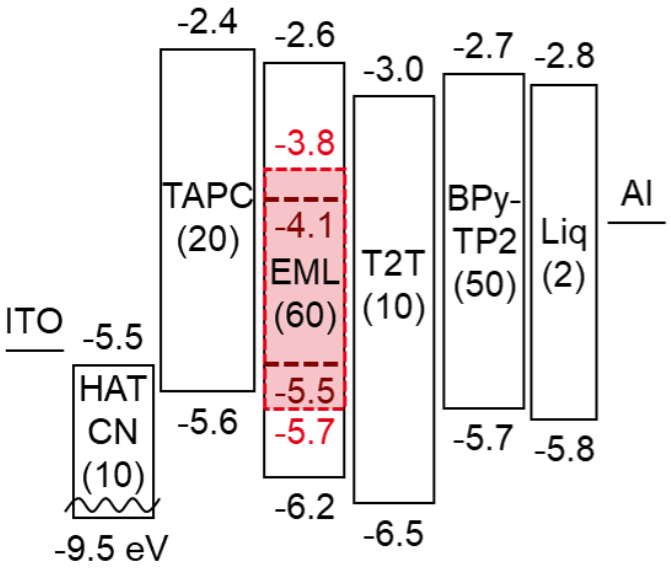

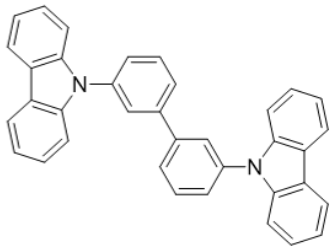

mCBP (EML host)

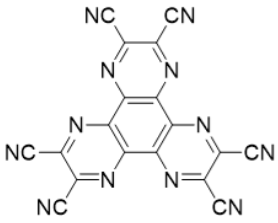

HATCN

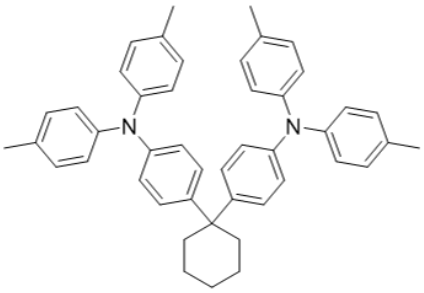

TAPC

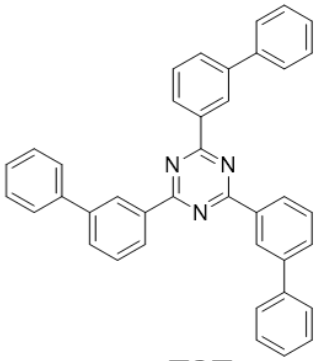

T2T

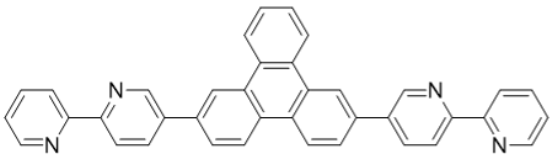

BPy-TP2

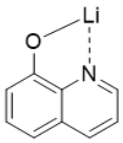

Liq

Optical characterization of organic thin films

The ground-state absorption spectra were measured using a spectrophotometer (LAMBDA950-PKA, PerkinElmer). The steady-state PL spectra were measured using a multichannel spectrofluorometer (FP-8600, JASCO). The PL quantum yield was measured using an absolute PL quantum yield measurement system (C13534-21, Hamamatsu Photonics) under the flow of argon gas with an excitation wavelength of 340 nm. The transient PL decay curves were obtained under Ar flow using a fluorescence lifetime spectrometer (C11367, Hamamatsu Photonics). The temperature dependence of transient PL spectra were obtained under vacuum condition using a streak camera (C10910, Hamamatsu Photonics), a Nd:YAG laser (PL2250, EKSPLA) as an excitation source with an excitation wavelength of 355 nm, and a cryostat (PS-HT-200, Nagase Techno-Engineering). The angle-dependent PL spectra and intensities were measured using a molecular orientation measurement system (C13472, Hamamatsu Photonics) and a multichannel spectrophotometer (C10027-01, Hamamatsu Photonics). The optical simulation of transition dipole orientation in co-deposited film and light-outcoupling efficiency of the TADF-OLED were performed using simulation software (Setfos, Fluxim).

Characterization of OLEDs

The current density–voltage–radiant flux characteristics of the OLEDs were measured using a semiconductor parameter analyzer (E5273A, Agilent Technologies) and a calibrated Si photodetector and an InGaAs photodetector (818-IG-L, Newport) connected to an optical power meter (1930C, Newport). The EL spectra of the OLEDs also measured using a multichannel spectrophotometer (C10027-02, Hamamatsu Photonics). The operational device lifetime of the TADF-OLEDs was obtained using a lifetime measurement system (EAS-26B, System Engineers), and that of TAF-OLEDs were obtained using a sourcemeter (2400, Keithley) and a multichannel spectrophotometer (C10028-01, Hamamatsu Photonics). For PPG sensing, a finger is placed on OLED/OPD integrated devices, and the time variation of scattered and reflected light intensity was processed by a detecting

circuit and an oscilloscope (DSO5034A, Agilent Technologies). All measurements were performed at room temperature.

DFT calculations

The computational studies were conducted using the computer facilities at the Research Institute for Information Technology, Kyushu University. The ground-state (S_0) geometry of TPA-PZTCN was optimized at the B3LYP/6-311+G(d) level using Gaussian 09, and the time-dependent DFT (TD-DFT) calculations were conducted at the B3LYP/6-311+G(d) level for the excited state calculation using the S_0 geometry. The overlap integral of natural transition orbitals (NTOs) in each excited state was calculated using the program Multiwfn [36].

Electrochemical characterization

Cyclic voltammetry (CV) was measured using CHI600 voltammetric analyzer at room temperature with a conventional three-electrode configuration consisting of a platinum disk working electrode, a platinum wire auxiliary electrode and an Ag wire pseudo-reference electrode with ferrocenium–ferrocene (Fc^+/Fc) as the internal standard. Argon purged dichloromethane was used as solvent for scanning the oxidation with tetrabutylammonium hexafluorophosphate ($TBAPF_6$) (0.1 M) as the supporting electrolyte. The cyclic voltammograms were obtained at a scan rate of 100 mV s^{-1}. The HOMO and LUMO levels are calculated to be –5.66 eV and –3.84 eV, respectively, by using HOMO (eV) = –e (E_{ox} + 5.1 V) and LUMO (eV) = –e (E_{red} + 5.1 V) [37].

References

1. M. A. Baldo, D. F. O'Brien, M. E. Thompson, S. R. Forrest, Excitonic singlet-triplet ratio in a semiconducting organic thin film. *Phys. Rev. B* **60**, 14422 (1999)

2. K. T. Ly, R. W. C. Cheng, H. W. Lin, Y. J. Shiau, S. H. Liu, P. T. Chou, C. S. Tsao, Y. C. Huang, Y. Chi, Near-infrared organic light-emitting diodes with very high external quantum efficiency and radiance. *Nat. Photon.* **11**, 63 (2017)

3. K. R. Graham. Y. Yang, J. R. Sommer, A. H. Shelton, K. S. Schanze, J. Xue, J. R. Reynolds, Extended Conjugation Platinum(II) Porphyrins for use in Near-Infrared Emitting Organic Light Emitting Diodes. *Chem. Mater.* **23**, 5305 (2011)

4. H. Uoyama, K. Goushi, K. Shizu, H. Nomura, C. Adachi, Highly efficient organic light-emitting diodes from delayed fluorescence. *Nature* **492**, 234 (2012)

5. S. Wang, X. Yan, Z. Cheng, H. Zhang, Y. Liu, Y. Wang, Highly Efficient Near-Infrared Delayed Fluorescence Organic Light Emitting Diodes Using a Phenanthrene-Based Charge-Transfer Compound. *Angew. Chem. Int. Ed.* **127**, 13260 (2015)

6. T. Yamanaka, H. Nakanotani, S. Hara, T. Hirohata, C. Adachi, Near-infrared organic light-emitting diodes for biosensing with high operating stability. *Appl. Phys. Express* **10**, 074101 (2017)

7. J. Brodeur, L. Hu, A. Malinge, E. Eizner, W. G. Skene, S. K. Cohen, Highly Efficient and Spectrally Narrow Near-Infrared Fluorescent OLEDs Using a TADF-Sensitized Cyanine Dye. *Adv. Opt. Mater.* **7**, 1901144 (2019)

8. Y. Yuan, Y. Hu, Y. X. Zhang, J. D. Lin, Y. K. Wang, Z. Q. Jiang, L. S. Liao, S. T. Lee, Over 10% EQE Near-Infrared Electroluminescence Based on a Thermally Activated Delayed Fluorescence Emitter. *Adv. Funct. Mater.* **27**, 1700986 (2017)

9. J. Xue, Q. Liang, R. Wang, J. Hou, W. Li, Q. Peng, Z. Shuai, J. Qiao, Highly Efficient Thermally Activated Delayed Fluorescence via J-Aggregates with Strong Intermolecular Charge Transfer. *Adv. Mater.* **31**, 1808242 (2019)

10. D. G. Congrave, B. H. Drummond, P. J. Conaghan, H. Francis, S. T. E. Jones, C. P. Grey, N. C. Greenham, D. Credgington, H. Bronstein, A Simple Molecular Design Strategy for Delayed Fluorescence toward 1000 nm. *J. Am. Chem. Soc.* **141**, 18390 (2019)

11. Q. Liang, J. Xu, J. Xue, J. Qiao, Near-infrared-II thermally activated delayed fluorescence organic light-emitting diodes. *Chem. Commun.* **56**, 8988 (2020)

12. Y. L. Zhang, Q. Ran, Q. Wang, Y. Liu, C. Hänisch, S. Reineke, J. Fan, L. S. Liao, High-Efficiency Red Organic Light-Emitting Diodes with External Quantum Efficiency Close to 30% Based on a Novel Thermally Activated Delayed Fluorescence Emitter. *Adv. Mater.* **31**, 1902368 (2019)

13. C. Li, R. Duan, B. Liang, G. Han, S. Wang, K. Ye, Y. Liu, Y. Yi, Y. Wang, Deep-Red to Near-Infrared Thermally Activated Delayed Fluorescence in Organic Solid Films and Electroluminescent Devices. *Angew. Chem. Int. Ed.* **56**, 11525 (2017)

14. K. Zhang, J. Liu, Y. Zhang, J. Fan, C. K. Wang, L. Lin, Theoretical Study of the Mechanism of Aggregation-Caused Quenching in Near-Infrared Thermally Activated Delayed Fluorescence Molecules: Hydrogen-Bond Effect. *J. Phys. Chem. C* **123**, 24705 (2019)

15. J. Kumsampao, C. Chaiwai, P. Chasing, T. Chawanpunyawat, S. Namuangruk, T. Sudyoadsuk, V. Promarak, A Simple and Strong Electron-Deficient 5,6-Dicyano[2,1,3]benzothiadiazole-Cored Donor-Acceptor-Donor Compound for Efficient Near Infrared Thermally Activated Delayed Fluorescence. *Chem. Asian J.* **15**, 3029 (2020)

16. D. H. Kim, A. D'Aléo, X. K. Chen, A. D. S. Sandanayaka, D. Yao, L. Zhao, T. Komino, E. Zaborova, G. Canard, Y. Tsuchiya, E. Choi, J. W. Wu, F. Fages, J. L. Bredas, J. C. Ribierre, C. Adachi, High-efficiency electroluminescence and amplified spontaneous emission from a thermally activated delayed fluorescent near-infrared emitter. *Nat. Photon.* **12**, 98 (2018)

17. H. Ye, D. H. Kim, X. Chen, A. S. D. Sandanayaka, J. U. Kim, E. Zaborova, G. Canard, Y. Tsuchiya, E. Y. Choi, J. W. Wu, F. Fages, J. L. Bredas, A. D'Aléo, J. C. Ribierre, C. Adachi, Near-Infrared Electroluminescence and Low Threshold Amplified Spontaneous Emission above 800 nm from a Thermally Activated Delayed Fluorescent Emitter. *Chem. Mater.* **30**, 6702 (2018)

18. A. Shahalizad, A. Malinge, L. Hu, G. Laflamme, L. Haeberlé, D. M. Myers, J. Mao, W. G. Skene, S. K. Cohen, Efficient Solution-Processed Hyperfluorescent OLEDs with Spectrally Narrow Emission at 840 nm. *Adv. Funct. Mater.* 2007119 (2020)

19. R. Englman, J. Jortner, The energy gap law for radiationless transition in large molecules. *Mol. Phys.* **18**, 145 (1970)

20. W. C. Chen, P. T. Chou, Y. C. Cheng, Low Internal Reorganization Energy of the Metal-Metal-to-Ligand Charge Transfer Emission in Dimeric Pt(II) Complexes. *J. Phys. Chem. C* **123**, 10225 (2019)

21. J. Gibson, A. P. Monkman, T. J. Penfold, The Importance of Vibronic Coupling for Efficient Reverse Intersystem Crossing in Thermally Activated Delayed Fluorescence Molecules. *ChemPhysChem* **17**, 2956 (2016)

22. H. Noda, H. Nakanotani, C. Adachi, Excited state engineering for efficient reverse intersystem crossing. *Sci. Adv.* **4**, eaao6910 (2018)

23. H. Noda, X. K. Chen, H. Nakanotani, T. Hosokai, M. Miyajima, N. Notsuka, Y. Kashima, J. L. Brédas, C. Adachi, Critical role of intermediate electronic states for spin-flip processes in charge-transfer-type organic molecules with multiple donors and acceptors. *Nat. Mater.* **18**, 1084 (2019)

24. G. Qian, B. Dai, M. Luo, D. Yu, J. Zhan, Z. Zhang, D. Ma, Z. Y. Wang, Band Gap Tunable, Donor−Acceptor−Donor Charge-Transfer Heteroquinoid-Based Chromophores: Near Infrared Photoluminescence and Electroluminescence. *Chem. Mater.* **20**, 6208 (2008)

25. G. Qian, Z. Zhong, M. Luo, D. Yu, Z. Zhang, Z. Y. Wang, D. Ma, Simple and Efficient Near-Infrared Organic Chromophores for Light-Emitting Diodes with Single Electroluminescent Emission above 1000 nm. *Adv. Mater.* **21**, 111 (2009)

26. H. Nakanotani, T. Higuchi, T. Furukawa, K. Masui, K. Morimoto, M. Numata, H. Tanaka, Y. Sagara, T. Yasuda, C. Adachi, High-efficiency organic light-emitting diodes with fluorescent emitters. *Nat. Commun.* **5**, 4016 (2014)

27. S. Wray, M. Cope, D. T. Delpy, J. S. Wyatt, E. O. R. Reynolds, Characterization of the near infrared absorption spectra of cytochrome aa_3 and haemoglobin for the non-invasive monitoring of cerebral oxygenation. *Biochim. Biophys. Acta.* **933**, 184 (1988)

28. D. Yokoyama, Molecular orientation in small-molecule organic light-emitting diodes. *J. Mater. Chem.* **21**, 19187 (2011)

29. K. Masui, H. Nakanotani, C. Adachi, Analysis of exciton annihilation in high-efficiency sky-blue organic light-emitting diodes with thermally activated delayed fluorescence. *Org. Electron.* **14**, 2721 (2013)

30. C. Murawski, K. Leo, M. C. Gather, Efficiency Roll-Off in Organic Light-Emitting Diodes. *Adv. Mater.* **25**, 6801 (2013)

31. T. Furukawa, H. Nakanotani, M. Inoue, C. Adachi, Dual enhancement of electroluminescence efficiency and operational stability by rapid upconversion of triplet excitons in OLEDs. *Sci. Rep.* **5**, 8429 (2015)

32. J. Lee, C. Jeong, T. Batagoda, C. Coburn, M. E. Thompson, S. R. Forrest, Hot excited state management for long-lived blue phosphorescent organic light-emitting diodes. *Nat. Commun.* **8**, 15566 (2017)

33. X. Wang, H. Li, Z. Su, F. Fang, G. Zhang, J. Wang, B. Chu, X. Fang, Z. Wei, B. Li, W. Li, Efficient organic near-infrared photodetectors based on lead phthalocyanine/C_{60} heterojunction. *Org. Electron.* **15**, 2367 (2014)

34. A. Bilgaiyan, F. Elsamnah, H. Ishidai, C. H. Shim, M. A. B. Misran, C. Adachi, R. Hattori, Enhancing Small-Molecule Organic Photodetector Performance for Reflectance-Mode Photoplethysmography Sensor Applications. *ACS Appl. Electron. Mater.* **2**, 1280 (2020)

35. Y. Shirai, A. J. Osgood, Y. Zhao, Y. Yao, L. Saudan, H. Yang, C. Y. Hung, L. B. Alemany, T. Sasaki, J. F. Morin, J. M. Guerrero, K. F. Kelly, J. M. Tour, Surface-Rolling Molecules. *J. Am. Chem. Soc.* **128**, 4854 (2006)

36. T. Lu, F. Chen, Multiwfn: A multifunctional wavefunction analyzer. *J. Comput. Chem.* **33**, 580 (2012)

37. C. M. Cardona, W. Li, A. E. Kaifer, D. Stockdale, G. C. Bazan, Electrochemical Considerations for Determining Absolute Frontier Orbital Energy Levels of Conjugated Polymers for Solar Cell Applications. *Adv. Mater.* **23**, 2367 (2011)

Chapter 5

Summary and future perspective

5.1 Summary

In this thesis, I aimed to improve the η_{EQE} of NIR-OLEDs, and proposed novel device architectures and material design guidelines for high η_{γ} and high φ_{PL} in the NIR region.

In **Chapter 2**, NIR-OLEDs employing a TADF host matrix were investigated to improve η_{γ} in NIR-OLEDs. Combined with the temperature dependent measurement of the PL intensity, it was found that the efficient RISC process in the TADF host molecule contributes to the enhancement of the NIR-EL that originates from conventional NIR-dye, leading to a sixfold larger η_{EQE} than that of non-TADF host based OLEDs. The TADF material was also shown to be useful as a bipolar host material for low driving voltage in OLEDs.

In **Chapter 3**, the exploitation of a singlet fission process was demonstrated for the first time in OLEDs research to further boost η_{γ}. The magnetic field dependence of the visible and NIR luminescence intensities clearly indicated that the triplet exciton generated by the singlet fission process contributes to the enhancement of the NIR-EL, resulting in the η_{γ} of over 100%.

In **Chapter 4**, a novel NIR-TADF molecule, TPA-PZTCN, was developed to improve η_{EQE} and suppress roll-off in NIR-OLEDs. TPA-PZTCN showed intense NIR emission (PL: 729 nm, φ_{PL}: 40.8%) and efficient RISC process (k_{RISC}: 7.6×10^4 s^{-1}), and it was found that TPA-PZTCN acts as a TADF assisting dopant for a NIR fluorescent molecule with longer emission wavelength. Using significant triplet harvesting ability of TPA-PZTCN, NIR-TADF-OLED (EL: 734 nm, η_{EQE}: 13.4%), and NIR-TAF-OLED (EL: 901 nm, η_{EQE}: 1.1%) with suppressed roll-off and long device operating lifetime were achieved. I also demonstrated that the NIR-OLEDs could be combined with a NIR-OPDs to realize all-organic PPG sensing at two wavelengths.

I summarize the obtained EQE and EL spectrum in **Figure 5-1**. I successfully achieved intensive NIR-EL in the wide NIR range of 700~1500 nm by applying exciton harvesting and multiplication mechanisms and a novel rigid molecular framework for NIR-OLEDs.

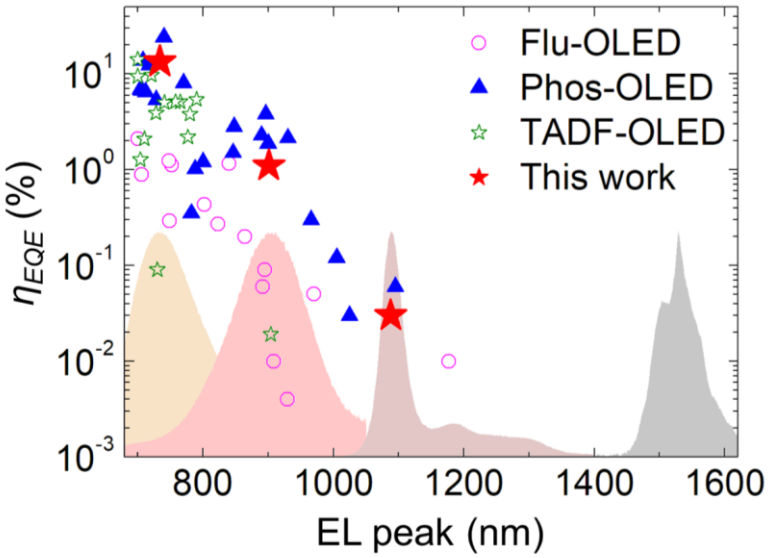

Fig. 5-1. The η_{EQE} and EL spectra of tested NIR-OLEDs

5.2. Future perspective

Nevertheless, compared to existing inorganic LEDs [1], quantum dot LEDs [2], perovskite LEDs [3], and phosphorescent OLEDs [4,5], the η_{EQE} values of NIR-SF-OLEDs and NIR-TADF-OLEDs reported in this thesis are still low. Thus, I finally summarize the future perspectives for advanced NIR emitters and NIR-OLEDs (**Figure 5-2**).

In **Chapter 3**, I demonstrated EL via singlet fission, and this can be seen as the first step toward the realization of an ultimate η_γ of 200% under electrical excitation. Although spin-statistics rules would still limit the theoretical η_γ to 125% in the presented system, an η_γ of 200% could be possible by first converting all of the electrically generated excitons to singlets. In fact, our group previously reported the harvesting of triplet excitons as delayed fluorescence by using resonant energy transfer from molecules exhibiting TADF to fluorescent emitters [6,7]. Thus, a path to an η_γ of 200% exists through the combination of TADF molecules to produce singlet excitons, singlet-fission sensitizers

to double the number of excitons while converting them to triplets, and NIR phosphors (not only organometallic complexes but also nanocrystals) to emit light from the triplets.

In addition, to further improve the φ_{PL} of NIR emitters, the suppression of the non-radiative deactivation processes is essential. A recent study on NIR phosphorescent materials based on platinum complexes have revealed that the energy gap law can be circumvented by reducing the reorganization energy based on "exciton delocalization" [8]. The key point of this concept is that effective reorganization energy (λ_{eff}) is reduced by the delocalization of one exciton on some molecules, as λ_{eff} is expressed by $\lambda_{eff} = \lambda / N$ (N: the number of molecules). So far, there are no reports focusing on TADF aggregates to achieve exciton delocalization for the enhancement of φ_{PL}. For D-A type TADF materials with large permanent dipole moment, however, exciton dissociation due to spontaneous orientation polarization inside the film has been reported [9,10]. Therefore, the development of non-polar TADF materials beyond D-A type is also required.

Here I note that, in addition to the enhancement in φ_{PL}, TADF aggregates are simultaneously beneficial for the reduction of driving voltage in NIR-OLEDs. So far, the high driving voltage of NIR-OLEDs, mainly caused by the charge trapping on guest molecules in the host-guest EML, have been one of the huge barrier for practical applications. Therefore, TADF aggregates are advantageous, because they potentially have bipolar charge-transporting ability [11,12] and do not require any host-guest system. This bipolar charge-transport of TADF aggregates is also beneficial for NIR-OLEDs, which require thicker film than that for visible OLEDs, due to the wavelength dependence of the light outcoupling efficiency [13]. Thus, I believe non-polar NIR-TADF aggregates would be one of the promising system for the enhancement of φ_{PL}, while maintaining the unity of γ and η_{γ} in NIR-OLEDs and decreasing the driving voltage.

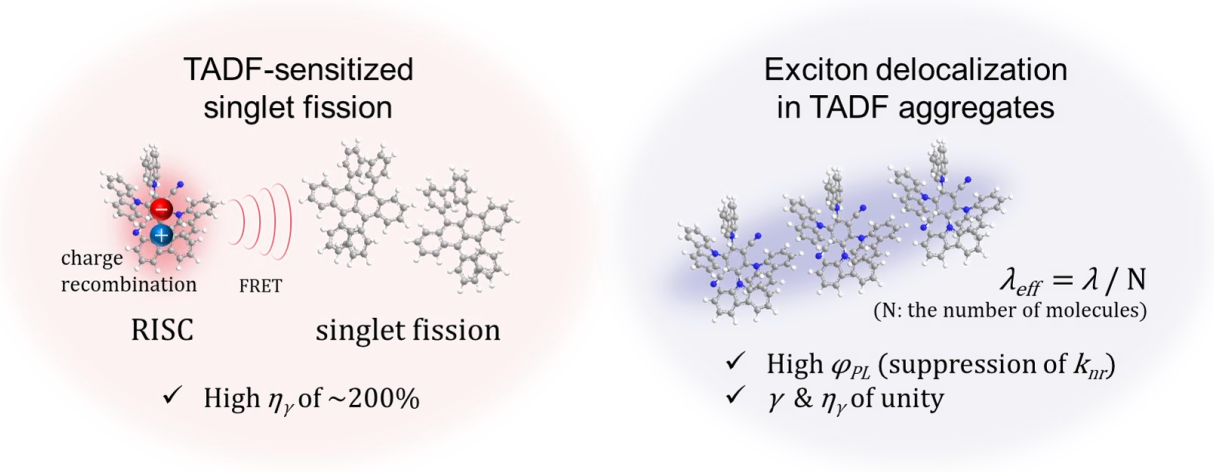

Fig. 5-2. Future perspective for high-efficiency NIR-OLEDs

Reference

1. J. Blondelle, H. D. Neve, P. Demeester, P. V. Daele, G. Borghs, R. Baets, 16% external quantum efficiency from planar microcavity LEDs at 940nm by precise matching of cavity wavelength. *Electron. Lett.* **31**, 1286 (1995)

2. M. Vasilopoulou, H. P. Kim, B. S. Kim, M. Papadakis, A. E. X. Gavim, A. G. Macedo, W. J. D. Silva, F. K. Schneider, M. A. M. Teridi, A. G. Coutsolelos, A. R. B. M. Yusoff, Efficient colloidal quantum dot light-emitting diodes operating in the second near-infrared biological window. *Nat. Photon.* **14**, 50 (2020)

3. W. Xu, Q. Hu, S. Bai, C. Bao, Y. Miao, Z. Yuan, T. Borzda, A. J. Barker, E. Tyukalova, Z. Hu, M. Kawecki, H. Wang, Z. Yan, X. Liu, X. Shi, K. Uvdal, M. Fahlman, W. Zhang, M. Duchamp, J. M. Liu, A. Petrozza, J. Wang, L. M. Liu, W. Huang, F. Gao, Rational molecular passivation for high-performance perovskite light-emitting diodes. *Nat. Photon.* **13**, 418 (2019)

4. K. T. Ly, R. W. C. Cheng, H. W. Lin, Y. J. Shiau, S. H. Liu, P. T. Chou, C. S. Tsao, Y. C. Huang, Y. Chi, Near-infrared organic light-emitting diodes with very high external quantum efficiency and radiance. *Nat. Photon.* **11**, 63 (2017)

5. K. R. Graham. Y. Yang, J. R. Sommer, A. H. Shelton, K. S. Schanze, J. Xue, J. R. Reynolds, Extended Conjugation Platinum(II) Porphyrins for use in Near-Infrared Emitting Organic Light Emitting Diodes. *Chem. Mater.* **23**, 5305 (2011)

6. H. Nakanotani, T. Higuchi, T. Furukawa, K. Masui, K. Morimoto, M. Numata, H. Tanaka, Y. Sagara, T. Yasuda, C. Adachi, High-efficiency organic light-emitting diodes with fluorescent emitters. *Nat. Commun.* **5**, 4016 (2014)

7. T. Higuchi, H. Nakanotani, C. Adachi, High-Efficiency White Organic Light-Emitting Diodes Based on a Blue Thermally Activated Delayed Fluorescent Emitter Combined with Green and Red Fluorescent Emitters. *Adv. Mater.* **27**, 2019 (2015)

8. Y. C. Wei, S. F. Wang, Y. Hu, L. S. Liao, D. G. Chen, K. H. Chang, C. W. Wang, S. H. Liu, W. H. Chan, J. L. Liao, W. Y. Hung, T. H. Wang, P. T. Chen, H. F. Hsu, Y. Chi, P. T. Chou, Overcoming the energy gap law in near-infrared OLEDs by exciton–vibration decoupling. *Nat. Photon.* **14**, 570 (2020)

9. T. Yamanaka, H. Nakanotani, C. Adachi, Slow recombination of spontaneously dissociated organic fluorophore excitons. *Nat. Commun.* **10**, 5748 (2019)

10. Y. Ueda, H. Nakanotani, T. Hosokai, Y. Tanaka, H. Hamada, H. Ishii, S. Santo, C. Adachi, Role of Spontaneous Orientational Polarization in Organic Donor–Acceptor Blends for Exciton Binding. *Adv. Opt. Mater.* **8**, 2000896 (2020)

11. R. Nagata, H. Nakanotani, C. Adachi, Near-infrared Electrophosphorescence up to 1.1 μm utilizing a Thermally Activated Delayed Fluorescence Molecule as triplet sensitizer, *Adv. Mater.* **29**, 1604265 (2017)

12. N. B. Kotadiya, P. W. M. Blom, G. J. A. H. Wetzelaer, Efficient and stable single-layer organic light-emitting diodes based on thermally activated delayed fluorescence. *Nat. Photon.* **13**, 765 (2019)

13. J. Brodeur, L. Hu, A. Malinge, E. Eizner, W. G. Skene, S. K. Cohen, Highly Efficient and Spectrally Narrow Near-Infrared Fluorescent OLEDs Using a TADF-Sensitized Cyanine Dye. *Adv. Opt. Mater.* **7**, 1901144 (2019)

Publication lists

Original papers

1) **Ryo Nagata**, Hajime Nakanotani, Chihaya Adachi, Near-infrared Electrophosphorescence up to 1.1 μm utilizing a Thermally Activated Delayed Fluorescence Molecule as triplet sensitizer, *Adv. Mater.* 29, 1604265 (2017).

2) **Ryo Nagata**, Hajime Nakanotani, William J. Potscavage Jr., Chihaya Adachi, Exploiting Singlet Fission in Organic Light-Emitting Diodes, *Adv. Mater.* 30, 1801484 (2018).

3) Umamahesh Balijapalli*, **Ryo Nagata***, Nishiki Yamada, Hajime Nakanotani, Masaki Tanaka, Anthony D'Aléo, Virginie Placide, Masashi Mamada, Youichi Tsuchiya, Chihaya Adachi, Highly Efficient Near-Infrared Electrofluorescence from a Thermally Activated Delayed Fluorescence Molecule, *Angew. Chem. Int. Ed.* (accepted). (*Equal contribution)

Joint papers

1) Ling-Song Cui, Shi-Bin Ruan, Fatima Bencheikh, **Ryo Nagata**, Lei Zhang, Ko Inada, Hajime Nakanotani, Liang-Sheng Liao, Chihaya Adachi, Long-lived efficient delayed fluorescence organic light-emitting diodes using n-type hosts, *Nat. Commun.* 8, 2250 (2017).

2) Masaki Tanaka, **Ryo Nagata**, Hajime Nakanotani, Chihaya Adachi, Understanding degradation of organic light-emitting diodes from magnetic field effects, *Commun. Mater.* 1, 18 (2020).

3) Masaki Tanaka, **Ryo Nagata**, Hajime Nakanotani, Chihaya Adachi, Precise Exciton Management of Quaternary Emission Layers for Highly Stable Organic Light-Emitting Diodes Based on Thermally Activated Delayed Fluorescence, *ACS. Appl. Mater. Interfaces* **12**, 50668 (2020).

4) Minghan Cai, Morgan Auffray, Dongdong Zhang, Yuewei Zhang, **Ryo Nagata**, Zesen Lin, Xun Tang, Chin-Yiu Chan, Yi-Ting Lee, Tianyu Huang, Xiaozeng Song, Youichi Tsuchiya, Chihaya Adachi, Lian Duan, Enhancing Spin-orbital Coupling in Deep-blue/blue TADF Emitters by Minimizing the Distance from the Heteroatoms in Donors to Acceptors, *Chem. Eng. J.* doi.org/10.1016/j.cej.2020.127591

Acknowledgements

The studies in this thesis were carried out at Adachi laboratory, Department of Chemistry and Biochemistry, Graduate School of Kyushu University from 2015-2021.

I deeply appreciate Professor Chihaya Adachi for supervising this thesis, providing excellent research environment, and supporting me in all of my works. I sincerely appreciate Professor Hiroyuki Furuta and Professor Ken Onda for co-supervising this thesis and giving me insightful advice from many perspectives. I would like to thank Associate Professor Hajime Nakanotani, Associate Professor Masashi Mamada, Assistant Professor Kenichi Goushi, Associate Professor Youichi Tsuchiya, Associate Professor Ryota Kabe (Okinawa Institute of Science and Technology Graduate University) for giving me a lot of expert advice. Especially, I would like to express my sincere gratitude to Associate Professor Hajime Nakanotani for his warm support in all of my works.

I would like to acknowledge Dr. William J. Potscavage Jr. for the calculation in Chapter 3, Dr. Umamahesh Balijapalli for the synthesis in Chapter 4, Dr. Masaki Tanaka for the discussion on device physics. I also sincerely appreciate Professor Reiji Hattori for giving me a lot of professional advice on pulseplethysmography in Chapter 4.

I would like to extend my gratitude to the former member of Adachi laboratory, Dr. Ko Yoshida, Dr. Munetomo Inoue, Dr. Hiroyuki Mieno, Dr. Hiroki Noda, Dr. Naoto Notsuka, Mr. Taro Furukawa, Dr. Yu Esaki, Mr. Hiroya Arai, Mr. Yu Shiihara, Ms. Momoka Miyajima. Also, I would like to acknowledge all the members in Adachi laboratory for their kind support not only for my works but also for my daily life. Especially, I sincerely appreciate Dr. Kazuya Jinnai for helping me get through the difficult times. I also deeply appreciate Shoshisha Foundation and Japan Society for the Promotion of Science for their financial support. Finally, I would like to express my sincere gratitude to my family for always supporting and encouraging me in my life.

January 2021, *Ryo Nagata*